











# NAVAL POSTGRADUATE SCHOOL

## Monterey, California



## THESIS

Y745

APPLICATION OF LASER DIFFRACTION TECHNIQUES  
TO PARTICLE SIZING IN SOLID PROPELLANT  
ROCKET MOTORS

by

E.D. Youngborg

December 1987

Thesis Advisor:

D.W. Netzer

Approved for public release; distribution is unlimited

T239339



## REPORT DOCUMENTATION PAGE

1a REPORT SECURITY CLASSIFICATION UNCLASSIFIED			1b RESTRICTIVE MARKINGS		
2a SECURITY CLASSIFICATION AUTHORITY			3 DISTRIBUTION/AVAILABILITY OF REPORT Approved for public release; distribution is unlimited		
2b DECLASSIFICATION/DOWNGRADING SCHEDULE			5 MONITORING ORGANIZATION REPORT NUMBER(S)		
4 PERFORMING ORGANIZATION REPORT NUMBER(S)			7a NAME OF MONITORING ORGANIZATION Naval Postgraduate School		
6a NAME OF PERFORMING ORGANIZATION Naval Postgraduate School		6b OFFICE SYMBOL (If applicable) Code 67		7b ADDRESS (City, State, and ZIP Code) Monterey, California 93943-5000	
6c ADDRESS (City, State, and ZIP Code) Monterey, California 93943-5000			9 PROCUREMENT INSTRUMENT IDENTIFICATION NUMBER		
8a NAME OF FUNDING SPONSORING ORGANIZATION Air Force Astronautics Laboratory		8b OFFICE SYMBOL (If applicable)		10 SOURCE OF FUNDING NUMBERS	
8c ADDRESS (City, State, and ZIP Code) Edwards Air Force Base, California 93523		PROGRAM ELEMENT NO		PROJECT NO F04611-87-X-00FO	TASK NO WORK UNIT ACCESSION NO
11 TITLE (Include Security Classification) APPLICATION OF LASER DIFFRACTION TECHNIQUES TO PARTICLE SIZING IN SOLID PROPELLANT ROCKET MOTORS					
12 PERSONAL AUTHOR(S) Youngborg, E.D.					
13a TYPE OF REPORT Master's Thesis		13b TIME COVERED FROM _____ TO _____		14 DATE OF REPORT (Year, Month, Day) 1987, December	
				15 PAGE COUNT 112	
16 SUPPLEMENTARY NOTATION					
17 COSATI CODES			18 SUBJECT TERMS (Continue on reverse if necessary and identify by block number)		
FIELD	GROUP	SUB-GROUP	Particle Sizing; Solid Propellant Rocket Motors		
19 ABSTRACT (Continue on reverse if necessary and identify by block number) <p>Measurements of forward scattered light were used to determine the particulate behavior in the combustor and across the exhaust nozzle of a small solid propellant rocket motor. A MALVERN 2600 was successful in measuring multimodal particle distributions, and a locally designed system was successfully applied to monomodal distributions. The propellant tested was a reduced smoke propellant containing one-percent zirconium carbide by weight. The results suggested that ZrC reacts to completion on or very near the propellant surface. Zirconium oxide (ZrO<sub>2</sub>) agglomerates are believed to form on the surface. Surface agglomerate size decreased with increasing pressures to approximately 500 psig. Agglomerates broke up in the nozzle convergence to approximately 18 microns, independent of the pressure or nozzle entrance particle size. Particle breakup occurred in the exhaust plume. System limitations, sources of error and suggested improvements are discussed.</p>					
20 DISTRIBUTION/AVAILABILITY OF ABSTRACT <input checked="" type="checkbox"/> UNCLASSIFIED/UNLIMITED <input type="checkbox"/> SAME AS RPT <input type="checkbox"/> DTIC USERS			21 ABSTRACT SECURITY CLASSIFICATION Unclassified		
22a NAME OF RESPONSIBLE INDIVIDUAL Prof. D.W. Netzer			22b TELEPHONE (Include Area Code) (408) 646-2980		22c OFFICE SYMBOL Code 67Nt

Approved for public release; distribution is unlimited

Application of Laser Diffraction Techniques to Particle  
Sizing in Solid Propellant Rocket Motors

by

E.D. Youngborg  
Lieutenant Commander, United States Navy  
B.S., U.S. Naval Academy, 1976

Submitted in partial fulfillment of the  
requirements for the degree of

MASTER OF SCIENCE IN AERONAUTICAL ENGINEERING

from the

NAVAL POSTGRADUATE SCHOOL  
December 1987



## ABSTRACT

Measurements of forward scattered light were used to determine the particulate behavior in the combustor and across the exhaust nozzle of a small solid propellant rocket motor. A MALVERN 2600 was successful in measuring multimodal particle distributions, and a locally designed system was successfully applied to monomodal distributions. The propellant tested was a reduced smoke propellant containing one-percent zirconium carbide by weight. The results suggested that ZrC reacts to completion on or very near the propellant surface. Zirconium oxide ( $\text{ZrO}_2$ ) agglomerates are believed to form on the surface. Surface agglomerate size decreased with increasing pressures to approximately 500 psig. Agglomerates broke up in the nozzle convergence to approximately 18 microns, independent of the pressure or nozzle entrance particle size. Particle breakup occurred in the exhaust plume. System limitations, sources of error and suggested improvements are discussed.

## TABLE OF CONTENTS

I.	INTRODUCTION -----	1
II.	THEORETICAL BACKGROUND -----	5
III.	EXPERIMENTAL APPARATUS -----	12
	A. INTRODUCTION -----	12
	B. ROCKET MOTOR -----	12
	C. LASER LIGHT SCATTERING APPARATUS -----	16
	D. DATA ACQUISITION AND REDUCTION -----	22
IV.	RESULTS AND DISCUSSION -----	25
	A. INTRODUCTION -----	25
	B. SYSTEM CALIBRATION -----	26
	C. RESULTS FROM REDUCED SMOKE PROPELLANT EVALUATION -----	30
	1. Test Conditions -----	30
	2. Zirconium Carbide Behavior -----	33
	3. Near Propellant Surface Data -----	35
	4. Nozzle Entrance Data -----	43
	5. Exhaust Nozzle Data -----	54
	6. SEM Analysis -----	80
	D. COMPARATIVE EVALUATION OF THE MALVERN 2600 AND THE LOCALLY DESIGNED LASER DIFFRACTION SYSTEM -----	82
	E. SOURCES OF MEASUREMENT ERROR (UNCERTAINTY) --	85
V.	CONCLUSIONS AND RECOMMENDATIONS -----	96
	LIST OF REFERENCES -----	99
	INITIAL DISTRIBUTION LIST -----	102

# LIST OF TABLES

3.1	PROPELLANT CHARACTERISTICS -----	17
3.2	LASER SPECIFICATIONS -----	22
4.1	CALIBRATION RESULTS -----	27
4.2	THERMOPHYSICAL PROPERTIES OF Zr, ZrC, AND ZrO <sub>2</sub> --	33
4.3	NEAR GRAIN SURFACE SCATTERING MEASUREMENT RESULTS -----	36
4.4	MOTOR CHAMBER SCATTERING MEASUREMENTS OBTAINED UPSTREAM FROM NOZZLE CONVERGING SECTION -----	44
4.5	EXHAUST SCATTERING MEASUREMENTS (P <sub>e</sub> = P <sub>critical</sub> ) -----	57
4.6	EXHAUST SCATTERING MEASUREMENTS (P <sub>e</sub> = P <sub>o</sub> ) -----	67

## LIST OF FIGURES

3.1	Schematic of a Laser Diffraction System -----	13
3.2	Scattering Properties of Particles as a Function of Size -----	14
3.3	Motor Components -----	15
3.4	Short Motor Components -----	15
3.5	NPS Light Scattering Apparatus -----	19
3.6	Hewlett Packard HP 9836S Computer and HP 6942A Multiprogrammer -----	20
3.7	MALVERN 2600 Particle Sizer -----	21
4.1	Calibration Profile for a Polydispersed Sample (14.9-24.4 Microns) -----	28
4.2	Calibration Profile for a Polydispersed Sample (8.5-10.4 Microns) -----	29
4.3	Volume Distribution, Bimodal Calibration Sample -----	31
4.4	Near Grain Scattering Measurement Results -----	37
4.5	Volume Distribution, Near Grain Test No. 1 (159 psig) -----	38
4.6	Volume Distribution, Near Grain Test No. 2 (188 psig) -----	39
4.7	Volume Distribution, Near Grain Test No. 3 (248 psig) -----	40
4.8	Volume Distribution, Near Grain Test No. 4 (448 psig) -----	42
4.9	Volume Distribution, Nozzle Entrance Test No. 1 (119 psig) -----	46
4.10	Volume Distribution, Nozzle Entrance Test No. 2 (124 psig) -----	47



4.11	Volume Distribution, Nozzle Entrance Test No. 3 (161 psig) -----	48
4.12	Volume Distribution, Nozzle Entrance Test No. 8 (252 psig) -----	50
4.13	Volume Distribution, Nozzle Entrance Test No. 9 (251 psig) -----	51
4.14	Volume Distribution, Nozzle Entrance Test No. 10 (370 psig) -----	52
4.15	Volume Distribution, Nozzle Entrance Test No. 11 (427 psig) -----	53
4.16	Nozzle Entrance Scattering Measurement Results -----	55
4.17	Comparative Results, Near Grain and Nozzle Entrance Data -----	56
4.18	Volume Distribution, Exhaust ( $P_e = P_{critical}$ ) Test No. 1 (147 psig) -----	58
4.19	Volume Distribution, Exhaust ( $P_e = P_{critical}$ ) Test No. 2 (212 psig) -----	59
4.20	Volume Distribution, Exhaust ( $P_e = P_{critical}$ ) Test No. 3 (450 psig) -----	60
4.21	Volume Distribution, Exhaust ( $P_e = P_{critical}$ ) Test No. 4 (421 psig) -----	61
4.22	Volume Distribution, Exhaust ( $P_e = P_{critical}$ ) Test No. 5 (371 psig) -----	62
4.23	Exhaust Profile ( $P_e = P_{critical}$ ) Test No. 6 (370 psig) -----	63
4.24	Exhaust Scattering Measurement Results ( $P_e = P_{critical}$ ) -----	66
4.25	Volume Distribution, Exhaust ( $P_e = P_o$ ) Test No. 1 (175 psig) -----	68
4.26	Volume Distribution, Exhaust ( $P_e = P_o$ ) Test No. 2 (125 psig) -----	69
4.27	Volume Distribution, Exhaust ( $P_e = P_o$ ) Test No. 3 (135 psig) -----	70

4.28	Volume Distribution, Exhaust ( $P_e = P_o$ ) Test No. 4 (79 psig) -----	71
4.29	Volume Distribution, Exhaust ( $P_e = P_o$ ) Test No. 5 (215 psig) -----	72
4.30	Volume Distribution, Exhaust ( $P_e = P_o$ ) Test No. 6 (436 psig) -----	73
4.31	Volume Distribution, Exhaust ( $P_e = P_o$ ) Test No. 7 (352 psig) -----	74
4.32	Volume Distribution, Exhaust ( $P_e = P_o$ ) Test No. 8 (300 psig) -----	75
4.33	Exhaust Scattering Measurement Results ( $P_e = P_o$ ) -----	78
4.34	Comparative Results, Exhaust ( $P_e = P_{critical}$ ) and Exhaust ( $P_e = P_o$ ) Data -----	79
4.35	SEM Photograph of Residue Collected from Exhaust Nozzle -----	81
4.36	SEM Photograph of Residue Collected from Exhaust Nozzle -----	81
4.37	Comparative Results, NPS and MALVERN Data for the Nozzle Entrance -----	84
4.38	Example of the Effects of a Reduced Field of View -----	86
4.39	Motor Profile, Nozzle Entrance Test No. 4 (175 psig) -----	87
4.40	Motor Profile, Nozzle Entrance Test No. 5 (125 psig) -----	88
4.41	Motor Profile, Nozzle Entrance Test No. 6 (135 psig) -----	89
4.42	Motor Profile, Nozzle Entrance Test No. 7 (79 psig) -----	90

### ACKNOWLEDGMENTS

The guidance of Professor David Netzer proved to be invaluable in the successful completion of the present research. The technical support of Mr. Harry Conner, Mr. Pat Hickey, and the diligent work of Mr. Don Harvey in preparing the exhaust nozzles were greatly appreciated.





## I. INTRODUCTION

The use of metallized propellants offers the advantage of improved solid rocket motor performance in terms of increased energy, specific impulse, and suppression of high frequency acoustic combustion instabilities. Aluminum is currently the primary metallic additive of choice when exhaust plume visibility is not a mission consideration. However, the requirement for reduced smoke propellants for use in tactical air-to-air applications has dictated the use of alternate high energy propellants which utilize only small amounts of additives such as zirconium, zirconium carbide, and aluminum oxide to provide acoustic stabilization.

The improvements achieved via such additives are not without penalty, certain loss mechanisms are introduced. The specific impulse efficiency of a propellant containing metal is generally less than that of a base propellant due to incomplete combustion of the metal in the motor and the presence of condensed metal and metal oxides in the nozzle flow. Particle-gas velocity lag represents the primary source of performance loss within the exhaust nozzle. Thermal lag generally has less effect on performance. Yet, neglecting thermal and velocity lag as loss mechanisms, the simple fact that the condensed particulates do not expand as

the other combustion gases expand, results in a reduction of available specific impulse.

Netzer et al. [Ref. 1], point out that the behavior of metal as it leaves the burning surface is not a well-defined phenomenon. Some particles upon reaching the burning surface depart immediately, while others agglomerate on the surface before passing into the gas flow. The mechanics of metal droplet combustion as discussed by Schorr [Ref. 2], indicate that resultant particles in the range of 1-2 microns and smaller are of significance in determining exhaust plume signature, while those particulates of 5 microns and greater are important in the determination of two-phase flow losses. The problem of predicting performance depends on an accurate determination of these two-phase flow losses which are a strong function of particle size. The aluminum oxide that results from the gas phase combustion of aluminum is generally less than two microns in size. These small particles have little velocity lag. Thus, making them smaller would serve little benefit.

Several complex computer codes attempt to model the combustion process in order to predict solid rocket motor performance. The SPP (Solid Performance Program) [Refs. 3,4], is one such code. These programs are semi-empirical in nature and require an a priori knowledge of particle size distribution entering the exhaust nozzle. This distribution

must be experimentally determined, as the problem is currently intractable with regard to analytic methods.

The following experimental methods have been employed in previous work at the Naval Postgraduate School:

- (a) collection of exhaust products
- (b) light transmission measurements
- (c) light scattering measurements
- (d) holography and high speed motion pictures.

A summary of previous research conducted at the Naval Postgraduate School combustion laboratory is contained in Reference 1. The present investigation focused on the use of light scattering techniques to determine particle size. The method is non-intrusive and suited to measurements in both the motor and exhaust nozzle environments. The speed of the flow precludes successful application of most holographic techniques within the exhaust nozzle.

Heretofore most studies have been directed at aluminized composites, and much is known about the combustion of aluminum. The behavior of other metallic additives have not been as fully explored. For example, zirconium carbide is used as a stability additive. However, it is not known whether surface agglomeration occurs, or whether the zirconium burns to zirconium oxide. Both of these processes will affect the size distribution and density of the particles in the gas phase. These in turn affect the

ability of the particles to provide damping for a specific frequency of pressure oscillation.

The goals of this investigation were:

- (1) to refine previously developed experimental and diagnostic techniques, and
- (2) to use the apparatus to determine the effects operating pressure and position within the motor and exhaust nozzle on the particle size distributions from a reduced smoke propellant.

The propellant studied was a low smoke, composite which contained one percent zirconium carbide by weight. The behavior of particulates at various positions in the motor and exhaust nozzle was examined as a function of chamber pressure.



## II. THEORETICAL BACKGROUND

The performance of a solid rocket motor utilizing metallized propellants is significantly dependent on the diameter of the condensed particulates present in the flow. A non-intrusive, in-situ method is the most desirable means to determine particle size, since the measurement is real time and the environmental conditions (pressure, temperature, gas composition, etc.) are undisturbed. The method chosen for the present research was the diffractively scattered light technique. Very large particles cannot be measured with this technique due to the transmitted light interference with the light which is scattered at very small forward angles. Very small particles scatter at larger angles, but the intensity is low, making detection difficult. Absorption and refraction also become important for very small particles. Particle concentrations are also limited to those which do not exhibit significant multiple scattering effects. Within these limits, the mean particle size is readily determined from diffraction techniques, but size distributions cannot easily be determined. In general, a distribution type must be selected a priori, i.e., Rosin-Rammler, log-normal or other such distribution must be assumed. Yet, the diffraction technique is non-intrusive and can be used in the internal motor and nozzle

environment, where velocities and particle concentrations can be high.

The scattering and absorption of a plane monochromatic electromagnetic wave by an isotropic homogeneous sphere is described by Mie's solution to Maxwell's equations [Ref. 5], and the general theory of scattering developed by Mie is presented by Van de Hulst [Ref. 6]. According to Mie's theory, the characteristics of scattered light depend upon the particle size, shape, internal structure, refractive index with respect to the surrounding medium, the scattering angle and the incident wave polarization and wavelength [Ref. 7]. The solution to Maxwell's equations for multiple scattering in a concentrated sample, where interaction of scattering centers is significant, presently represents an intractable problem, even if boundary conditions could be specified. Even the solution without multiple scattering is quite complex and difficult to incorporate into diagnostic equipment.

When the particles are much larger or much smaller than the wavelength of the incident light, the equations simplify to Fraunhofer diffraction and Rayleigh scattering, respectively. The light scattered from particles within these restricted ranges can be measured and used to readily determine particle size. The size of particles of interest in solid propellant combustion depend on the application. When considering two phase flow losses, particle sizes of

interest are generally five microns or greater. Jones [Ref. 8], has shown that Fraunhofer diffraction can be used for particles as small as one micron when a He-Ne laser is used. Fraunhofer diffraction is applicable in the case of larger particles because the forward scattered light in the center lobe is due principally to diffraction. The mechanisms of reflection and absorption do not significantly contribute to the center lobe in this instance (this was shown by Hodgkinson [Ref. 9]). If these latter effects are present to a significant extent, then the complete Mie equations must be used.

The classical results of Fraunhofer diffraction from particles, i.e., the discrete rings associated with a monodispersion, are typically not observed in practical combustion experiments. Typically, the particulates are polydispersed and, in many cases, a multimodal polydispersion is present. The intensity distribution due to a monodispersion is given by Fraunhofer diffraction [Ref. 10] as,

$$\frac{I(\theta)}{I(0)} = \left[ \frac{2J_1(\alpha \sin \theta)}{\alpha \sin \theta} \right]^2 \quad (1)$$

where  $J_1$  is the first order Bessel function,  $\alpha = \pi D/\lambda$ ,  $\theta$  is the scattering angle for the forward direction,  $D$  is the particle diameter, and  $\lambda$  is the wavelength of the incident

light. When considering small angles ( $\theta < 15^\circ$ ), the expression simplifies to,

$$\frac{I(\theta)}{I(0)} = \left[ \frac{2J_1(\alpha\theta)}{\alpha\theta} \right]^2. \quad (2)$$

Dobbins [Ref. 11] showed that the normalized integrated intensity of forward scattered light from a polydispersion of large particles is given as,

$$\frac{I(\theta)}{I(0)} = \frac{\int_0^{D_\infty} \left[ \frac{2J_1(\alpha\theta)}{\alpha\theta} \right]^2 N_r(D) D^4 dD}{\int_0^{D_\infty} N_r(D) D^4 dD} \quad (3)$$

where  $N_r(D)$  is a distribution function describing the proportion of particles with diameter  $D$  in the sample. Dobbins et al. [Ref. 11] used the Upper Limit Distribution Function (ULDF) developed by Mugele and Evans [Ref. 12] and the same approach was followed in a portion of this investigation. The volume-to-surface mean diameter (Sauter mean diameter)  $D_{32}$  of a polydispersion is defined by,

$$D_{32} \equiv \frac{\int_0^{D_\infty} N_r(D) D^3 dD}{\int_0^{D_\infty} N_r(D) D^2 dD}. \quad (4)$$



The significance of  $D_{32}$  (versus  $D_{43}$ , etc.) is that the illumination profiles for different size distributions of the ULDF plotted against  $(\pi D_{32}\theta/\lambda)$  are brought into near coincidence [Ref. 11].

Buchele [Ref. 10] showed that for  $\pi D_{32}\theta/\lambda$  less than three, a gaussian curve can be used for the scattered light intensity which closely matches the theoretical intensity profile for a polydispersion obtained by integrating Equation (3). The gaussian expression presented by Buchele is given as,

$$\frac{I(\theta)}{I(0)} = \exp[-(.57\pi D_{32}\theta/\lambda)^2] \quad (5)$$

The data reduction technique developed by Netzer and Harris [Refs. 1,13] is based on Buchele's work. The method involves comparison of the experimentally obtained intensity profile with that produced by Equation (5). Use of Equation (5) requires the value of  $I(0)$ , the forward scattered intensity at theta equal zero. Since transmitted light dominates at very low scattering angles,  $I(0)$  cannot be measured. A ratioing technique eliminates this problem. Equation (5) can be used to ratio  $I(\theta_2)/I(\theta_1)$  as follows,

$$\frac{I(\theta_2)}{I(\theta_1)} = \exp\{-D_{32}^2(\frac{.57\pi}{\lambda})^2(\theta_2^2 - \theta_1^2)\} . \quad (6)$$

This eliminates the need to determine  $I(0)$ . However,  $I(\theta_1)$  at the "minimum" forward angle  $\theta_1$  must be taken from the experimentally measured profile at a location where the transmitted light effects are not significantly present. The resultant profile  $I(\theta_2)/I(\theta_1)$  versus  $\theta_2$  can then be generated for a specified  $D_{32}$ .  $D_{32}$  is varied interactively until the profile generated by Equation (6) matches the measured profile. This procedure yields  $D_{32}$ . However, this approach has an obvious disadvantage in that it is only accurate if the polydispersion is monomodal.

A Malvern 2600 particle sizer was also used in the present investigation. The Malvern software is similarly based upon Fraunhofer diffraction. However, it is based on the inversion of the measured scattered data to obtain a particle size distribution. The Malvern allows use of a selected type of particle size distribution (Rosin Rammler, log-normal, normal) or of a model independent mode. The model independent method is described by the Malvern 2600 Reference Manual [Ref. 14] as a constrained non-linear least squares method, which is able to measure multi-modal particle distributions with high resolution. The obvious advantages of the Malvern 2600 are the ability to measure multi-modal particle size distributions, and it has been independently tested. Dodge et al. [Ref. 15] conducted a comparison of the Malvern device and a phase doppler system and found that there was excellent agreement in point

measured Sauter mean diameters between the deconvoluted laser diffraction data and the phase doppler data. The Malvern system is currently one of the most widely used laser diffraction devices and it shows great promise for application to particle sizing in solid rocket motors.

Other work has been done in the area of analytic methods that appears to provide the basis for refinements in particle sizing and determination of particle size distributions. Koo and Hirleman [Ref. 16] evaluated the use of integral transform techniques on Fraunhofer diffraction patterns. These techniques offer the advantage of direct inversion of scattering data to obtain a size distribution.

### III. EXPERIMENTAL APPARATUS

#### A. INTRODUCTION

Laser diffraction systems have become widely used in the field of particle and droplet size measurements. Fraunhofer diffraction is the underlying principle involved. Hodgkinson [Ref. 9] demonstrated that for particles greater than several microns in size, the primary contribution in the near forward small angle region is from diffraction rather than reflection or refraction and Jones [Ref. 8] has proved that in this same region, Fraunhofer diffraction may be applied to particles as small as one micron when a helium-neon laser is chosen as the source of illumination. Figure 3.1 details a simple schematic for a laser light diffraction particle sizer. Such a system typically consists of a He-Ne laser source, beam expander (spatial filter and collimating lens), Fourier transform lens, and a detector.

Typically, small particles diffract light at large angles and large particles diffract light at small angles. Figure 3.2 depicts the diffraction process. Note that the undiffracted light is focused to a single point.

#### B. ROCKET MOTOR

The series of experiments conducted required the use of two small solid propellant rocket motors. The motor depicted in Figure 3.3 is the same as that used by Pruitt

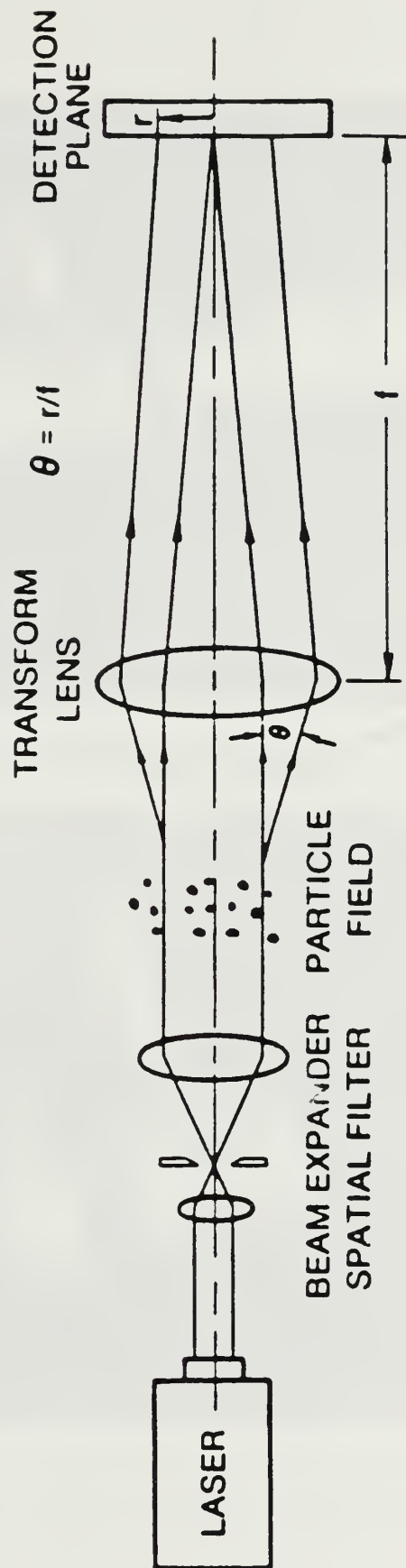


Figure 3.1 Schematic of a Laser Diffraction System [Ref. 16]



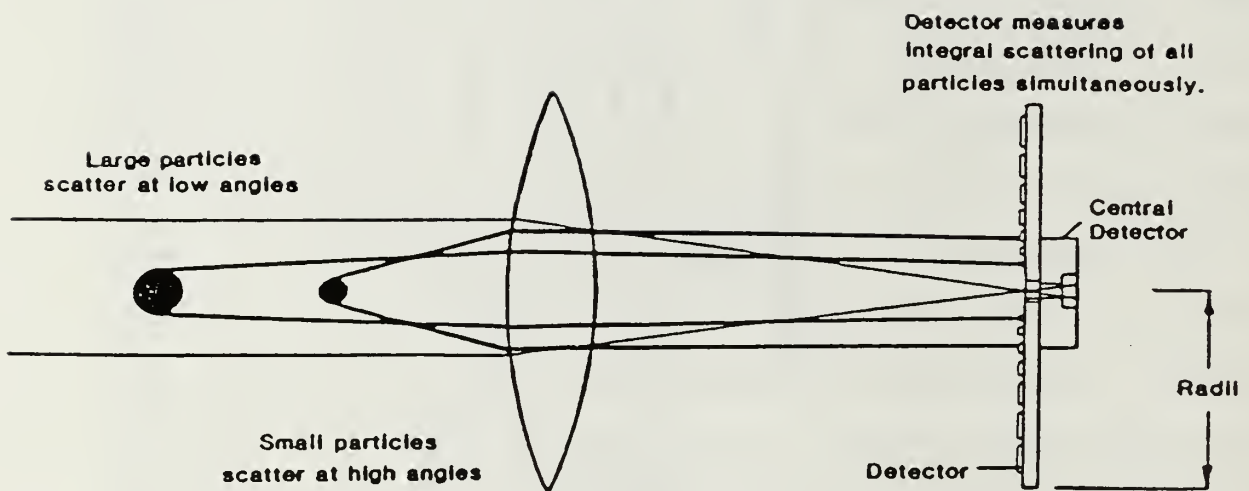


Figure 3.2 Scattering Properties of Particles as a Function of Size [Ref. 14]

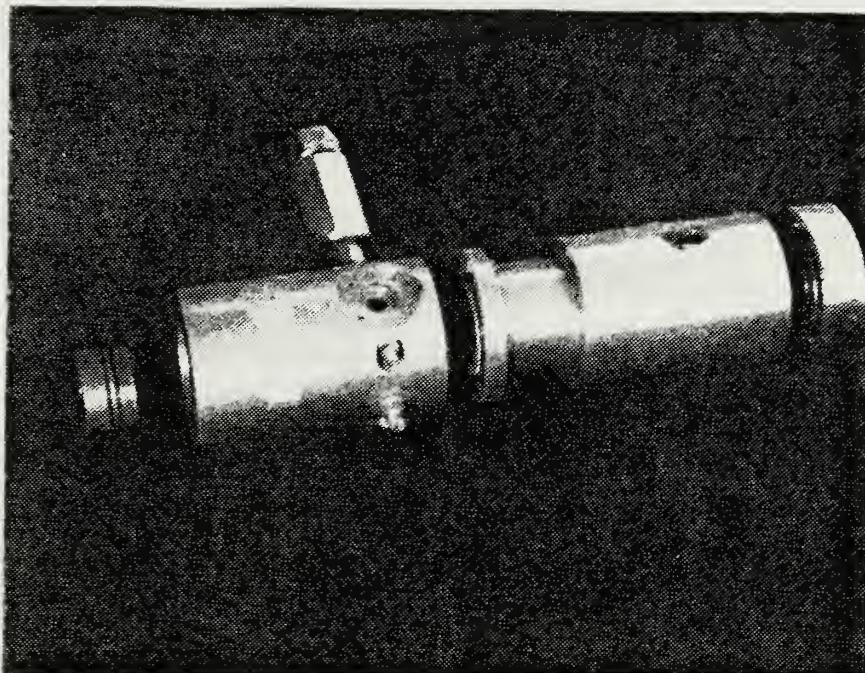


Figure 3.3 Motor Components

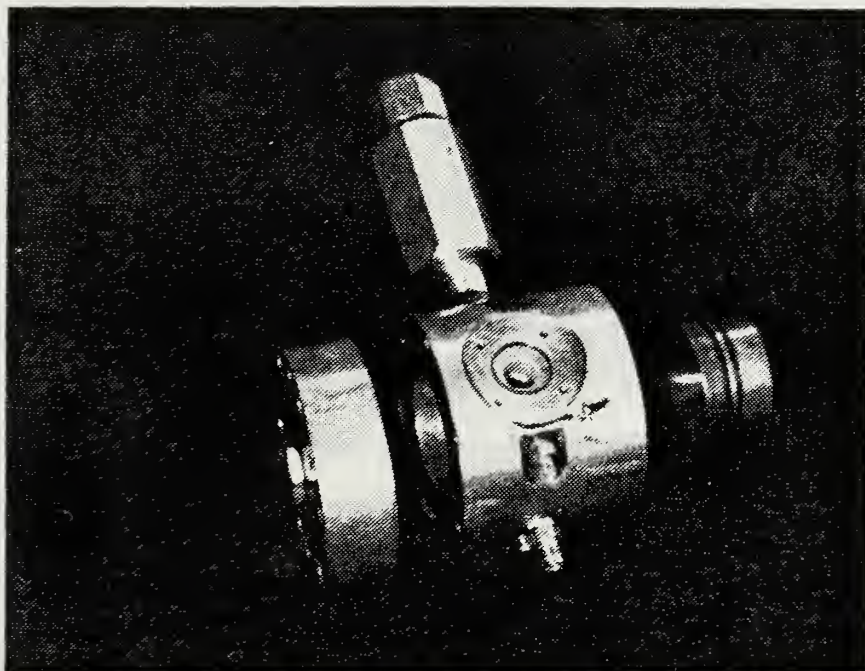


Figure 3.4 Short Motor Components

[Ref. 17]. The chamber diameter was 2.00 inches and the propellant was cylindrical, 1.98 inches in diameter and 1.00-1.25 inches thick. All tests conducted were done with end burning grains. The long motor (Fig. 3.3) was used to obtain in-situ measurements of particle size prior to the nozzle entrance and in the exhaust. Figure 3.4 depicts the short motor which was used to obtain in-situ particle size measurements just aft of the propellant burning surface. This particular motor had been used previously in connection with holographic imaging. For additional specifications see Reference 18.

Both motors were windowed, and the windows were kept clean using a nitrogen purge. The nitrogen was "spread" using a sintered metal sleeve which was inserted into the aperture.

Ignition was accomplished using a  $\text{BKNO}_3$  ignitor which was fired by means of a nichrome filament energized by a 12 VDC source.

The propellant was bonded into the motor casing with a self-vulcanizing silicone rubber (RTV). The propellant studied was a reduced smoke propellant with 87% solids loading. Table 3.1 presents the major propellant ingredient weight percentages.

### C. LASER LIGHT SCATTERING APPARATUS

The locally designed laser diffraction system makes use of an 8 mWatt He-Ne source in the same general configuration

TABLE 3.1  
PROPELLANT INGREDIENTS

<u>Ingredient</u>	<u>Approx. Wt. %</u>
R45M	9.2
RDX	4.0
AP	82.0
ZrC	1.0

depicted in Figure 3.1. (A complete description of the apparatus is contained in Reference 20 [see Figures. 3.5 and 3.6]). The scattered light is passed through a wide-pass laser line filter and a 500 mm focal length Fourier transform lens, which focuses the light onto the detector. The detector is a linear photodiode array (Reticon RL 1024G) which has 1024 photodiodes on 25 micron centers. The array is mounted on a "mother" board which contains the sample-and-hold circuits. Each photodiode measures the intensity of the scattered light and outputs a proportional voltage. The array is scanned at a rate of 33 kHz and a 6 msec blanking pulse is used to sequence the sweeps. The range of scattering angles within the field of view is determined by a number of factors. The upper limit of scattering angle is determined by the diameter and focal length of the focusing lens, the distance between the focusing lens and the particles, the diameter of the motor window, and the height/position of the diode array [Ref. 1]. The range of



scattering angles for this investigation was .01-.06 radians, corresponding to an offset of 5 mm of the array and .02-.07 radians corresponding to a 10 mm offset. Because of the very small detectors, the system is not capable of measuring very weak scattering intensities.

The second system utilized was a commercially available particle size analyzer manufactured by MALVERN Instruments. The particular instrument used in this series of experiments was the MALVERN 2600 HSD. Figure 3.7 depicts the MALVERN 2600 system, which utilizes a 2 mW He-Ne laser with a collimated beam diameter of 9 mm (Table 3.2 details laser specifications). One of the principle advantages of the MALVERN system is its use of an annular photodiode array. The array is a monolithic detector which consists of 31 rings. It has increasing thicknesses of the annular detector elements with increasing circumference, resulting in an increase of detector area as radius increases. Ring arrays permit much weaker intensities to be measured than can be accomplished with linear arrays. The dynamic range of the instrument is 180:1 on any of the three range settings, with an advertized accuracy of plus or minus 4% of volume mean diameter [Ref. 19]. The detector may be used in conjunction with any one of three interchangeable Fourier transform lens, with focal lengths of 63, 100 and 300 mm [Ref. 14]. The respective size classes associated with each lens are 1.2-118, 1.9-188 and 5.8-564 microns, with a sub-class



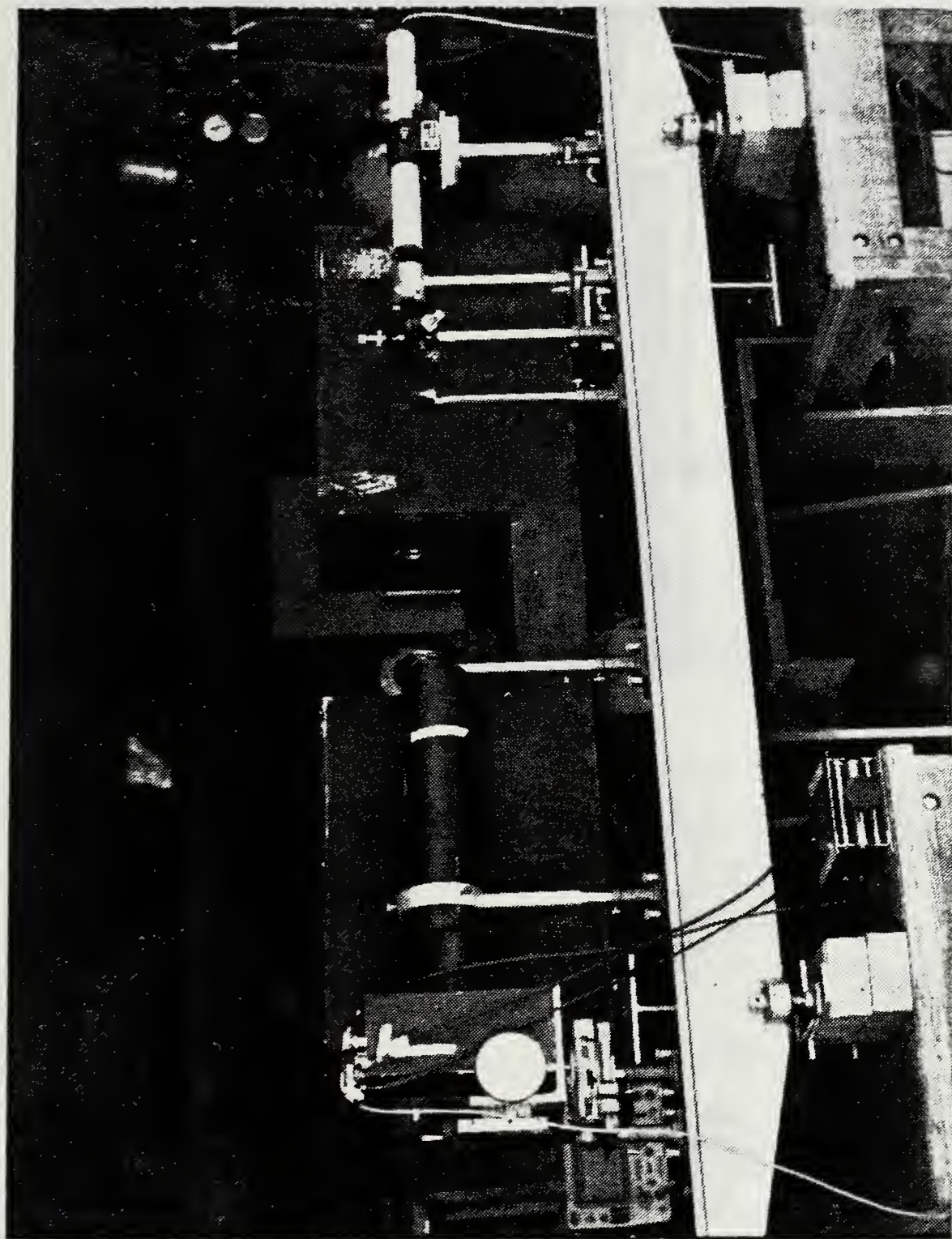


Figure 3.5 NPS Light Scattering Apparatus

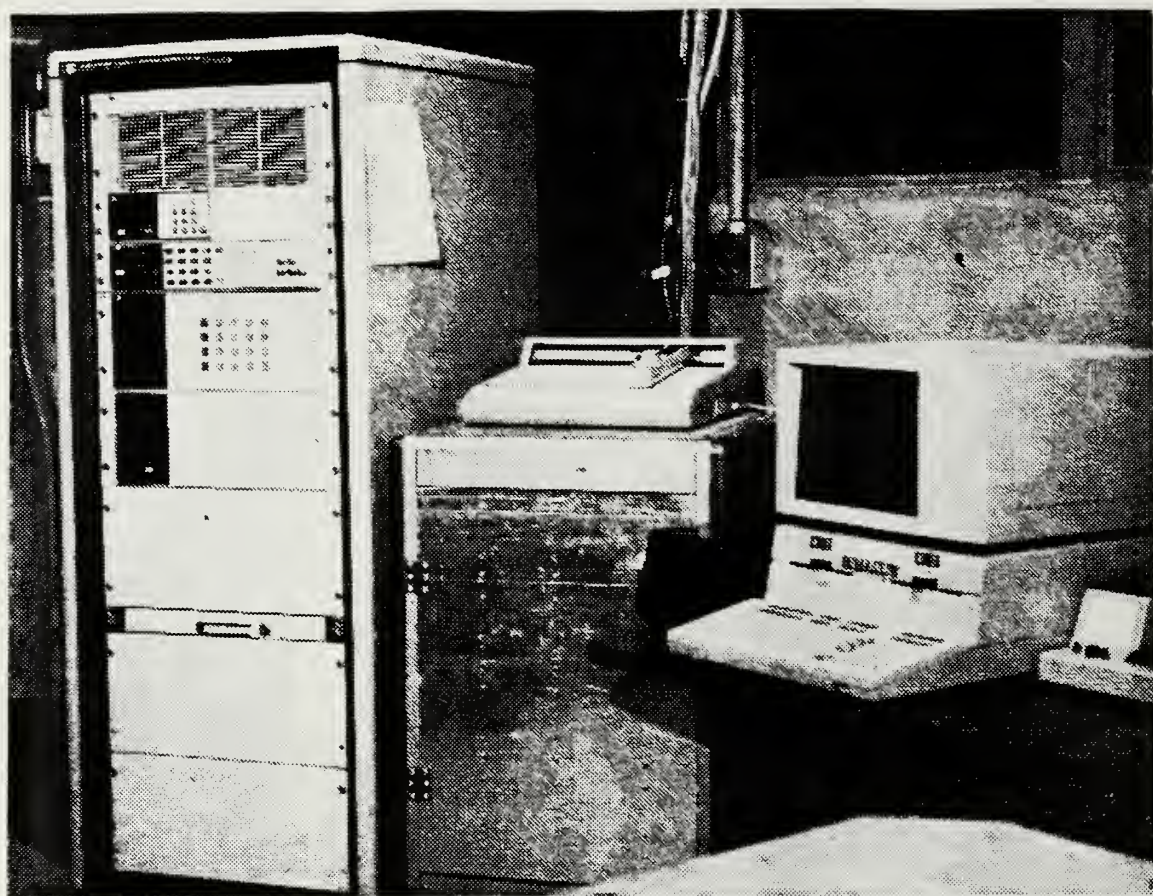
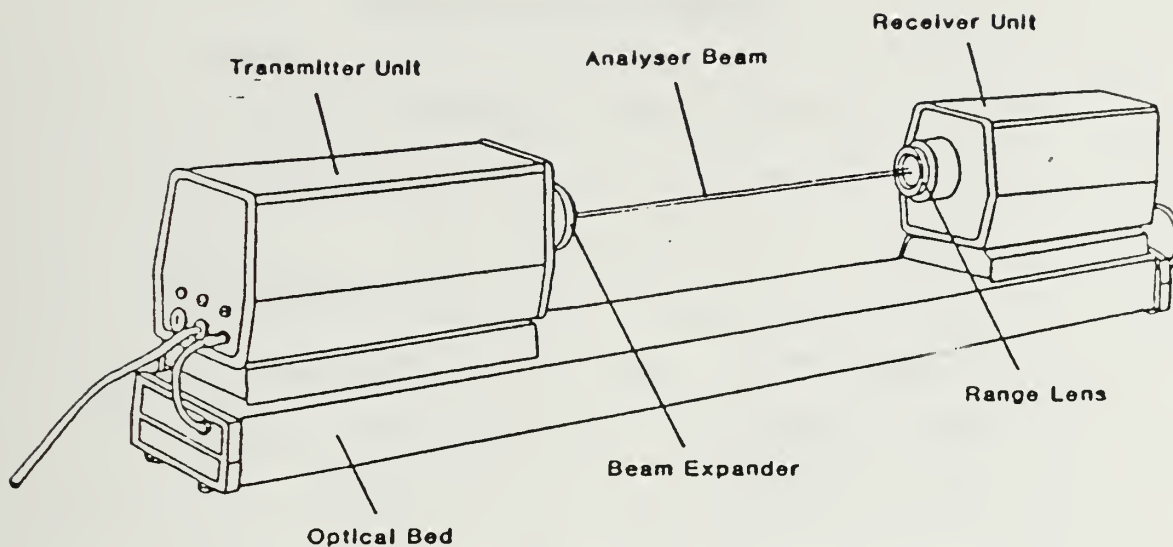
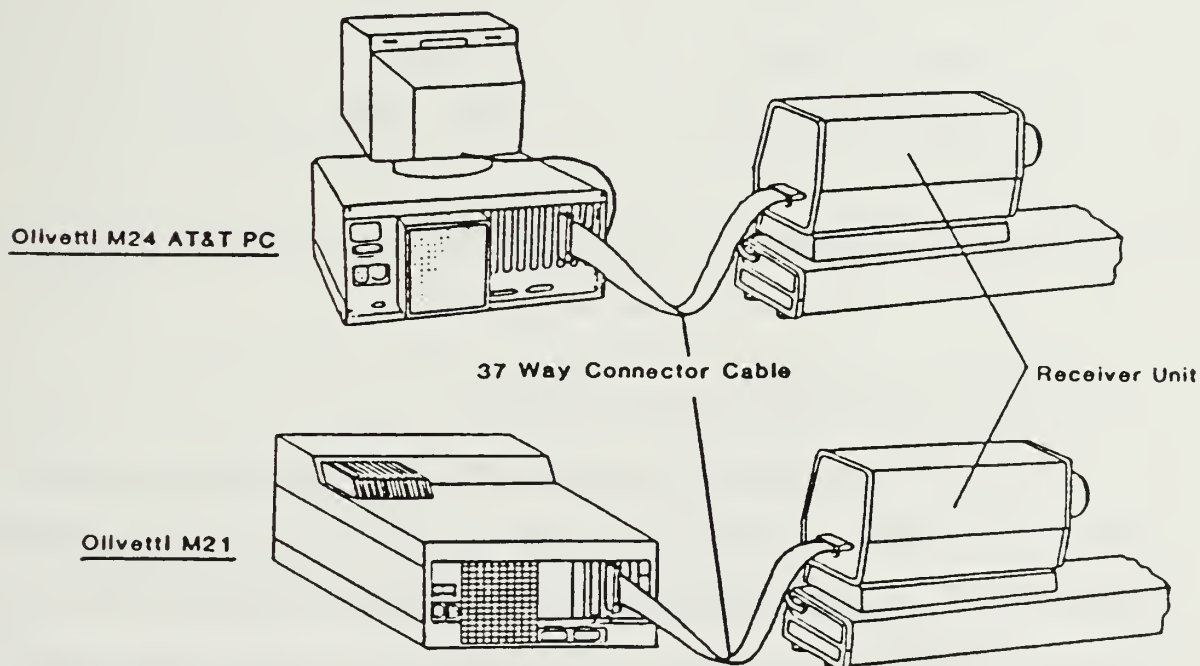


Figure 3.6 Hewlett Packard HP 9836S Computer and  
HP 6942A Multiprogrammer





2600 Optical Unit - Components & Controls



Computer to Optical Unit Connection

Figure 3.7 MALVERN 2600 Particle Sizer [Ref. 14]

TABLE 3.2

## LASER SPECIFICATIONS

## A. Helium-Neon Laser (Locally Designed System)

1. Manufacturer:	Spectra-Physics
2. Model:	147
3. Type:	He-ne Class 111B
4. Output Power:	8 mWatt
5. Beam Diameter:	.92 mm
6. Beam Divergence:	.87 mrad

## B. Helium-Neon Laser (MALVERN System)

1. Manufacturer:	MALVERN Instruments
2. Model:	2600
3. Type:	He-Ne Class 111B
4. Output Power:	2 mWatt
5. Beam Diameter:	9 mm
6. Beam Divergence:	Not Available

which extends down to .5 microns [Ref. 14]. The 100 mm lens was used for this set of experiments.

## D. DATA ACQUISITION AND REDUCTION

The data acquisition system associated with the locally designed laser diffraction system consisted of a Hewlett Packard 6942A multiprogrammer which was controlled by an HP 9836S computer. The data acquisition program developed by Harris [Ref. 13] was the system driver in the acquisition

mode. In the course of a motor firing sequence, a background measurement was recorded prior to ignition. This mean intensity profile was then subtracted from the mean intensity profile measured with particles present. This procedure accounts for noise present due to ambient light and corrects for the characteristics of individual diodes. The raw data were displayed on the HP 9836S CRT so that any erroneous scans could be excluded prior to data reduction.

A symmetric moving average type digital filter was then applied to the profile in order to smooth the curve [Ref. 1]. This type filter does not have the phase lag that is inherent in analog filters. The data reduction algorithm is based on the work done by Buchelle [Ref. 10], and is fully described in Reference 20. The chief disadvantage of the method lies in the fact that there is no way to account for the actual distribution of the particulates. The Sauter mean diameter (SMD) determined by this algorithm will be that which is associated with the dominant mode (within the field of view of the array) of a multimodal polydispersed sample.

The MALVERN system represents a vast improvement, in that not only is SMD determined, but the volume distribution is characterized as well. The MALVERN 2600 data acquisition system is centered about an AT&T 6300 PC. The system driver is the MALVERN Master-Sizer operating system. This version of the MALVERN software uses a command-based language that



allows the user to specify the pertinent parameters associated with the operation of the instrument. The Master-Sizer program allows the user to select from any one of four models. The model types available are Rosin-Rammler, log-normal, normal, and model independent. The model independent option of the Master-Sizer program is a process of constrained least squares fitting of theoretical scattering characteristics to observed data [Ref. 14]. It is usual to allow the best fit result to be obtained with no assumed form of size distribution and this allows the characterization of polydispersed multimodal distributions with high resolution [Ref. 14]. The capability of characterizing multimodal distributions is invaluable in work dealing with the combustion of metallized propellants, in that the distribution of particulates is most often multimodal. It is for this reason that the model independent mode was used exclusively throughout this investigation.

#### IV. RESULTS AND DISCUSSION

##### A. INTRODUCTION

This investigation was based on three major objectives:

- (1) refine previously developed experimental and diagnostic techniques by identifying specific causal factors of measurement error,
- (2) incorporate the use of a commercial particle size analyzer (MALVERN 2600) to validate and quantify the operating limits of the locally designed laser diffraction system and,
- (3) use the apparatus to determine the effects of operating pressure and position within the motor and exhaust nozzle on particle size distribution associated with the combustion of a reduced smoke propellant.

Previous investigations at NPS had been based on the method of Buchele [Ref. 10] which yields Sauter mean diameter, but does not provide any information as to the actual distribution of particulate size. The introduction of the MALVERN system allowed for a characterization of volume distribution. The common parameter between the locally designed system and the MALVERN was Sauter mean diameter ( $D_{32}$ ). This parameter provided the basis for comparison of the two diffraction systems. Both systems were used in the initial evaluation of the reduced smoke propellant. Once the limitations of the locally designed instrument were established, the MALVERN was used more extensively to gather data in both the motor and exhaust. The distinct advantage of being able to characterize multimodal particle size

distributions made the MALVERN the better suited instrument for the through motor measurements. In the exhaust, the annular detector of the MALVERN system allowed for the measurement of much weaker intensities as opposed to the locally designed system (which is also referred to as the NPS system).

## B. SYSTEM CALIBRATION

Among the methods available for calibration of laser diffraction instruments, the more commonly used include the calibration reticle and use of commercially prepared samples of known diameter. The latter approach was used in this investigation. The types of samples used included polystyrene spheres, glass beads and aluminum oxide powders. In each case, the sample material was suspended in a solution of distilled water.

The locally designed system was calibrated using the polystyrene spheres, with diameters of 5.1, 9.6 and 20.0 microns, respectively. Table 4.1 contains the results of these calibration tests. Figures 4.1 and 4.2 are representative samples of calibration results.

The MALVERN 2600 was calibrated using three different materials, polystyrene spheres, glass beads and an aluminum oxide powder. Results are presented in Table 4.1. Calibrations from the two systems were in good agreement. System alignment was completed with the container of water in the optical path and a background measurement was taken

TABLE 4.1

## CALIBRATION RESULTS

NPS LASER DIFFRACTION SYSTEM

<u>Particle Material</u>	<u>Median* Diameter (<math>\mu\text{m}</math>)</u>	<u>Range of* Diameters (<math>\pm 2\sigma</math>) (<math>\mu\text{m}</math>)</u>	<u>S.D. (<math>\mu\text{m}</math>) *</u>	<u>S.D. (%) *</u>	<u>Scattering Measurement <math>D_{32}</math> (<math>\mu\text{m}</math>)</u>
Polystyrene	5.1	4.6-6.4	.49	9.6	5.4
Polystyrene	9.6	8.5-10.4	.50	5.2	9.4
Polystyrene	20.0	14.9-24.4	2.40	12.0	20-21

\* Manufacturers Data (Duke Scientific Corporation)

MALVERN 2600

<u>Particle Material</u>	<u>Median* Diameter (<math>\mu\text{m}</math>)</u>	<u>Range of* Diameters (<math>\pm 2\sigma</math>) (<math>\mu\text{m}</math>)</u>	<u>S.D. (<math>\mu\text{m}</math>) *</u>	<u>(S.D. (%) *)</u>	<u>Scattering Measurement <math>D_{32}</math> (<math>\mu\text{m}</math>)</u>
Polystyrene	5.1	4.6-6.4	.49	9.6	5.5
Polystyrene	20.0	14.9-24.4	2.40	12.0	20.8
<u>Particle Material</u>	<u>Range of Particle Size (<math>\mu\text{m}</math>)</u>	<u>Mean Diameter (<math>\mu\text{m}</math>)</u>	<u>Scattering Measurement <math>D_{32}</math> (<math>\mu\text{m}</math>)</u>		
Aluminum Oxide	1-20**	5-8**	7.3		
Glass Beads	37-44**	40**	40.1		

\*\* Manufacturers Data

# CURVE FIT RESULTS INTENSITY VS. THETA

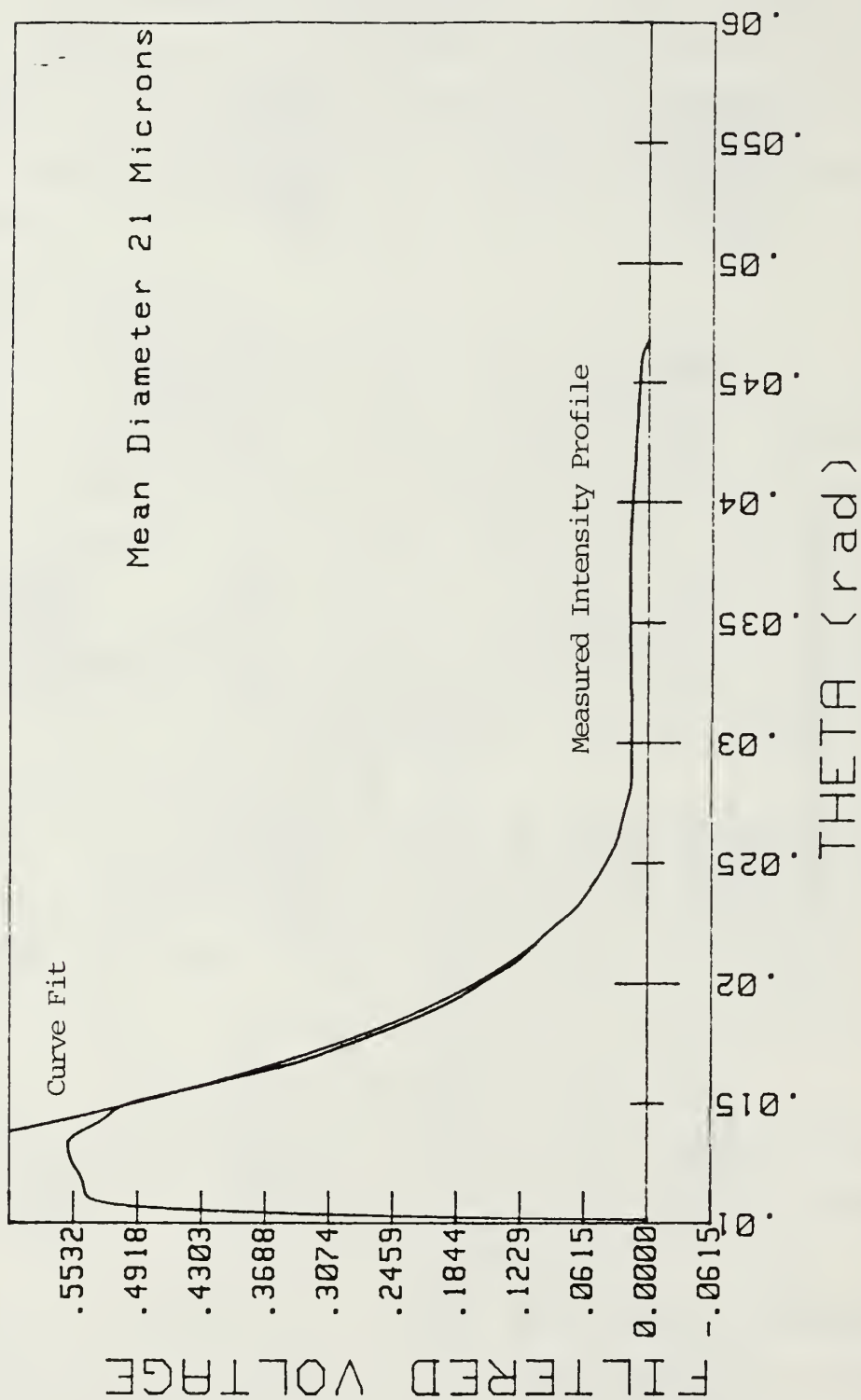


Figure 4.1 Calibration Profile for a Polydispersed Sample (14.9-24.4 Microns)



# CURVE FIT RESULTS INTENSITY vs. THETA

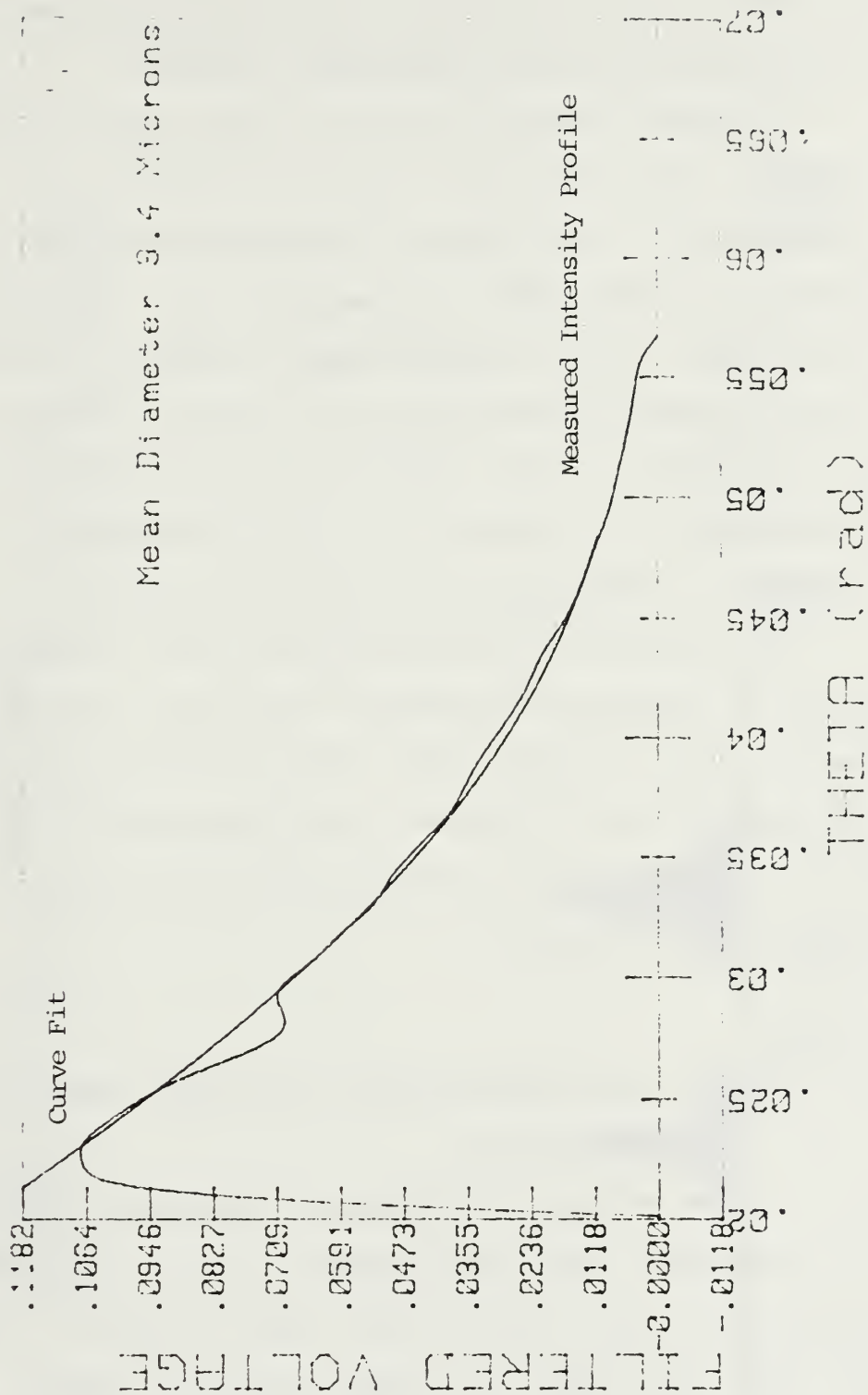


Figure 4.2 Calibration Profile for a Polydispersed Sample (8.5-10.4 Microns)

prior to introducing particles. A glass rod was used to stir the mixture to ensure that the particulates remained in suspension during the measurement process.

A primary concern early in the investigation was to validate the ability of the MALVERN to accurately characterize a multimodal distribution when the system was operated in the Model Independent mode. In order to test this facet of the Master-Sizer program, a polydispersed bimodal sample consisting of 5.1 and 20.0 micron particles was prepared. The results are depicted as a volume distribution in Figure 4.3. The respective modes are centered at approximately 5.5 and 21.0 microns.

When multiple scattering becomes significant, the mean particle diameters determined from single scattering theory are too small. Gulder [Ref. 28] has determined empirical corrections for the Malvern when obscuration is greater than 0.5. This correction was utilized, when required, in the present investigation.

## C. RESULTS FROM REDUCED SMOKE PROPELLANT EVALUATION

### 1. Test Conditions

The series of experiments conducted covered a range of pressures from approximately 70 to 450 psig. The experiments were divided into three pressure classes, 150, 250 and 400 psig. At each class of chamber pressure,

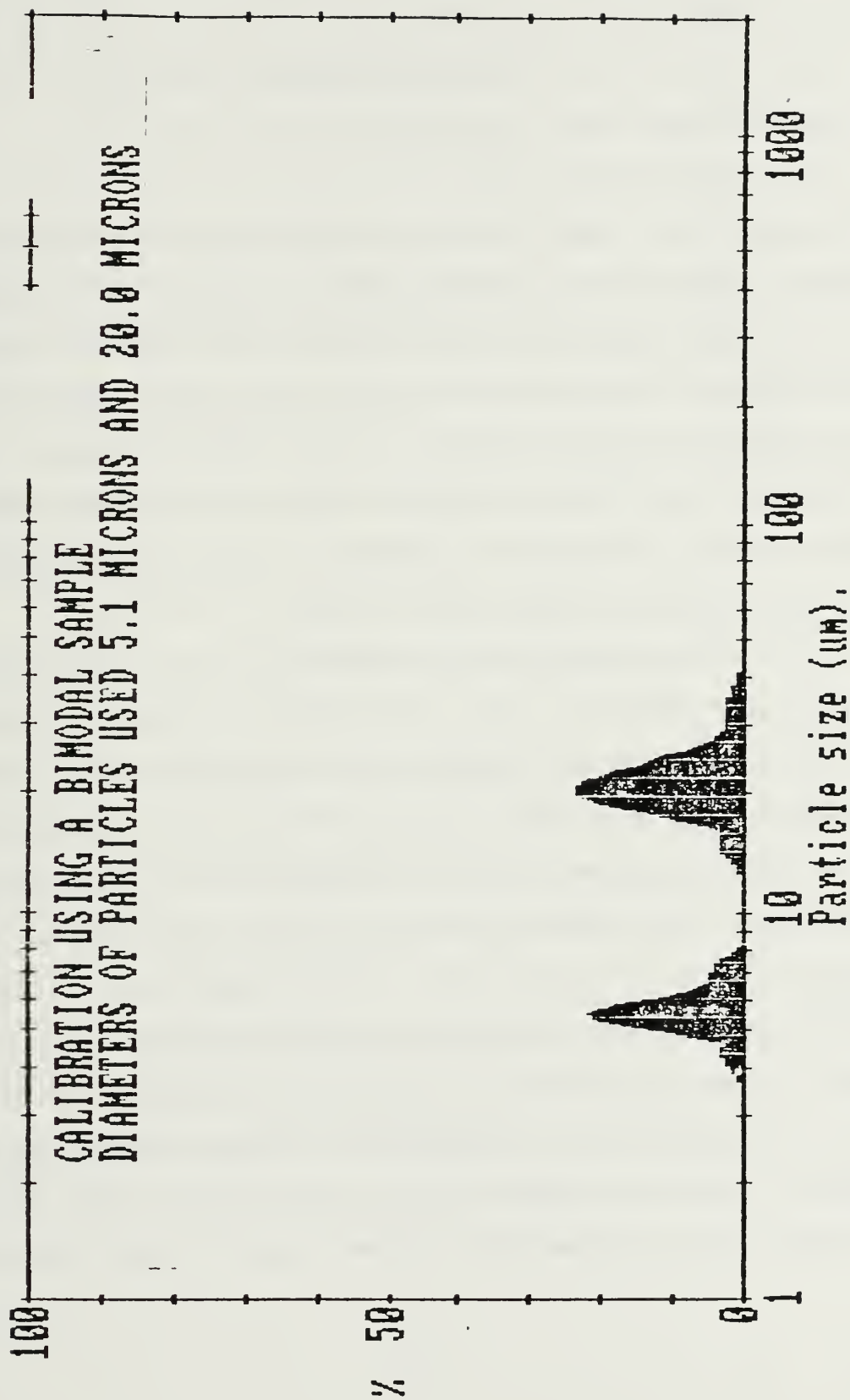


Figure 4.3 Volume Distribution, Bimodal Calibration Sample

scattering measurements were made at the following locations:

- (a) near grain (end burning)
- (b) prior to the nozzle entrance
- (c) exhaust ( $P_e = P_{\text{critical}}$ )
- (d) exhaust ( $P_e = P_o$ ).

A total of 32 tests were completed, 24 of which produced usable data. Three tests failed to produce data because the burst disk ruptured, three tests of the short motor were invalidated because the nitrogen purge system failed to keep the window surfaces clean, one test failed because of an O-ring failure in the motor joint, and for one test, data were not obtained because the pressure threshold to trigger the acquisition of data was set too high.

The nozzles were designed/sized for isentropic flow conditions using  $\gamma = 1.2$ . The ratio of specific heats was determined using PEPCODE, an equilibrium, adiabatic combustion code. The value of gamma obtained in this manner was 1.21. Because nozzle efficiencies should be quite high (97-99%), the isentropic assumption was made. Deviations in pressures can be attributed to the variations in ignition characteristics and propellant properties from run to run, and some small amount of nozzle throat erosion.

The propellant composition was provided by the Naval Weapons Center at China Lake, California. The zirconium carbide in the propellant varied in size from 2-20 microns,

with a  $D_{32}$  of 5.1 microns. The information is provided here as an introduction to the discussion of surface agglomeration on the burning grain.

## 2. Zirconium Carbide Behavior

The size of agglomerates that form on the surface of burning metallized solid propellants are determined by many factors, including metallic powder type, propellant type, size of original metal particulates, concentration of metal, motor chamber pressure, and the burning rate of the propellant. The effect of chamber pressure on agglomerate size has been observed to be quite strong for aluminum. As chamber pressure and burning rate increase, the agglomerates become smaller [Refs. 21,22].

Zirconium carbide has been observed to burn vigorously on the surface of reduced smoke propellants containing AP and HTPB [Ref. 23]. If zirconium carbide (ZrC) burns stoichiometrically with oxygen it results in a temperature of approximately 4400°K. This resultant temperature is much greater than the melting temperature of  $ZrO_2$  (2988°K). Table 4.2 delineates the temperatures relevant to the discussion.

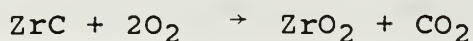
A plausible behavior of the ZrC is that as the material is exposed at the grain burning surface, oxygen ( $O_2$ ) from the ammonium perchlorate (AP) flame attacks the carbon to produce either carbon monoxide (CO) or carbon dioxide ( $CO_2$ ). Oxygen from water vapor may also be



TABLE 4.2  
THERMOPHYSICAL PROPERTIES OF Zr, ZrC, AND ZrO<sub>2</sub>

<u>Material</u>	<u>Melting Temperature (°K)</u>	<u>Boiling Temperature (°K)</u>
Zr	2127 [Ref. 24]	4700 [Ref. 24]
ZrC	3523 [Ref. 26]	-
ZrO <sub>2</sub>	2988 [Ref. 24]	4573 [Ref. 25]

NOTE: Adiabatic flame temperature for the propellant was determined to be 2916°K and the adiabatic flame temperature for the reaction



is approximately 4400°K.

involved. The oxygen then reacts with the zirconium to produce a porous ZrO<sub>2</sub> surface layer [Ref. 24]. The oxide should be a liquid since the local temperature at the particle surface (as a result of the surface combustion of ZrC or Zr with O<sub>2</sub>) should be much greater than the melting temperature of ZrO<sub>2</sub> (2988°K). The low burning rate associated with the relatively low chamber pressures allows time for the molten ZrO<sub>2</sub> on adjacent particles to stick together to form large agglomerates on the grain burning surface, prior to passing into the flow. At higher burning rates (pressures) the particles would be ejected from the surface more rapidly, resulting in smaller agglomerates.

### 3. Near-Propellant Surface Data

The test results obtained near the grain surface are summarized in Table 4.3.  $D_{32}$  values are plotted in Figure 4.4. As can be seen directly from these results, there was a strong dependence on chamber pressure of the agglomerate size produced from the ZrC. At the lower pressures (159 and 188 psig), the distribution of particulates ejected from the grain surface were trimodal and bimodal, respectively. Figures 4.5 and 4.6 detail the characterization of the particulate distributions. The dominant modes were centered at approximately 30-37 microns and 65 microns.

The Sauter mean diameters determined from the scattering data were 63.5 microns for the run at 159 psig and 72.8 microns for the run at 188 psig. This was considered to be good repeatability, run-to-run, allowing for variations in the combustion process from grain to grain. As discussed above, many of the ZrC particles, upon reaching the burning surface, apparently react to form  $ZrO_2$  and agglomerate before being ejected into the gas flow.

Test number three of the near grain results (248 psig) showed a reduction in Sauter mean diameter, with a measured  $D_{32}$  of 32.2 microns. The distribution of particulates at this pressure was still essentially bimodal as depicted by Figure 4.7. However, the dominant modes of the distribution were now centered at approximately 12-13 microns and 27 microns. There was also a small number of

TABLE 4.3

## NEAR GRAIN SURFACE SCATTERING MEASUREMENT RESULTS

<u>Test No.</u>	<u>Wt % Metal</u>	<u>Data Obtained at Measured Pressure (psig)</u>	<u>Max Pressure (psig)</u>	<u>Burn Time (sec)</u>	<u>Throat Diam, m</u>	<u>D<sub>32</sub> (microns)</u>
1	1.0 ZrC	159	170	6.2	.200	63.5
2	1.0 ZrC	188	192	5.8	.200	72.8
3	1.0 ZrC	248	254	5.3	.177	32.2
4	1.0 ZrC	448	450	1.3	.150	15.2

NOTE: (1) All measurements represent MALVERN data.

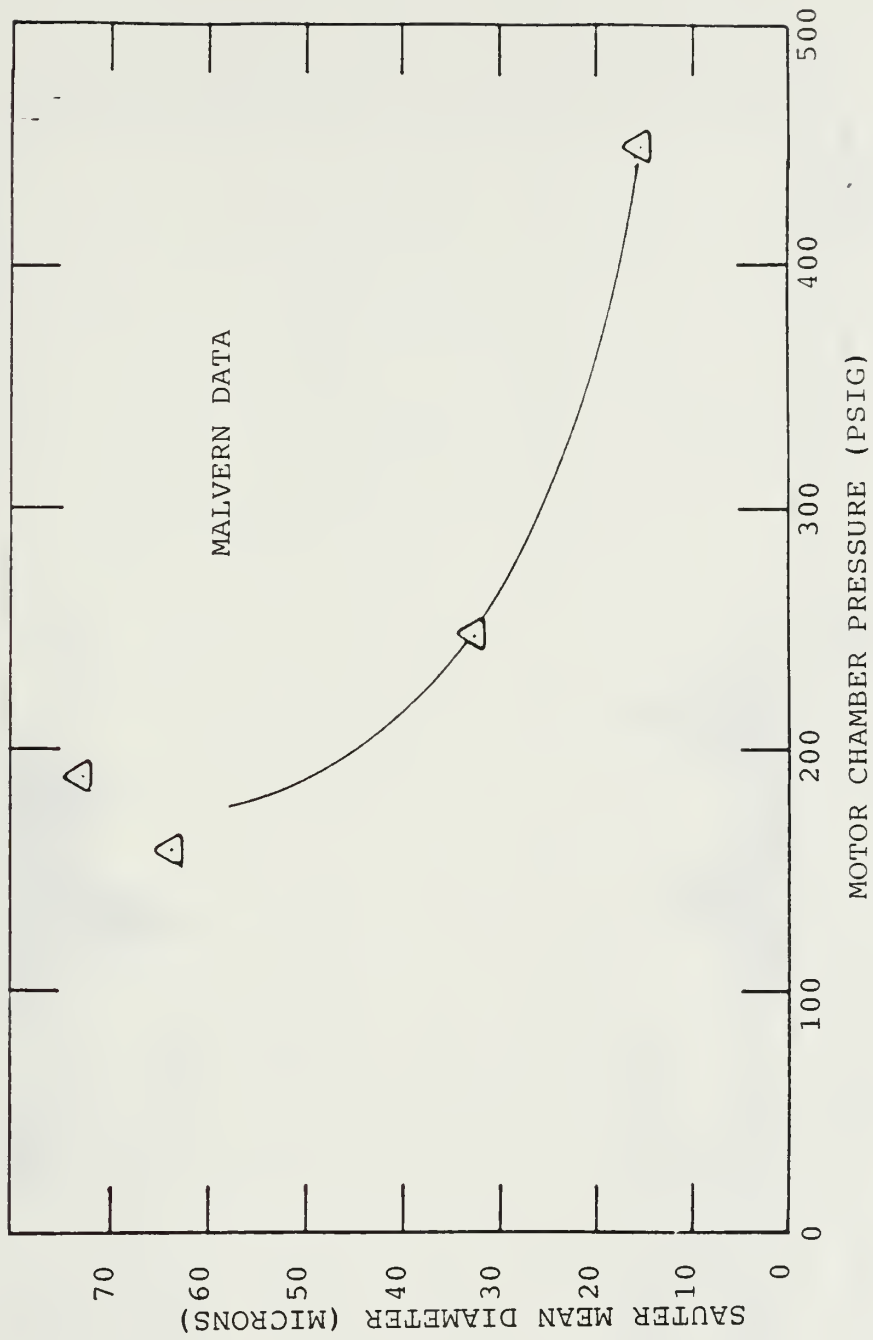


Figure 4.4 Near Grain Scattering Measurement Results

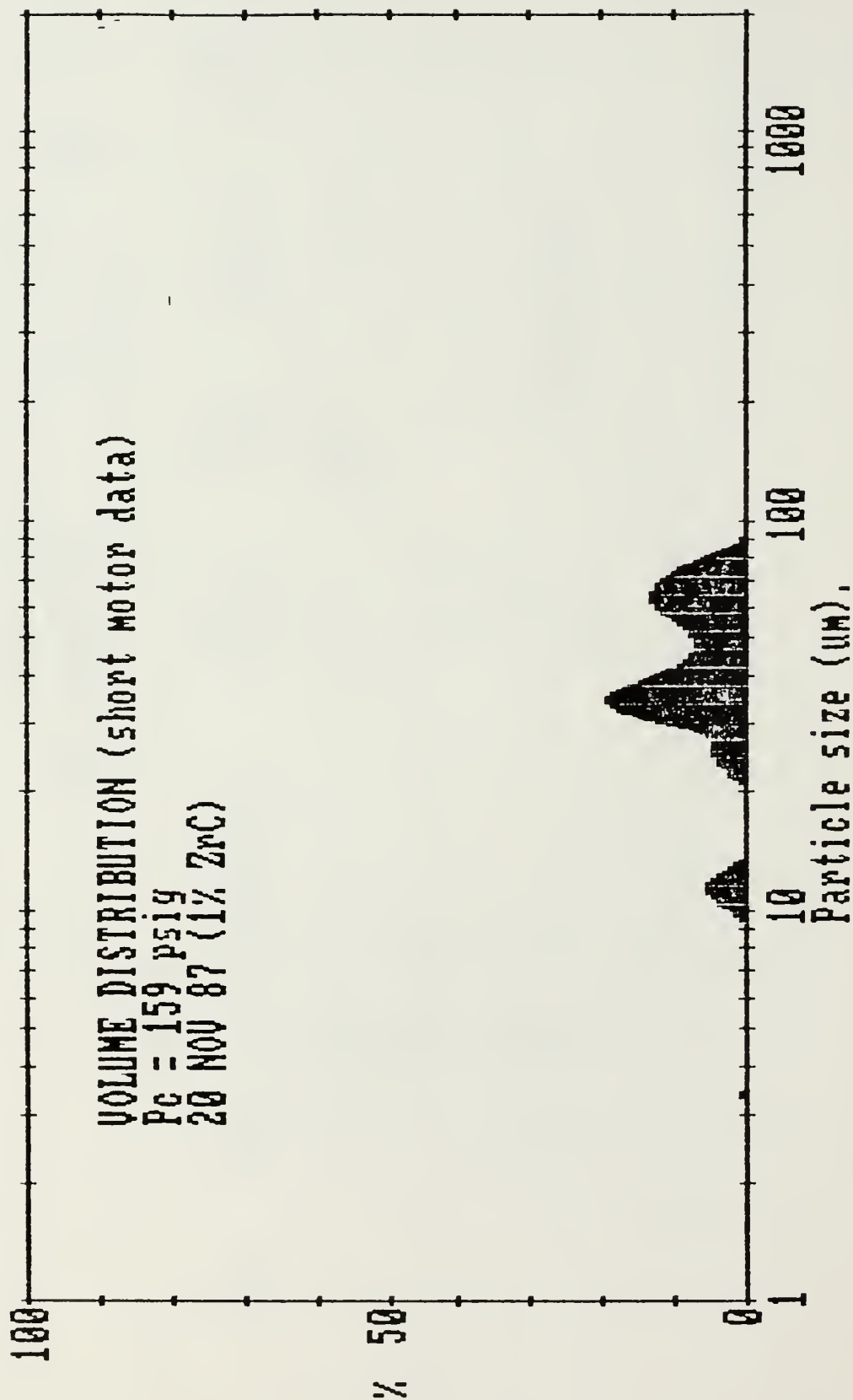


Figure 4.5 Volume Distribution Near Grain Test No. 1 (159 psig)



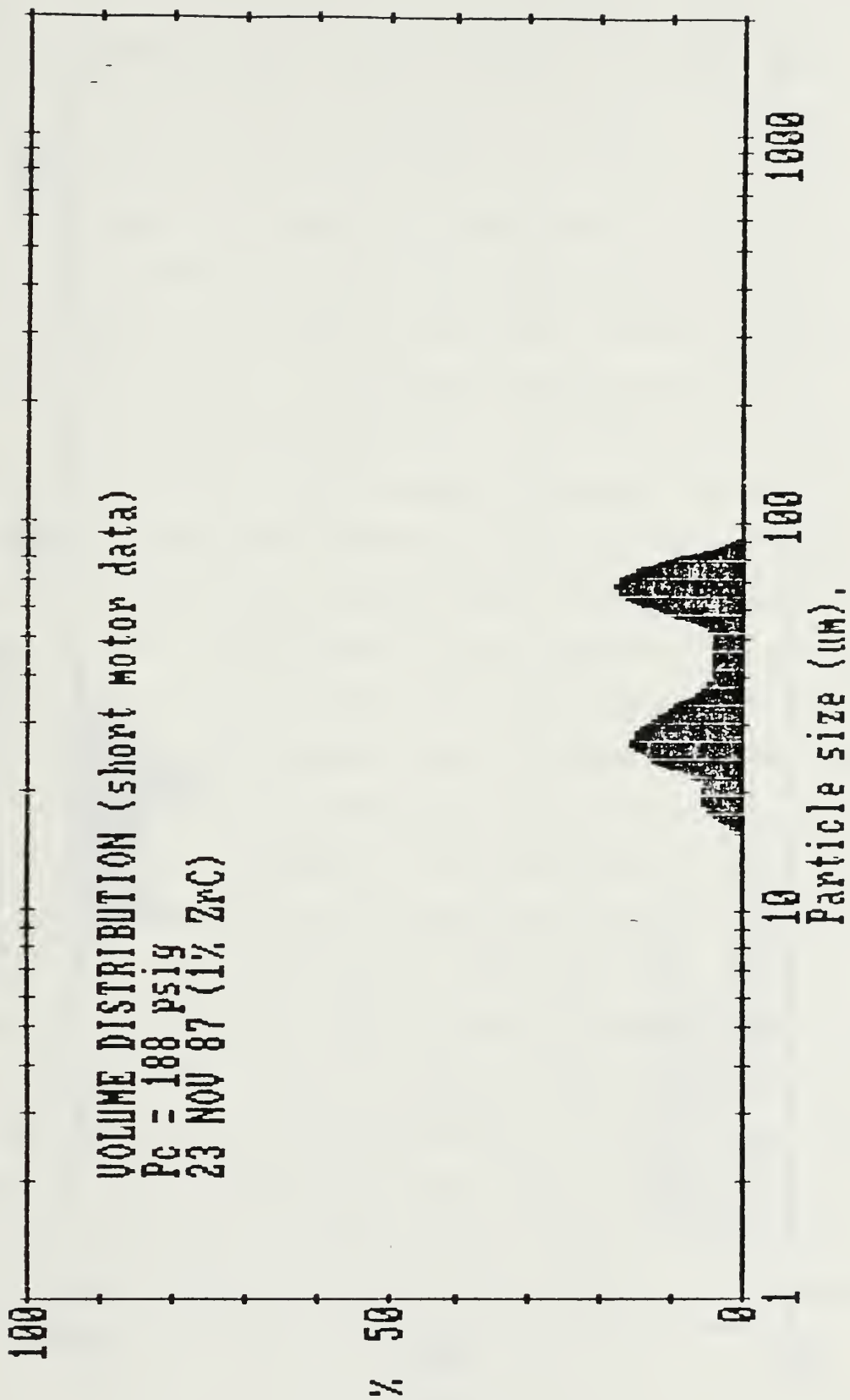


Figure 4.6 Volume Distribution, Near Grain Test No. 2 (188 psig)

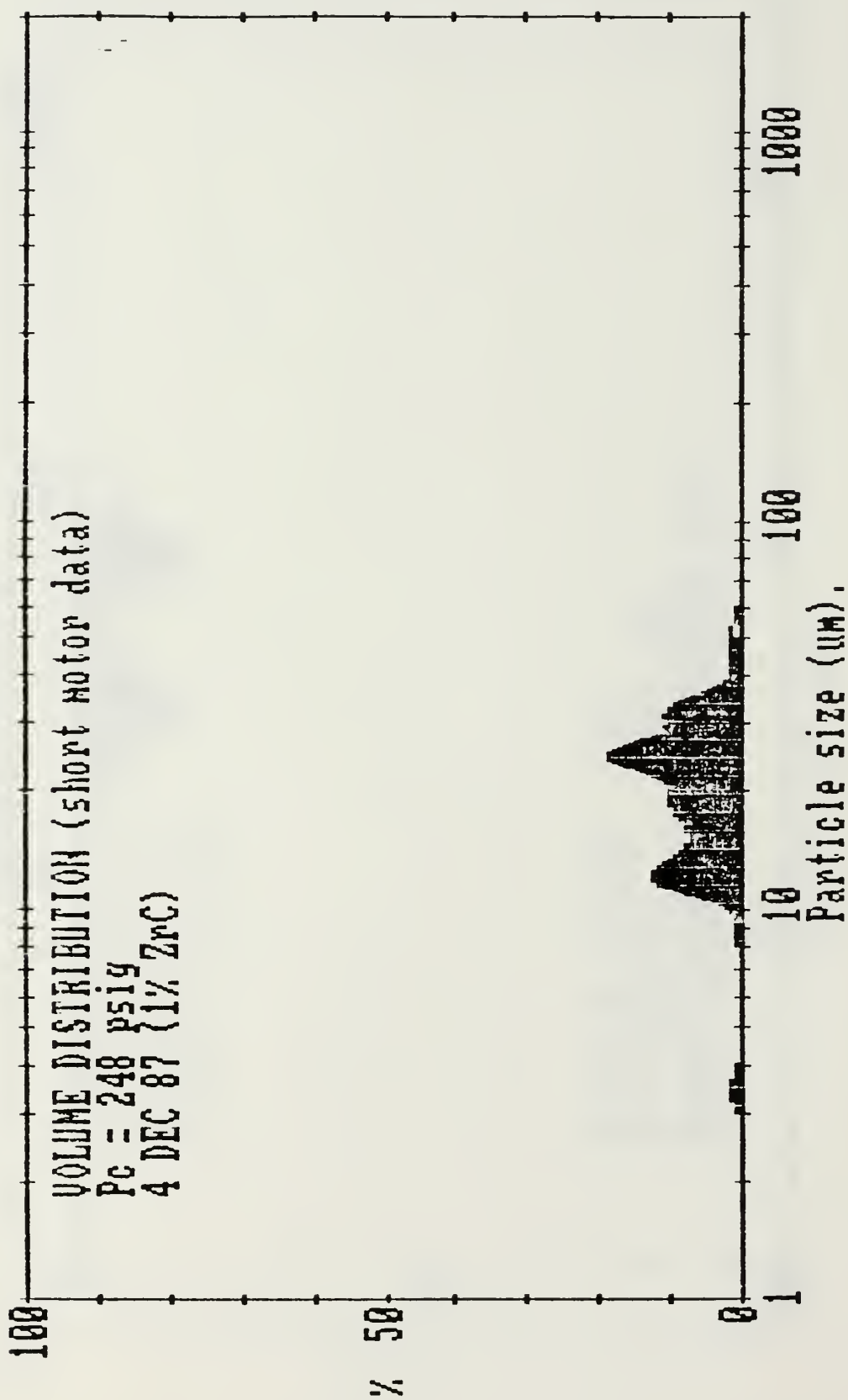


Figure 4.7 Volume Distribution, Near Grain Test No. 3 (248 psig)

particulates in the range of 3-4 microns, indicating that some of the particulates at this pressure (248 psig) were ejected directly into the gas stream. The 448 psig test resulted in a  $D_{32}$  of 15.2 microns. Figure 4.8 reveals that the distribution of particulates continued to be bimodal. It is apparent from Figure 4.8 that a much larger portion of the original metal (ZrC) particles was ejected directly into the gas flow, as evidenced by the well-defined mode centered between 3-4 microns. The general observation here was that as motor chamber pressure was increased, the size of agglomerates on the grain surface decreased, similar to the behavior of aluminized propellants reported in References 21 and 22. It was also observed that a greater number of the original ZrC particulates were apparently immediately ejected into the gas flow as they reached the burning surface as chamber pressure was increased. In all cases, the distributions of particulates near the burning surface were bimodal or trimodal. The quantities of particles in the smallest modes of the trimodal data were quite small.

The most difficult obstacles to overcome in obtaining near grain light scattering measurements were: (1) keeping the window surfaces clean, as the ignition process (due to its close proximity to the windows) made it difficult to effectively purge these surfaces, and (2) multiple scattering effects due to dense concentrations of particulate matter in the near grain region. The problem of

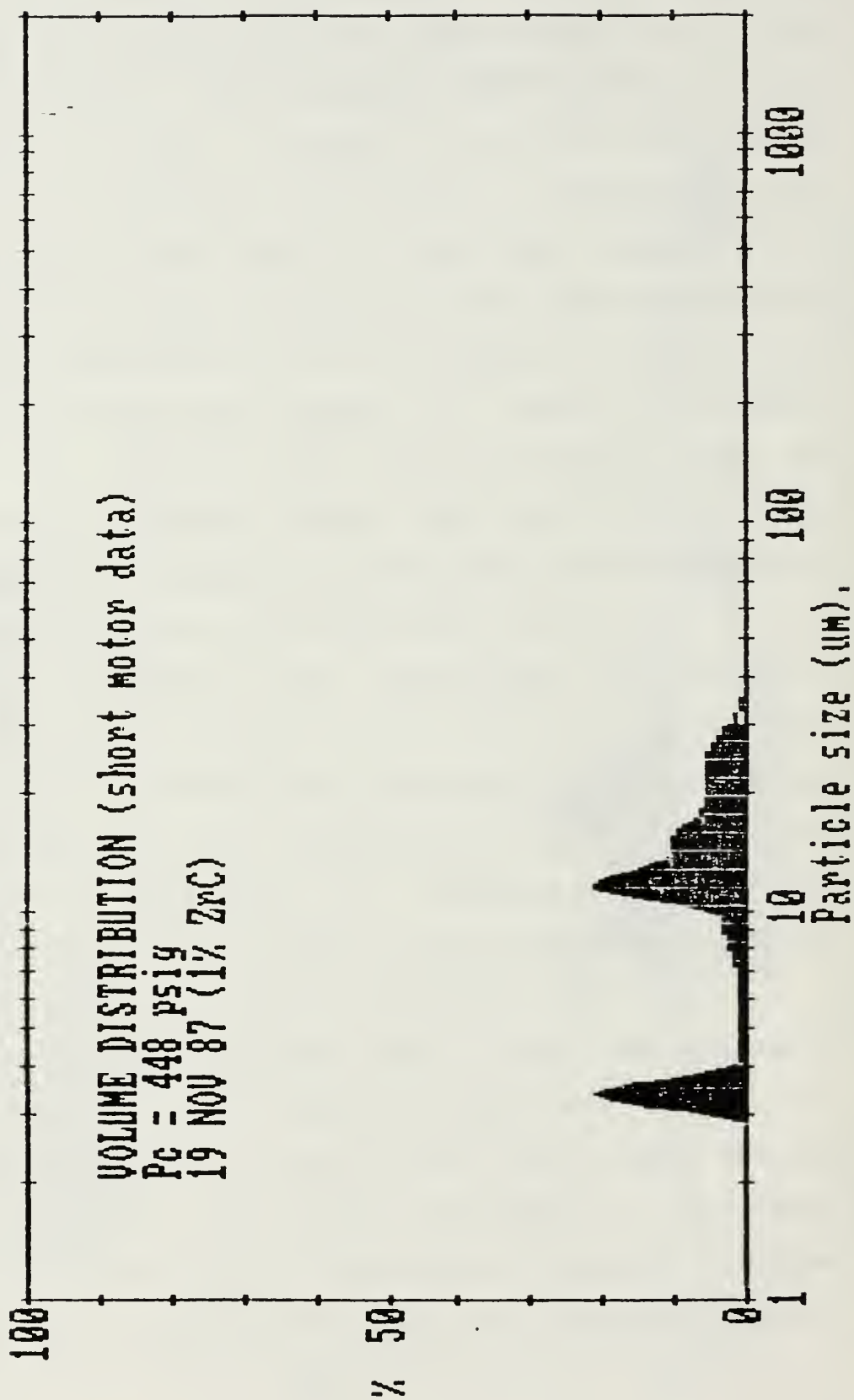


Figure 4.8 Volume Distribution Near Grain Test No. 4 (448 psig)

multiple scattering has been addressed above. The empirical corrections presented by Gulder [Ref. 28 ] are for a Malvern system operated in the model independent mode. This mode was also used in the current investigation. When obscuration is approximately 0.99, the measured  $D_{32}$  is approximately a factor of two too small. Gomi [Ref. 27 ] has also discussed the effects of multiple scattering. For monodispersed spheres Netzer and Powers [Ref. 1 ] have also presented data for correcting  $D_{32}$  for high obscurations.

The more difficult problem that had to be overcome in the near grain region was effectively purging the window surfaces. The only alternative here was to repeat the experiment until usable data were obtained. As noted earlier, three of the tests conducted in the near grain region were invalidated due to the fact that the window surfaces had become contaminated as a result of the ignition process.

#### 4. Nozzle Entrance Data

Table 4.4 presents the results from the measurements obtained prior to the nozzle entrance. These data allow one to examine the change in particle size across the nozzle when compared to the exhaust data which are contained in Tables 4.5 and 4.6. The  $D_{32}$  data obtained using the MALVERN are also plotted in Figure 4.16. Figure 4.17 plots these same data together with the MALVERN data obtained near the



TABLE 4.4

MOTOR CHAMBER SCATTERING MEASUREMENTS OBTAINED UPSTREAM  
FROM NOZZLE CONVERGING SECTION

Test No.	Wt % Metal	Data Obtained At Measured Pressure (psig)	Max Pressure (psig)	Burn Time (sec)	t <sub>res</sub> (msec)	D <sub>32</sub> (microns)
1*	1.0 ZrC	119	130	6.5	43	88.3
2*	1.0 ZrC	124	139	7.2	49	81.1
3	1.0 ZrC	161	173	6.0	52	30.7
4**	1.0 ZrC	175	185	7.9	74	24.0
5**	1.0 ZrC	125	138	7.2	49	29.0
6**	1.0 ZrC	135	141	6.7	49	30.0
7**	1.0 ZrC	79	85	10.2	47	38.0
8	1.0 ZrC	252	255	5.7	74	49.0
9	1.0 ZrC	251	263	6.1	79	48.0
10	1.0 ZrC	370	382	4.6	86	32.0
11	1.0 ZrC	427	429	5.4	117	27.6
12**	1.0 ZrC	300	331	6.0	93	19.0
13**	1.0 ZrC	352	388	5.8	104	18.0

\* Denotes data obtained by Pruitt [Ref. 17].

\*\* Denotes data obtained from NPS laser diffraction system; all other data were obtained using the MALVERN 2600.

burning surface. Figures 4.9, 4.10 and 4.11 characterize the volume distributions associated with the 150 psig class of experiments. Note in Figures 4.9 and 4.10 that the distributions remained bimodal in nature, with the dominant modes being centered at approximately 35 and 68-70 microns in the case of Figure 4.9 and at approximately 27 and again at 68-70 microns in the case of Figure 4.10. In the case of Figure 4.11, note that the profile was trimodal, but shifted toward the smaller end, with dominant modes centered at approximately 3-4 microns, 20 microns and at 38-40 microns. The Sauter mean diameter obtained from the scattering data was 30.7 microns (Test No. 3). A post-test alignment check done with the MALVERN system in the align mode revealed that some significant window contamination had occurred, but physical examination of the windows showed very little evidence of contamination. The results of this one test, although questionable, are included for completeness. Comparison of the Sauter mean diameters and volume distribution profiles for near grain and nozzle entrance measurements completed for the 150 psig class reveal only slight differences. This occurred even though the residence time ( $t_{res}$ ) was approximately 45 milliseconds.

As discussed above the equilibrium adiabatic flame temperature was 2916°K. The actual temperature may have been somewhat less than this due primarily to heat loss through the uninsulated, stainless steel walls of the

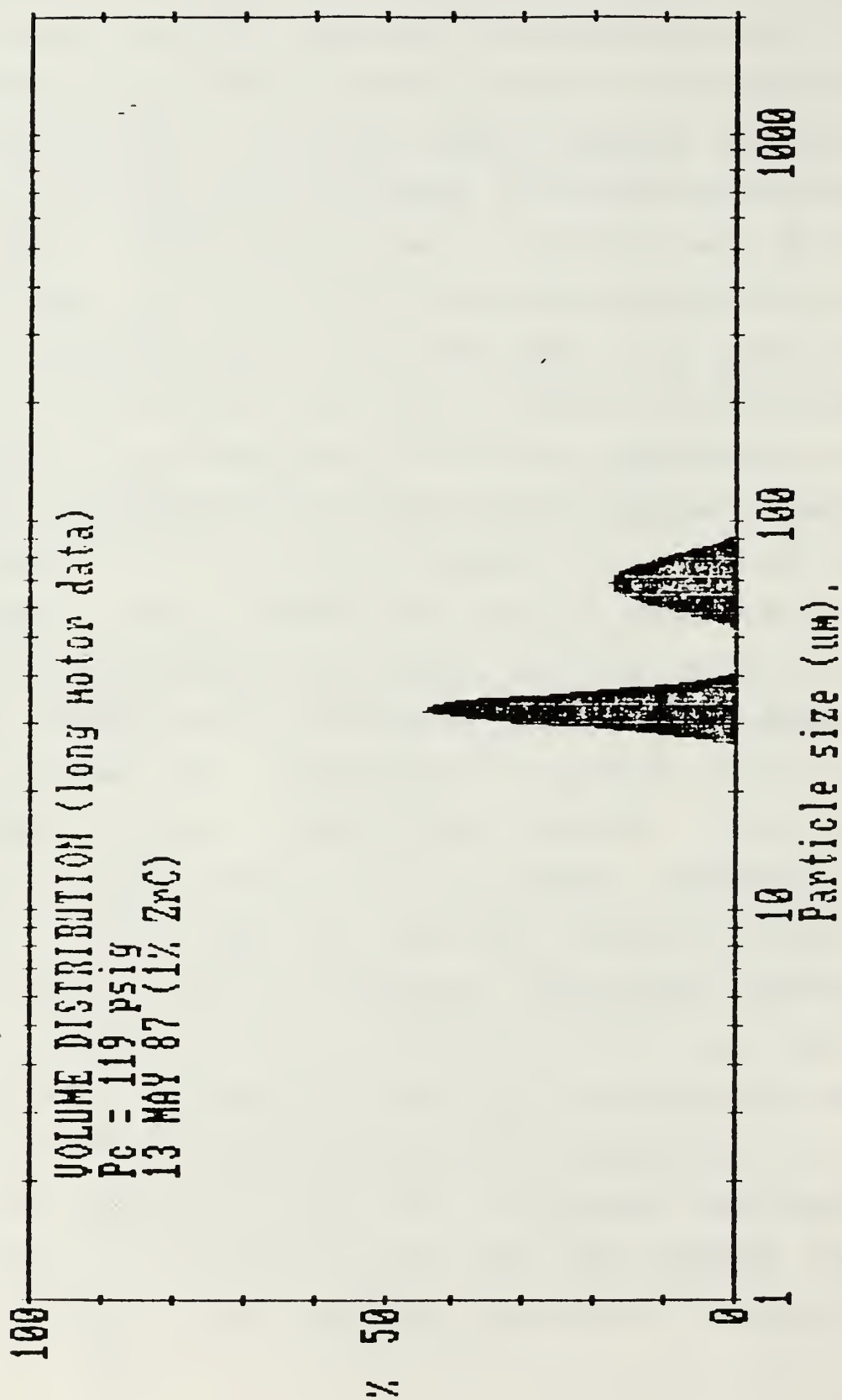


Figure 4.9 Volume Distribution Nozzle Entrance Test No. 1 (119 psig)

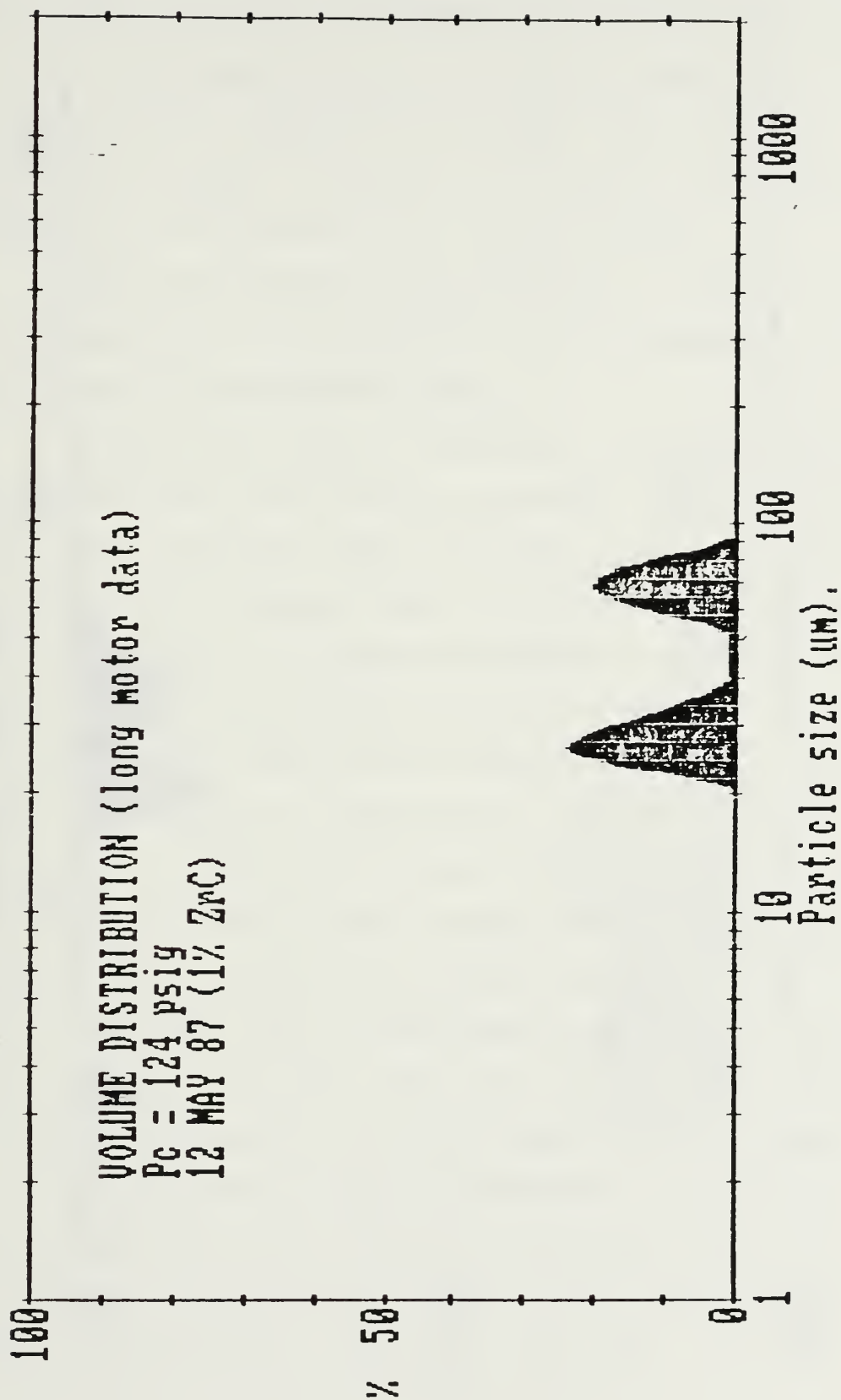


Figure 4.10 Volume Distribution, Nozzle Entrance Test No. 2 (124 psig)

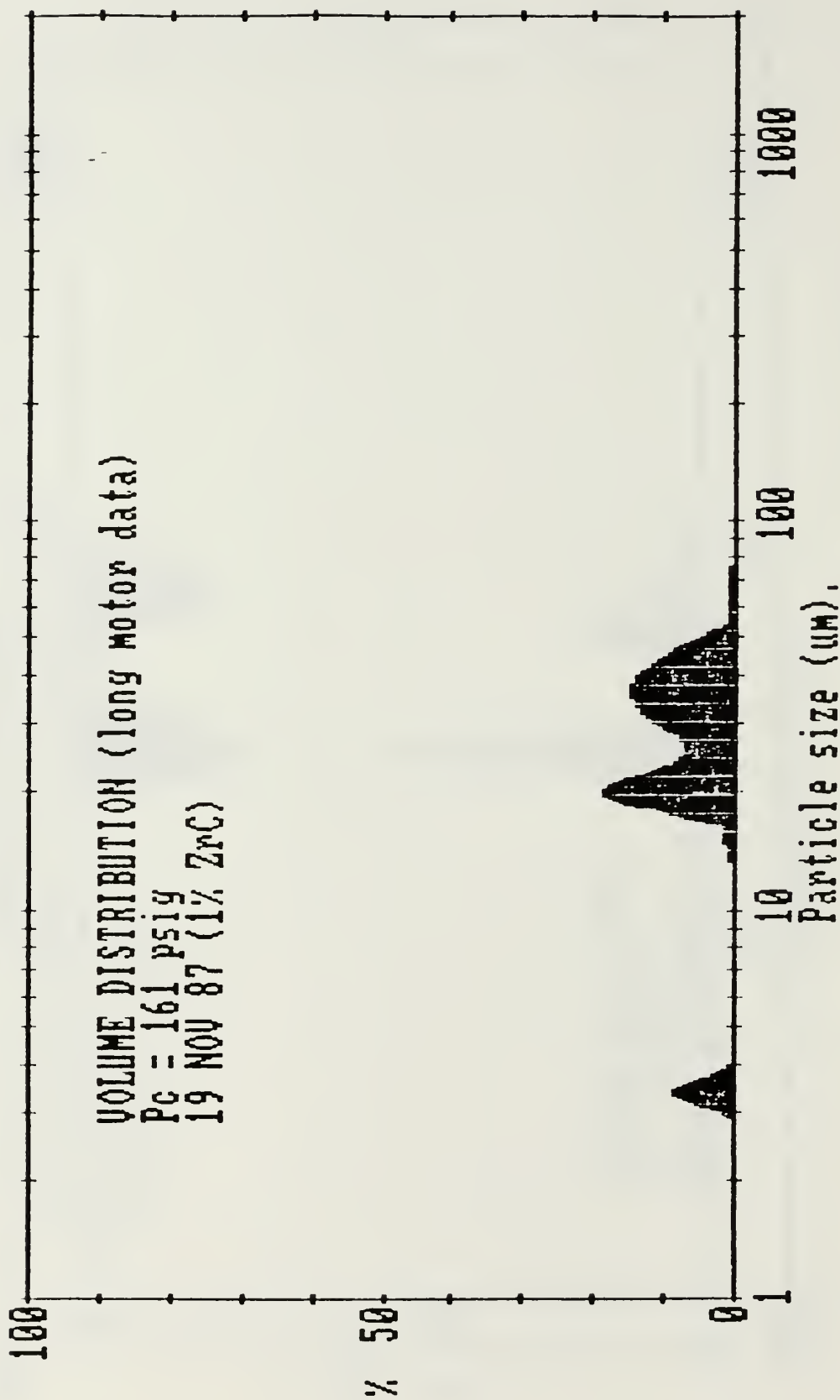


Figure 4.11 Volume Distribution, Nozzle Entrance Test No. 3 (161 psig)



combustor, and to the nitrogen gas used to purge the viewing windows. The observed particle behavior would be expected if the ZrC is completely consumed near (or on) the propellant surface, resulting in liquid  $\text{ZrO}_2$  particles flowing in a low velocity ( $M \ll .1$ ) environment.

The NPS scattering data included in Table 4.4 will be discussed later in conjunction with the comparison of the MALVERN and NPS measurement systems.

Figures 4.12 and 4.13 represent the volume distributions associated with the runs completed for the 250 psig class. This represents data for tests 8 and 9 of Table 4.4. The Sauter mean diameter (SMD) determined from scattering measurements was 49.0 microns corresponding to test number 8 and 48.0 microns associated with test number 9. This again represented good test-to-test repeatability. The dominant modes were centered at approximately the same locations for both tests. Comparison of these data with that obtained in the near grain surface region showed that there was approximately a 16 micron particle growth over the length of the motor. Note that only one measurement was taken in the near grain region. If the point was valid, then particle collisions and/or wall collisions/shedding may be suspected.

Test numbers 10 and 11 represent data obtained for the 400 psig class runs. The SMD's determined were 32.0 and 27.6 microns, respectively. Figures 4.14 and 4.15 are the volume distribution profiles for tests 10 and 11,

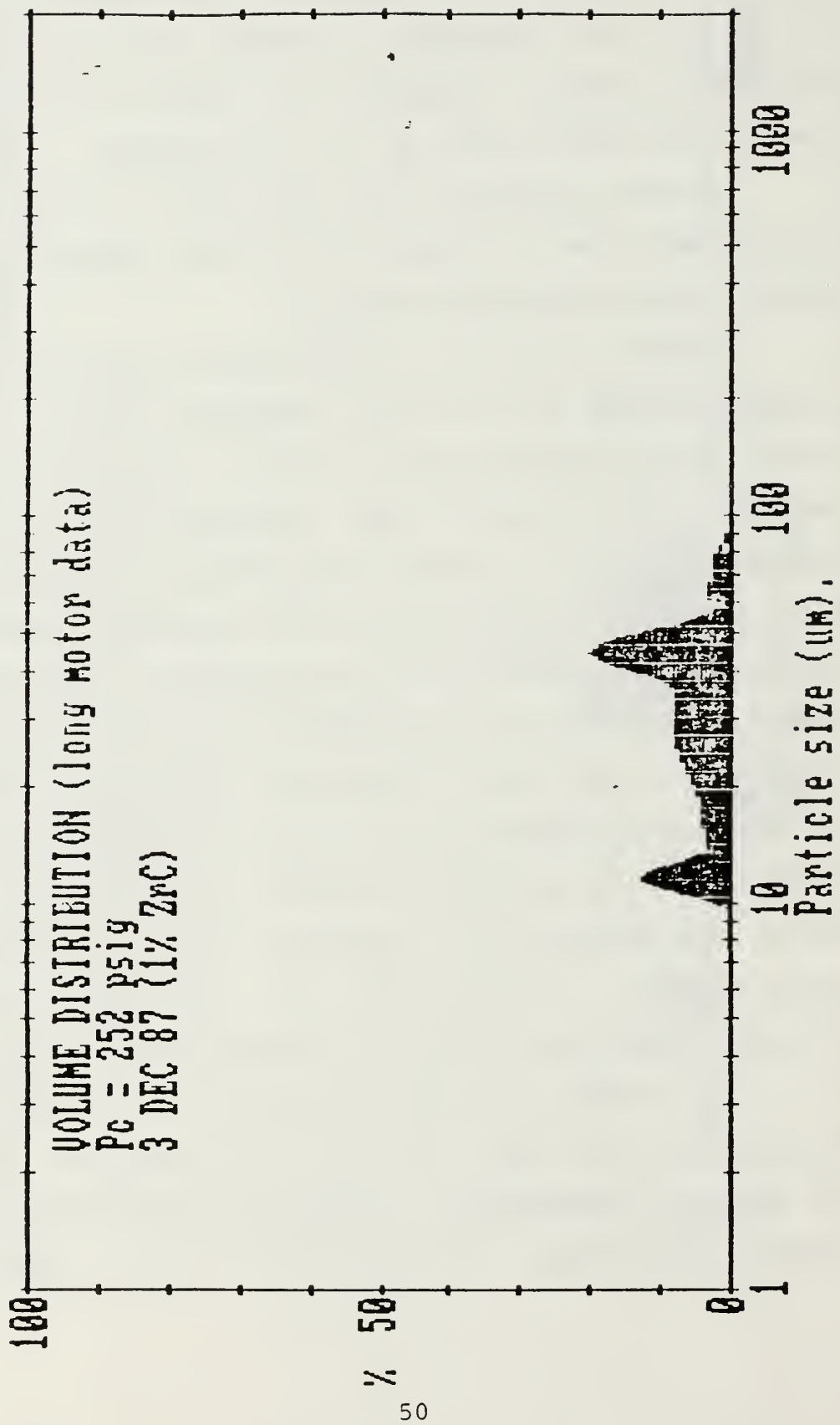


Figure 4.12 Volume Distribution, Nozzle Entrance Test No. 8 (252 psig)

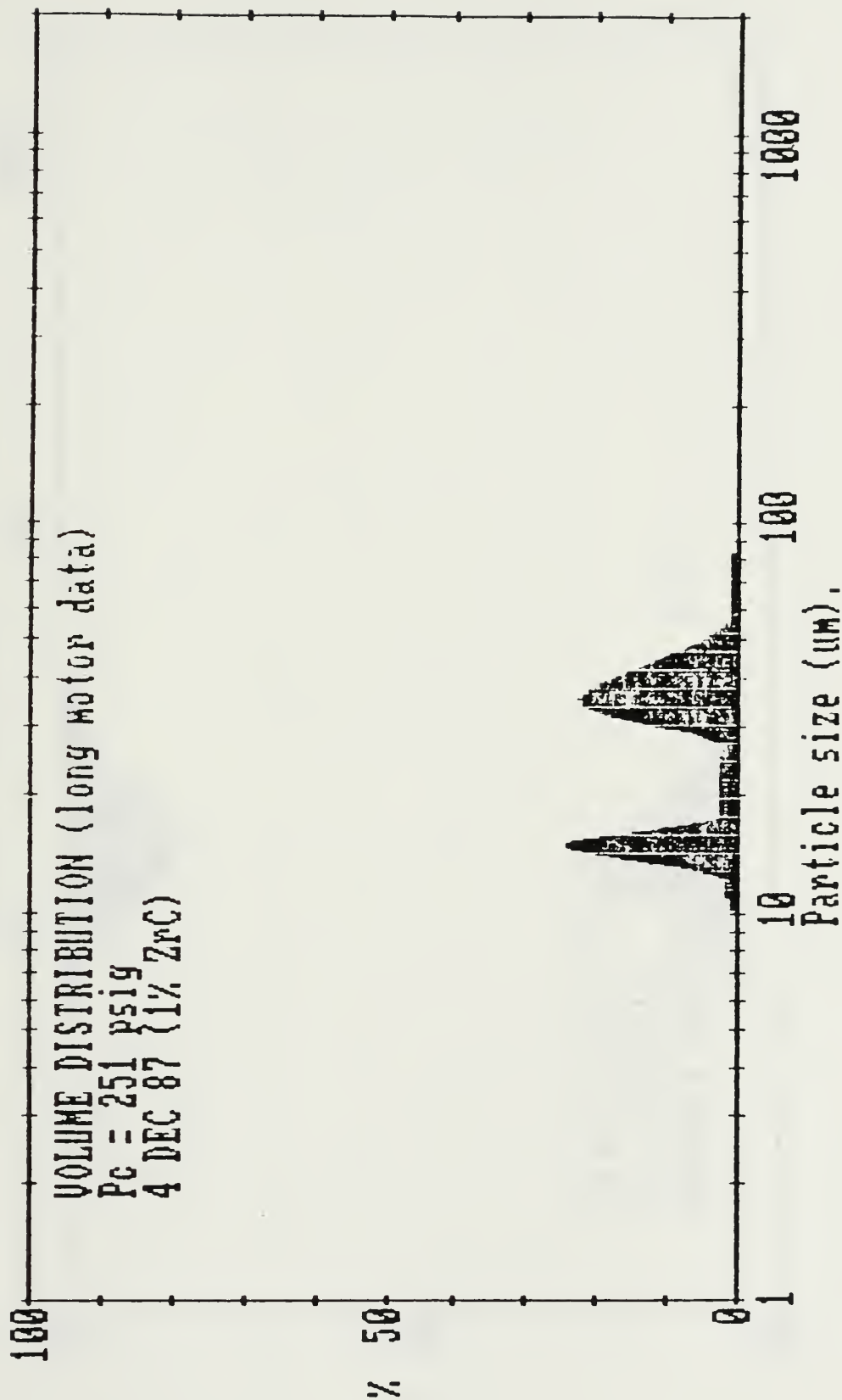


Figure 4.13 Volume Distribution, Nozzle Entrance Test No. 9 (251 psig)

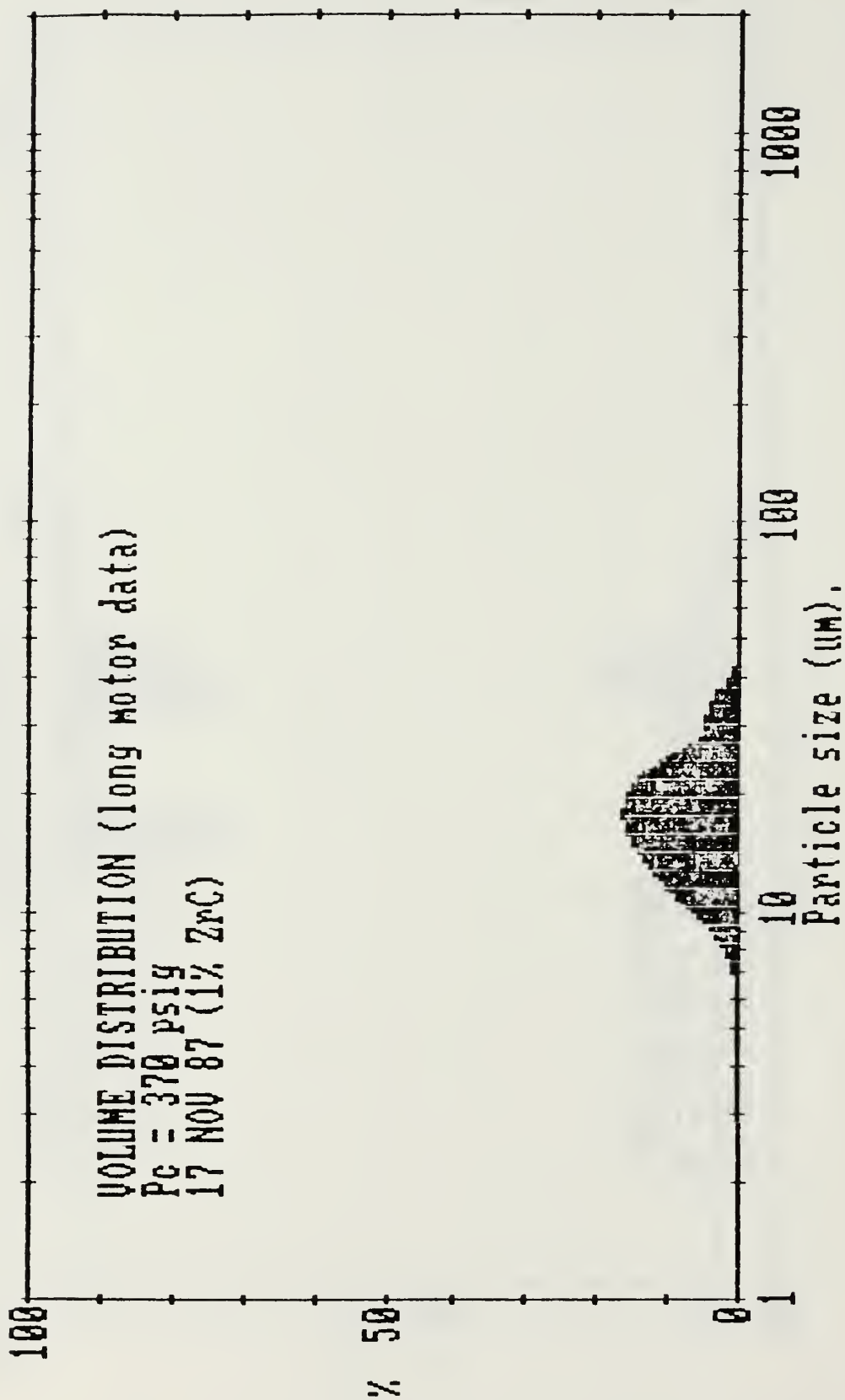


Figure 4.14 Volume Distribution, Nozzle Entrance Test No. 10 (370 psig)

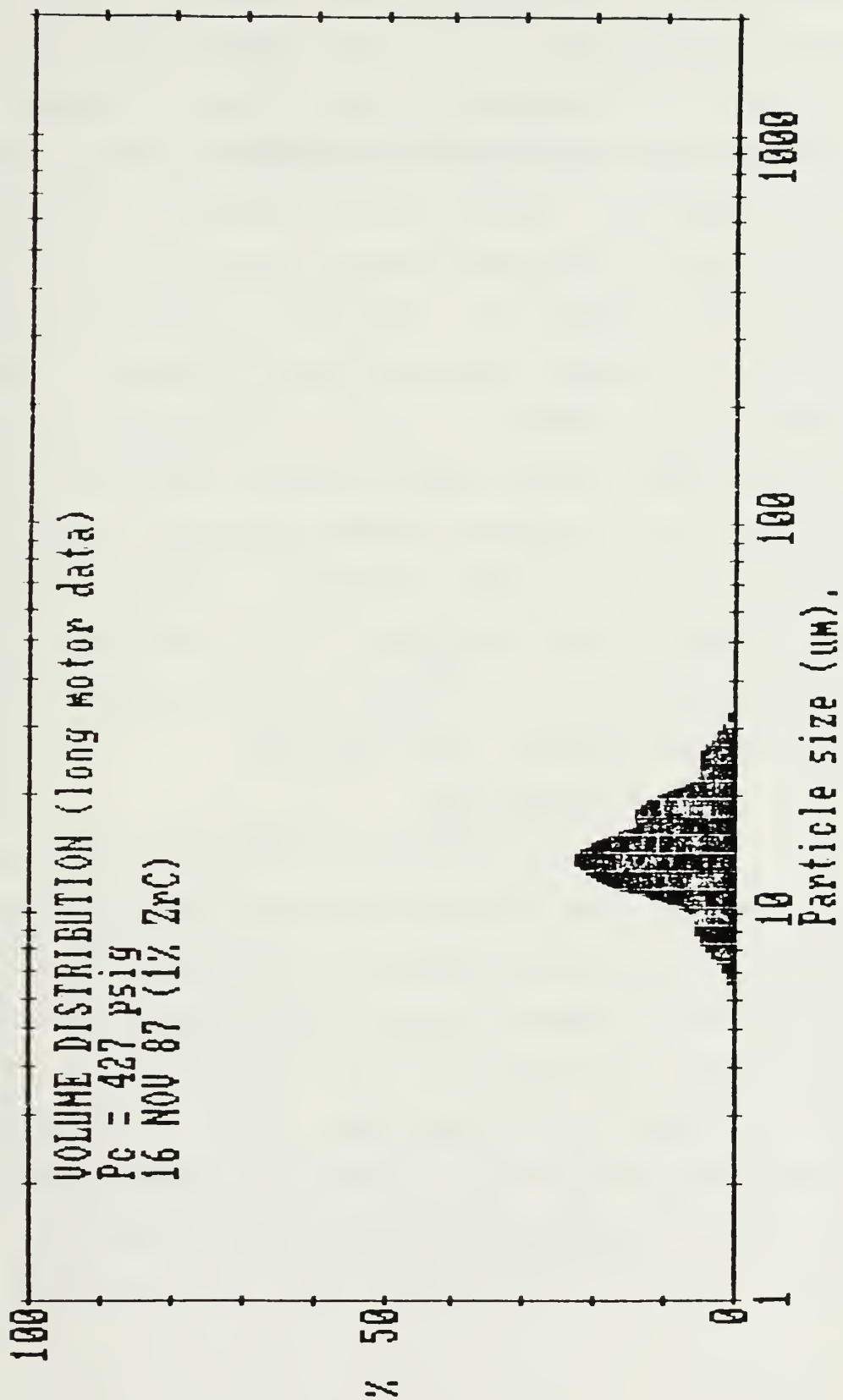


Figure 4.15 Volume Distribution, Nozzle Entrance Test No. 11 (427 psig)



respectively. Note that each was monomodal in nature. By comparing these profiles to those obtained near the grain surface, it was observed that the 3-4 micron diameter particles were eliminated as they passed along the length of the combustor. Again, if ZrC is assumed to react to  $\text{ZrO}_2$  on or near the propellant surface, particle collisions could explain this observation. There was an appreciable increase in particle diameter from near the grain surface to the nozzle entrance section. Figure 4.16 is a graphical depiction of SMD plotted against chamber pressure. Note that the SMD decreases with increasing chamber pressure. Figure 4.17 presents the data for both near-grain and nozzle-entrance measurements. From this figure, it is clear that particle growth/agglomeration occurred across the length of the combustor for pressures above 200 psi.

#### 5. Exhaust Nozzle Data

Table 4.5 is a listing of test results obtained in the exhaust for the condition of nozzle exit plane pressure equal to the critical pressure at the nozzle throat. The nozzles used in these tests had a  $45^\circ$  converging section and a short flat (.01"-.015") in the throat section. All nozzles were truncated at the throat after the .01"-.015" flat. Figures 4.18, 4.19, 4.20, 4.21 and 4.22 present the volume distributions associated with tests one through five, respectively. Figure 4.23 presents the results obtained on

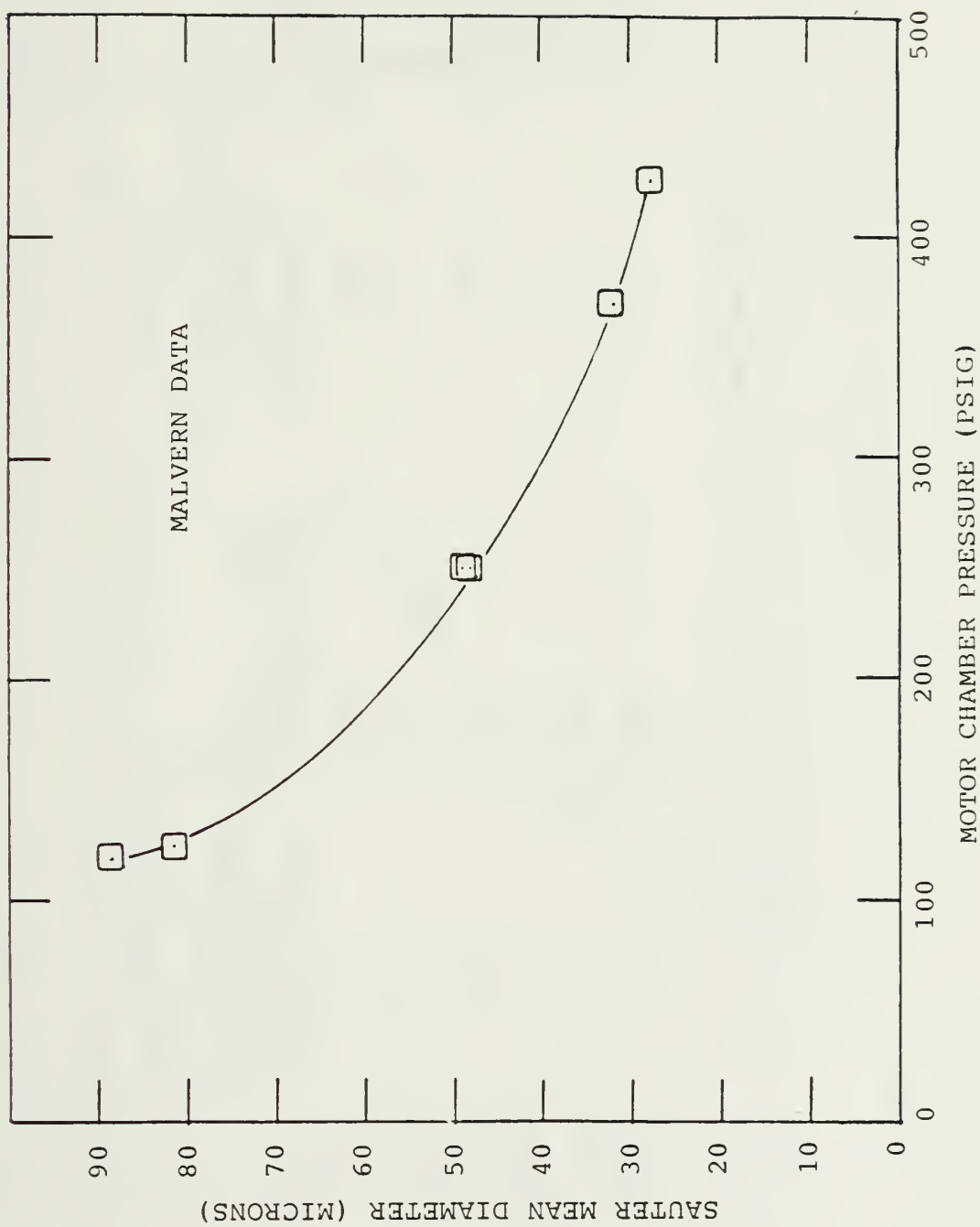


Figure 4.16 Nozzle Entrance Scattering Measurement Results

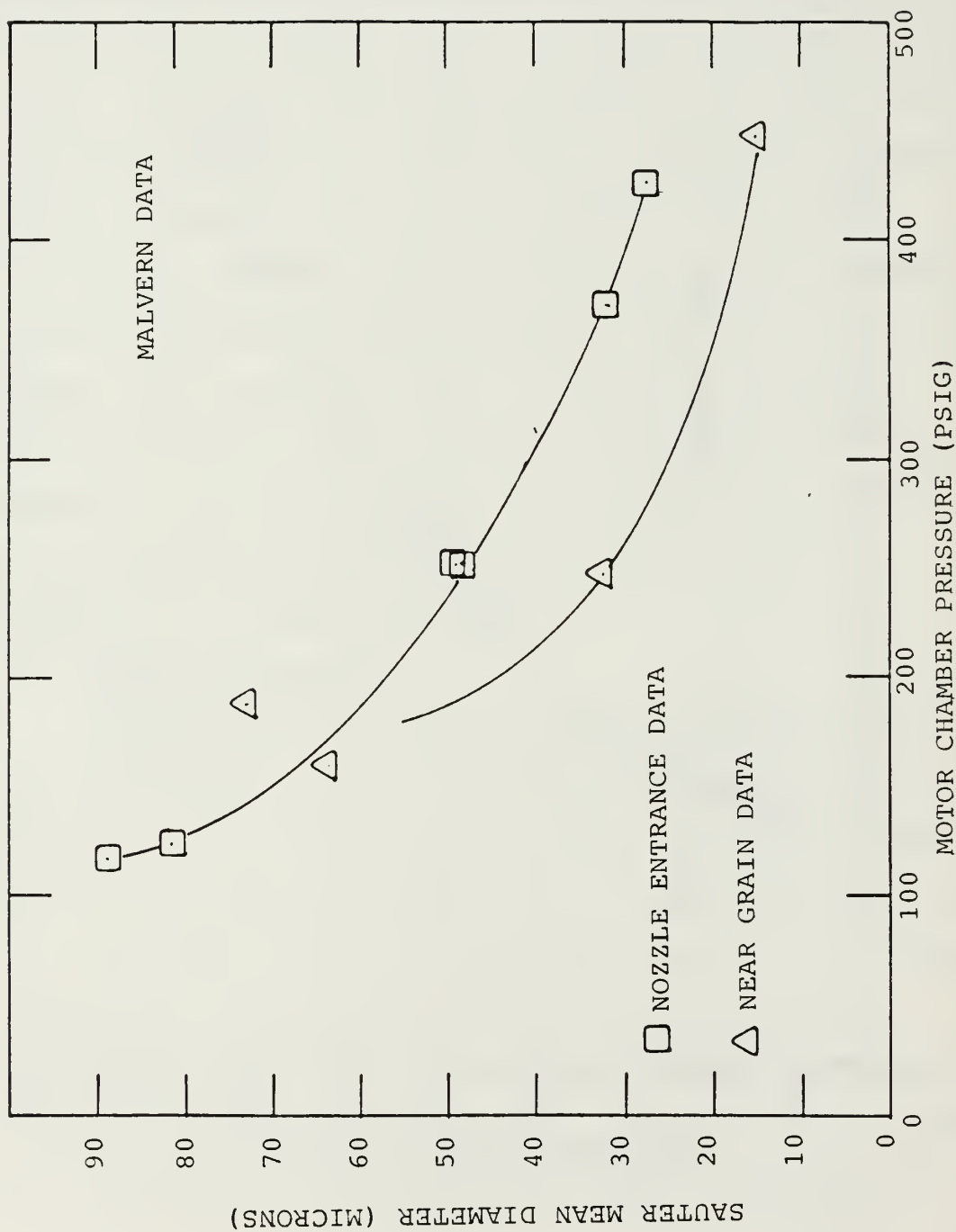


Figure 4.17 Comparative Results Near Grain and Nozzle Entrance Data

TABLE 4.5

EXHAUST SCATTERING MEASUREMENTS ( $P_e = P_{\text{critical}}$ )

Test No.	Wt % Metal	Data Obtained at Measured Pressure (psig)	Max Pressure (psig)	Burn Time (sec)	Measurement Location in (inches) Behind Exit Plane of Nozzle	D <sub>32</sub> (microns)
1	1.0 ZrC	147	153	7.1	1.08	8.1
2	1.0 ZrC	212	224	5.2	0.6	19.1
3	1.0 ZrC	450	452	3.4	1.08	14.8
4	1.0 ZrC	421	532	5.2	0.6	19.1
5	1.0 ZrC	371	376	5.3	0.6	19.1
6*	1.0 ZrC	370	382	4.6	2.7	16.0

\* Denotes data obtained from NPS laser diffraction system, all other data were obtained using the MALVERN 2600.

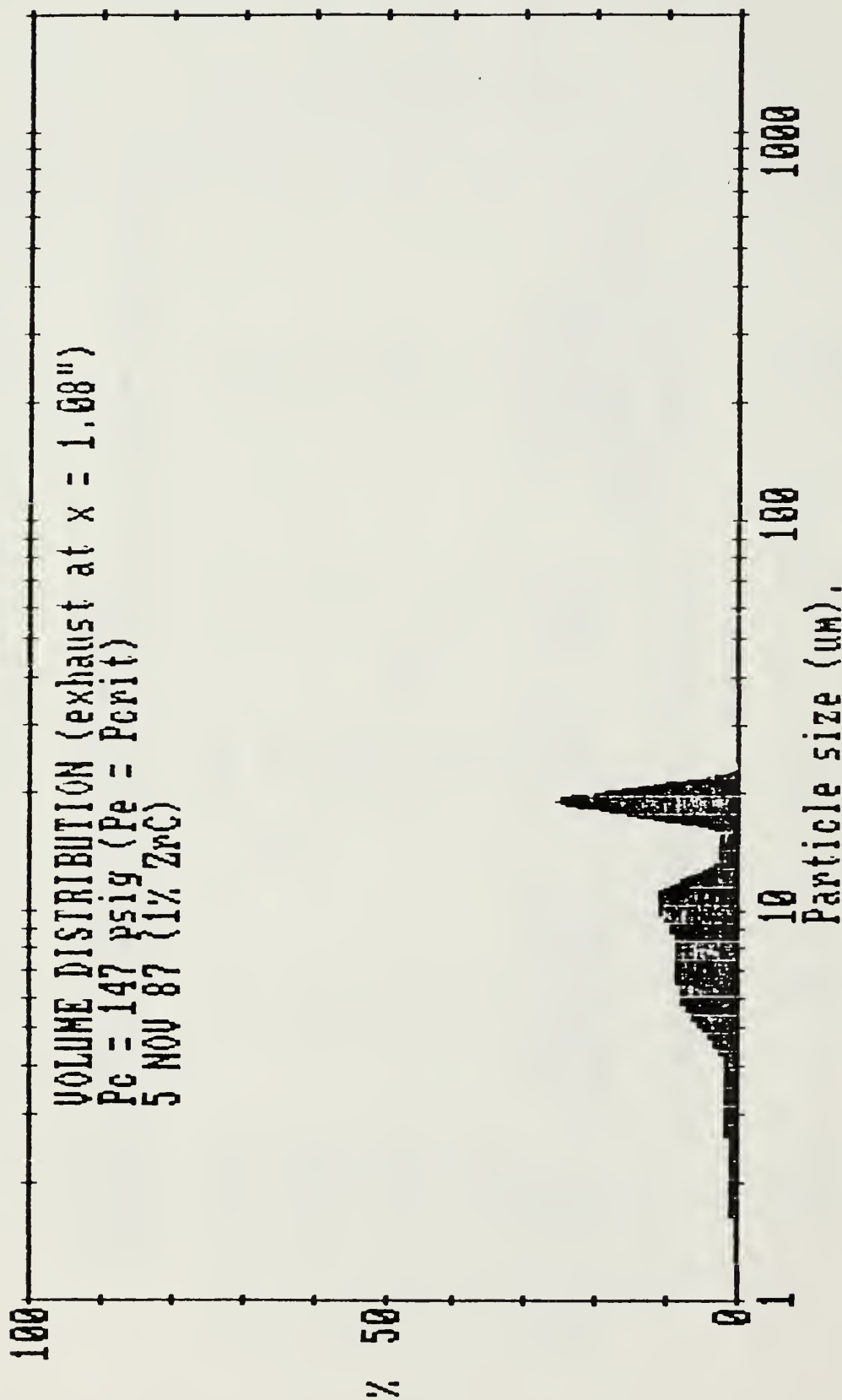


Figure 4.18 Volume Distribution, Exhaust ( $P_e = P_{critical}$ ) Test No. 1 (147 psig)



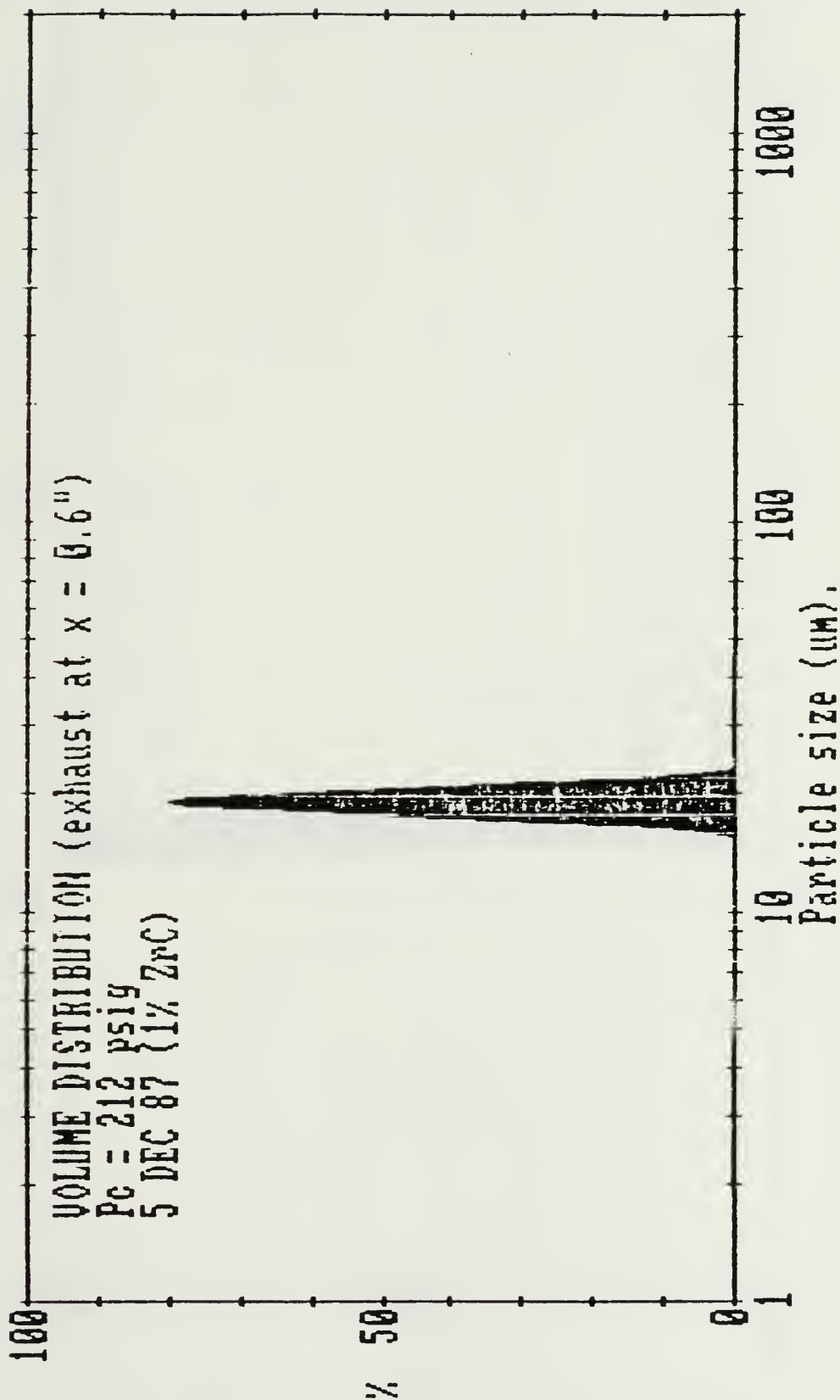


Figure 4.19 Volume Distribution, Exhaust ( $P_e = P_{critical}$ ) Test No. 2 (217 psig)

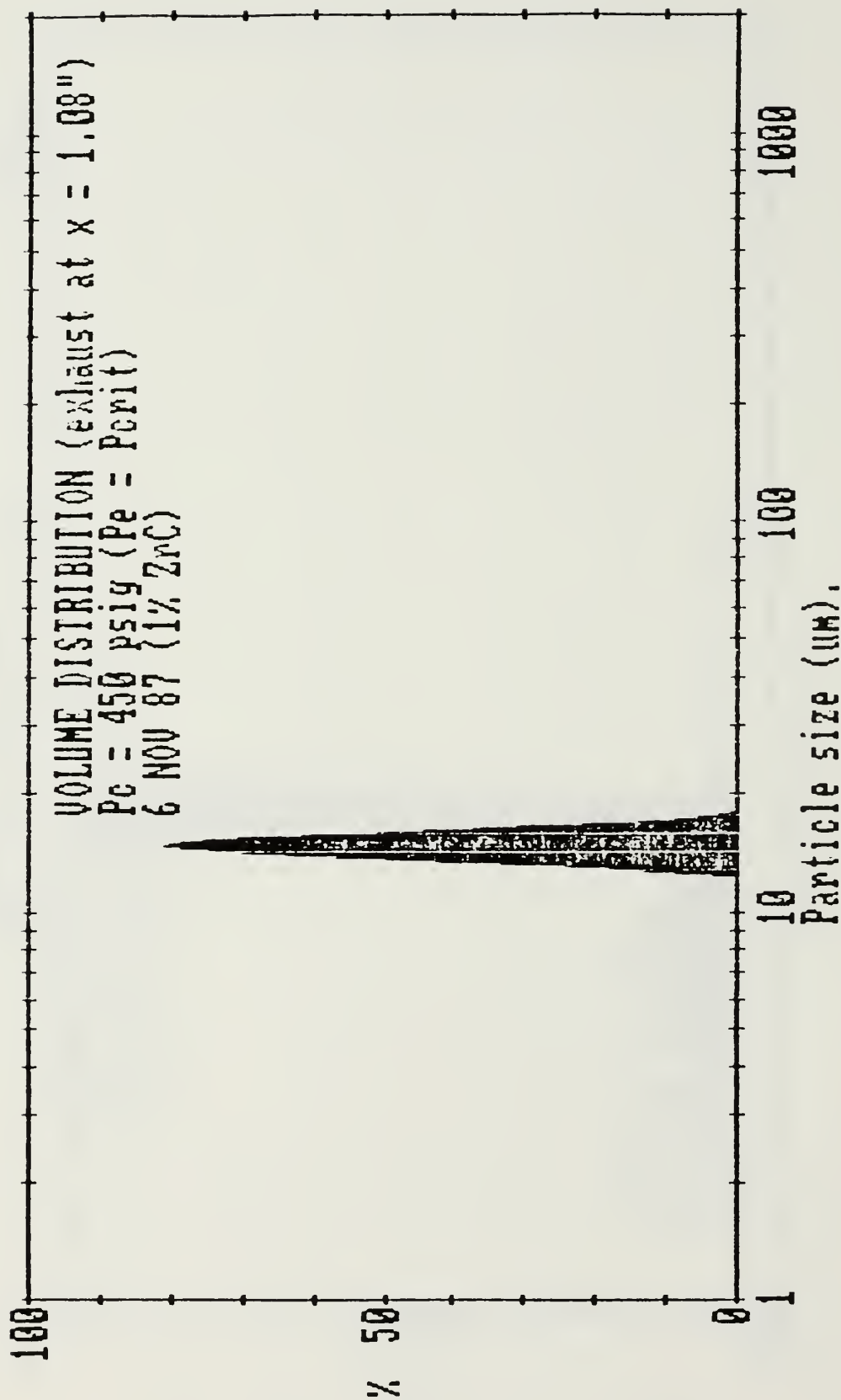


Figure 4.20 Volume Distribution, Exhaust ( $P_e = P_{critical}$ ) Test No. 3 (450 psig)

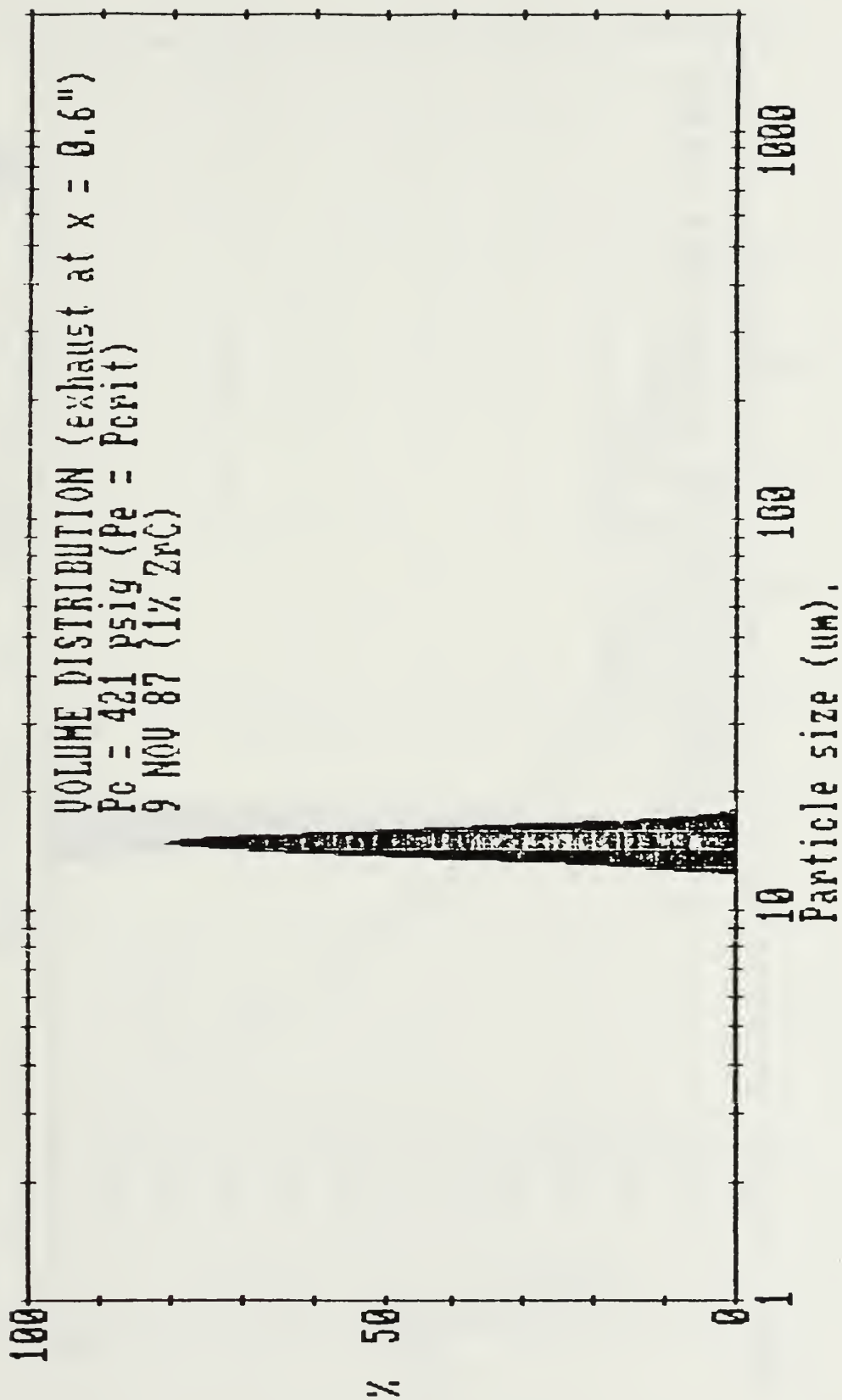


Figure 4.21 Volume Distribution, Exhaust ( $P_e = P_{critical}$ ) Test No. 4 (421 psig)

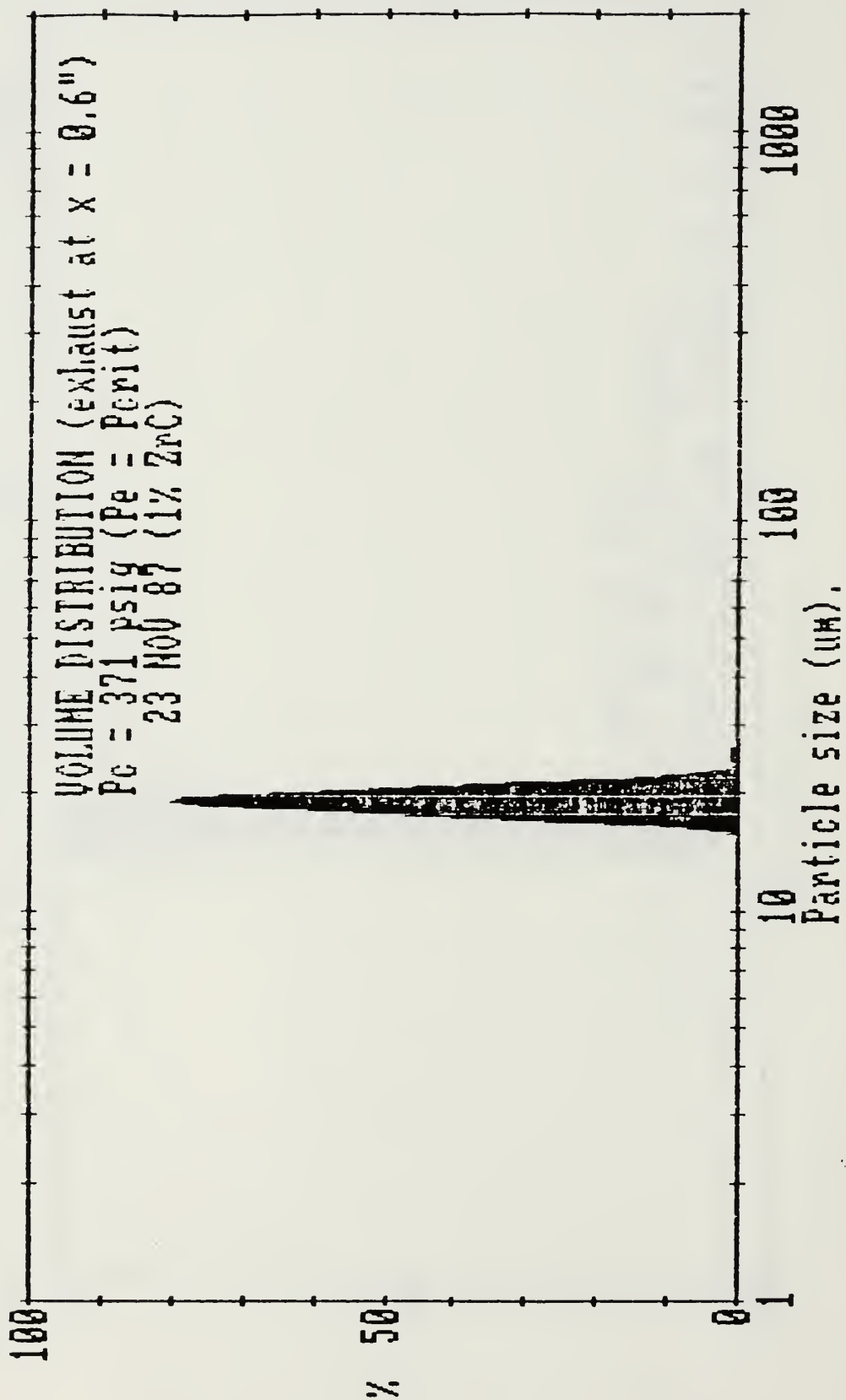


Figure 4.22 Volume Distribution, Exhaust ( $P_e = P_{critical}$ ) Test No. 5 (371 psig)

# CURVE FIT RESULTS INTENSITY vs. THETA

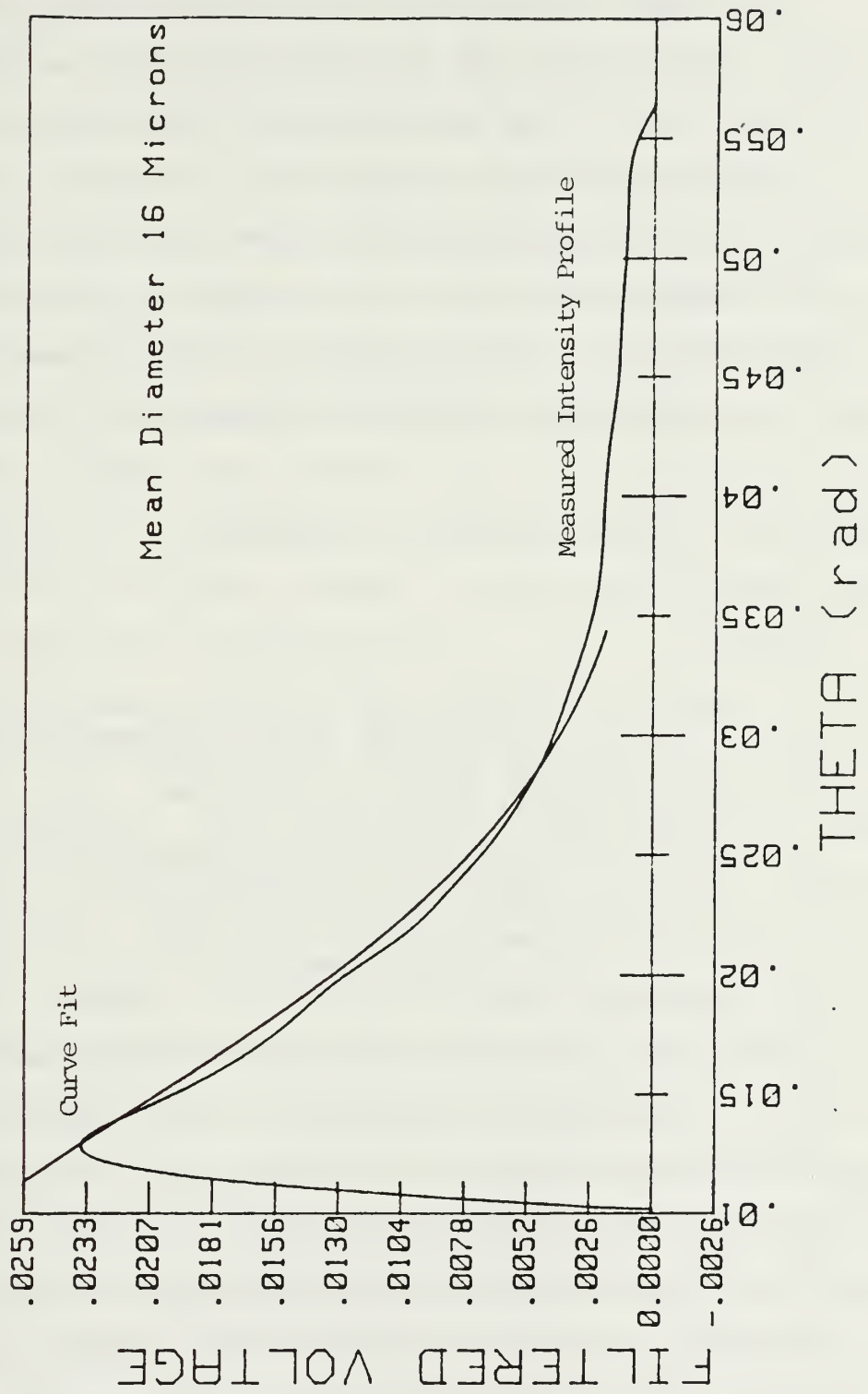


Figure 4.23 Exhaust Profile ( $P_e = P_{critical}$ ) Test No. 6 (370 psig)



test 6 using the NPS system. The distance downstream of the nozzle exit plane varied slightly as noted in Table 4.5 due to the geometry of the apparatus and set-up. All the distributions were monomodal with the exception of the test conducted at the lowest pressure (147 psig). Here a second broadly distributed mode was observed, which covered a range of approximately 4.5-12.0 microns. Except for this point, the SMD varied only slightly as chamber pressure was increased.

The Weber number is defined as

$$We = d_{ag} \rho_g (u_g - u_{ag})^2 / \sigma$$

where:

$d_{ag}$  = the diameter of an agglomerate (m)

$\rho_g$  = the density of the gas

$u_{ag}$  = the velocity of the agglomerate

$u_g$  = the velocity of the gas

$\sigma$  = the surface tension.

It is the ratio of inertial forces to surface tension forces. Gany [Ref. 22] found the Weber number to be a good correlation parameter in the analysis of the break-up of aluminum oxide agglomerates in the nozzle environment. Gany [Ref. 22] notes that for low Weber numbers the droplets are spherical, and tend to distort when the Weber number exceeds about four (for aluminum oxide). The distortion continues

to increase as Weber number increases until break-up occurs for Weber numbers in the range of 12-20 [Ref. 22].

Figure 4.24 is a plot of SMD versus motor chamber pressure. It is apparent from the curve that the agglomerates broke up into nearly the same size in the converging section of the nozzle, irrespective of chamber pressure (unless very low) or particle size entering the nozzle.

The equilibrium adiabatic combustion temperature was approximately the same as the melting temperature for  $\text{ZrO}_2$ . Thus, even though some thermal lag can be expected, the particles could be expected to rapidly solidify as the gas expansion in the nozzle occurs. This would prevent any further reduction in particle size.

Table 4.6 contains the results obtained in the exhaust for the condition of nozzle exit pressure equal to ambient pressure. The nozzles all had converging half angles of  $45^\circ$  and diverging half angles of  $15^\circ$ . Nozzle throat diameter and exit diameter were determined using isentropic relations for a ratio of specific heats equal to 1.2. Figures 4.25 to 4.32 present the volume distributions associated with tests 1 through 8, respectively. It is interesting to note that all the distributions were multimodal with the exception of test number 5, which was run at 215 psig. The primary factor which differentiated test five from the other tests was the distance behind the nozzle exit plane at which the measurements were obtained.

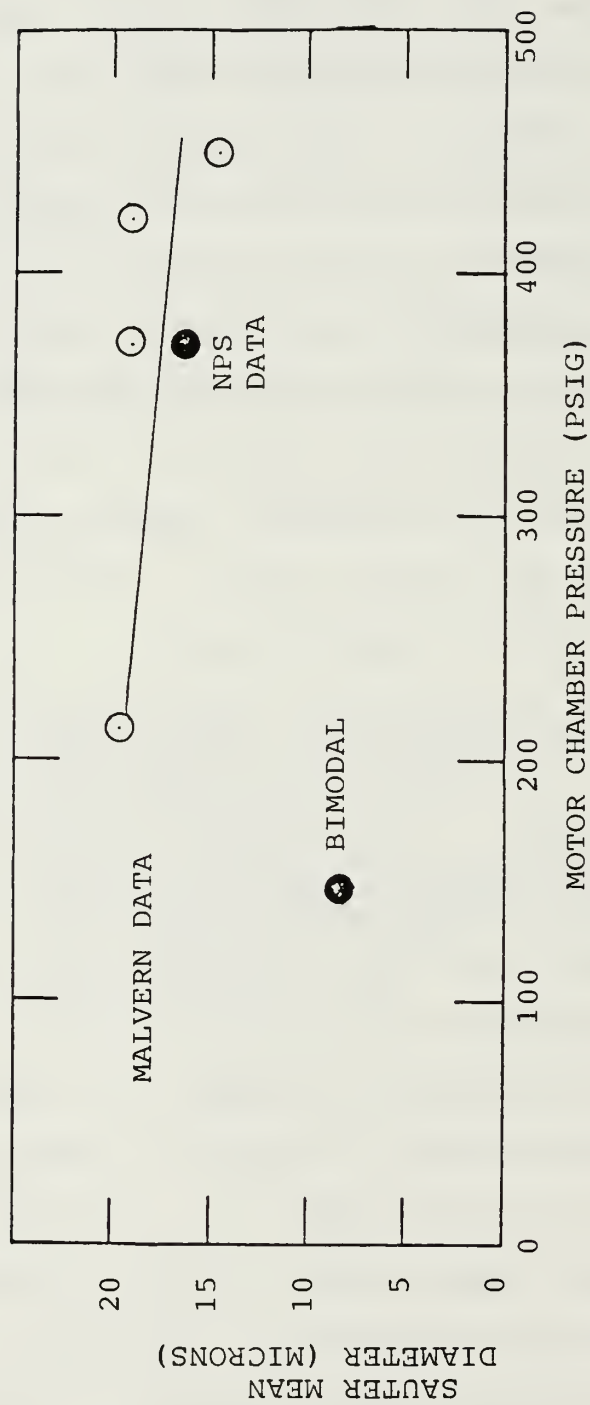


Figure 4.24 Exhaust Scattering Measurement Results ( $P_e = P_{critical}$ )

TABLE 4.6

EXHAUST SCATTERING MEASUREMENTS ( $P_e = P_o$ )

Test No.	Wt % Metal	Data Obtained at Measured Pressure (psig)	Max Pressure (psig)	Burn Time (sec)	Measurement Location	
					In Inches Behind Exit Plane of Nozzle	$D_{32}$ (microns)
1	1.0 ZrC	175	185	7.9	2.7	7.6
2	1.0 ZrC	125	138	7.2	2.7	8.3
3	1.0 ZrC	135	141	6.7	2.7	6.5
4*	1.0 ZrC	79	85	10.2	1.7	6.2
5	1.0 ZrC	215	220	5.1	0.6	19, 1.
6	1.0 ZrC	436	442	5.3	2.7	1.9
7	1.0 ZrC	352	388	5.8	2.7	3.4
8	1.0 ZrC	300	331	6.0	2.7	No Data

\* Denotes run made with graphite nozzle which had no converging section. It had a knife edged orifice which diverged at a 45° half angle.

NOTE: All data were obtained using the MALVERN 2600.

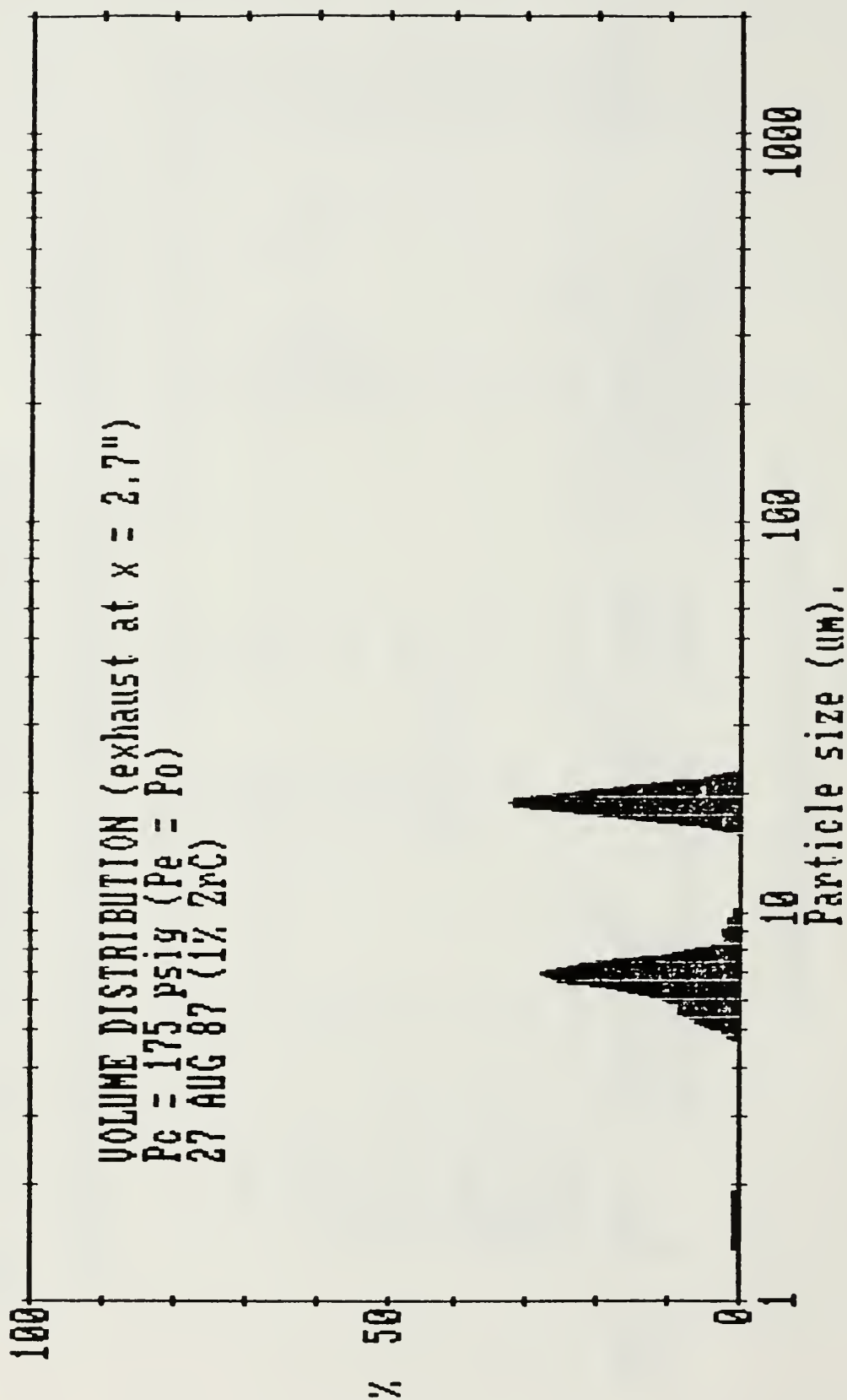


Figure 4.25 Volume Distribution, Exhaust ( $P_e = P_o$ ) Test No. 1 (175 psig)



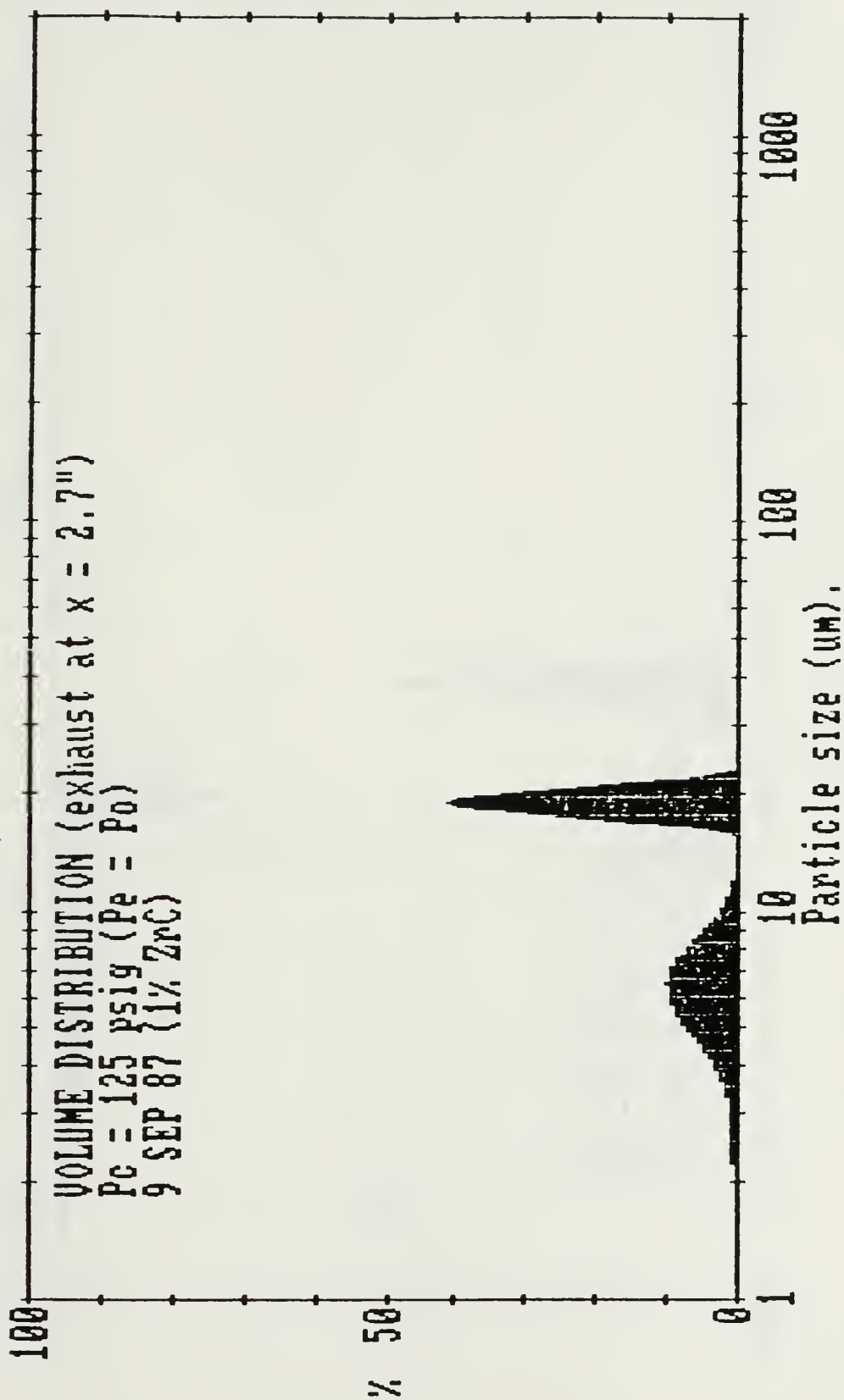


Figure 4.26 Volume Distribution, Exhaust ( $P_e = P_o$ ) Test No. 2 (125 psig)

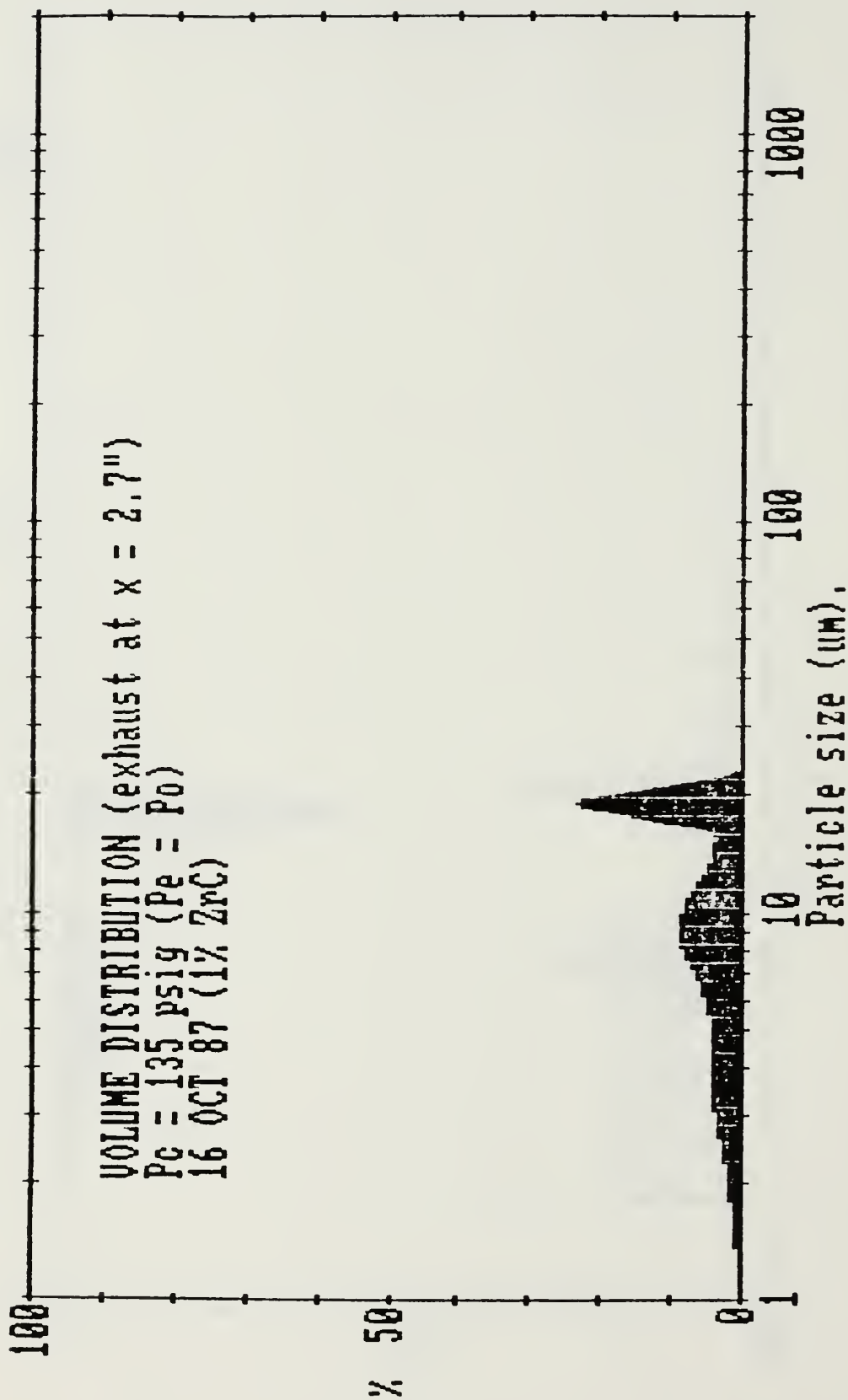


Figure 4.27 Volume Distribution, Exhaust ( $P_e = P_o$ ) Test No. 3 (135 psig)

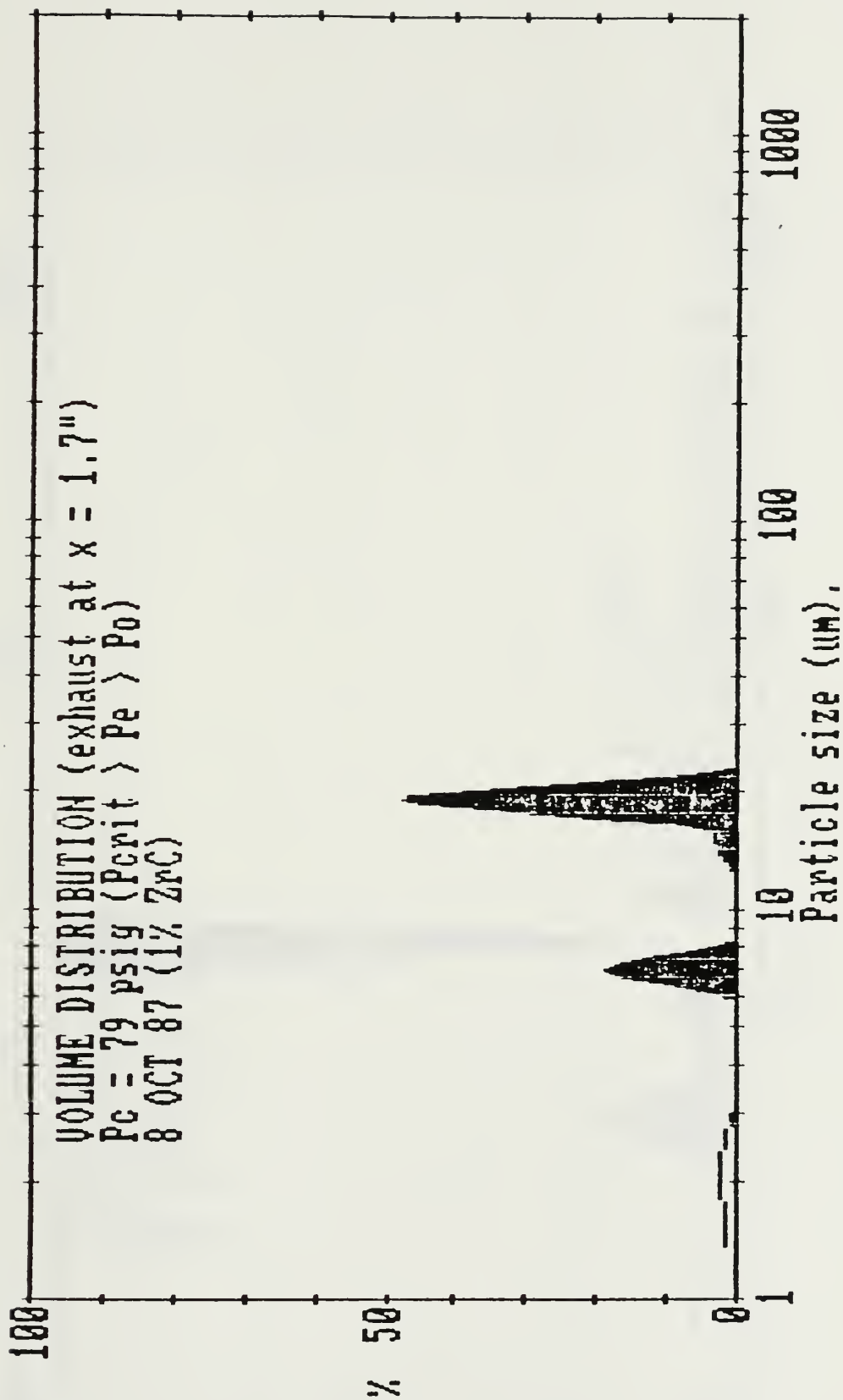


Figure 4.28 Volume Distribution, Exhaust ( $P_e = P_o$ ) Test No. 4 (79 psig)

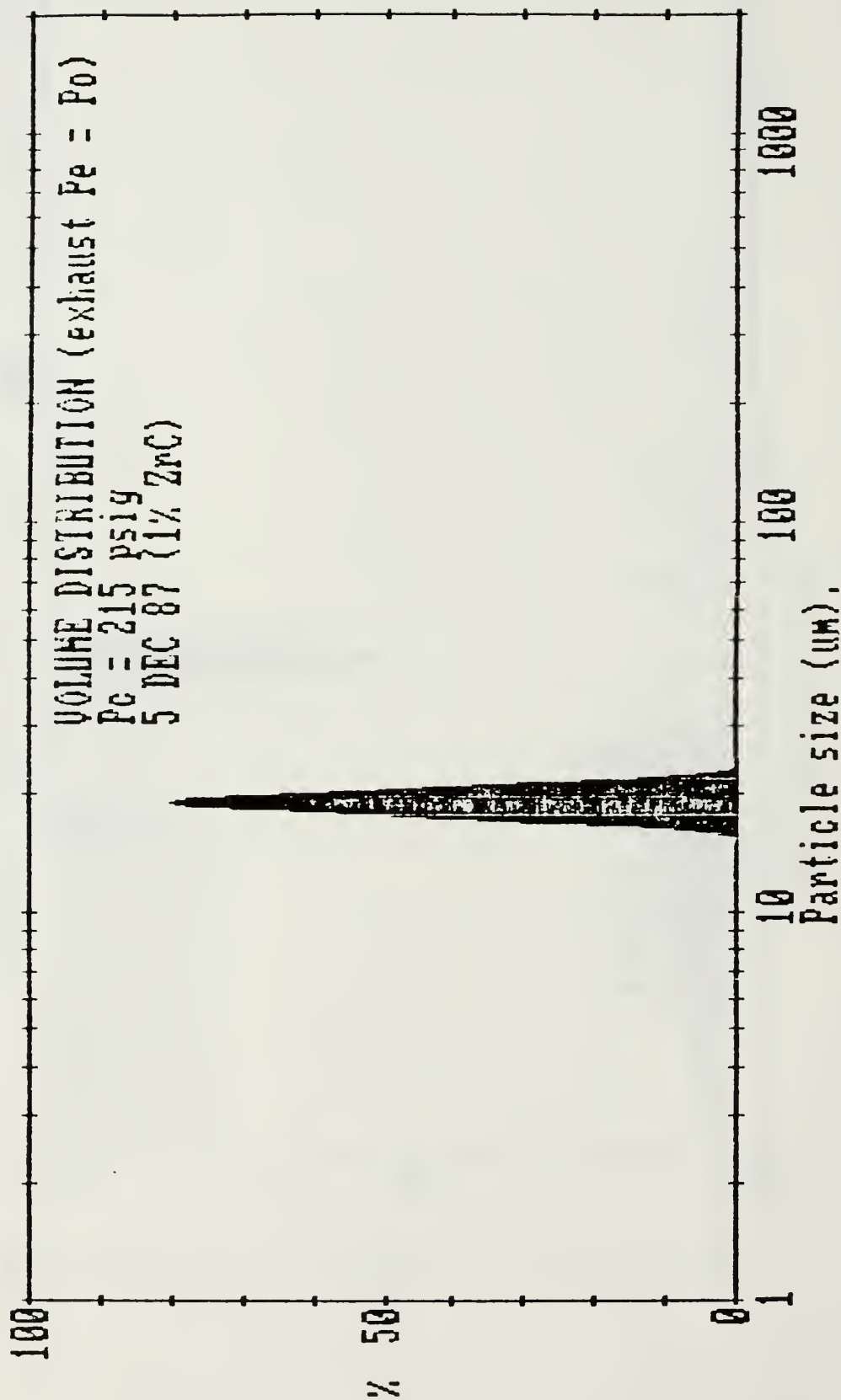


Figure 4.29 Volume Distribution, Exhaust ( $P_e = P_o$ ) Test No. 5 (215 psig)

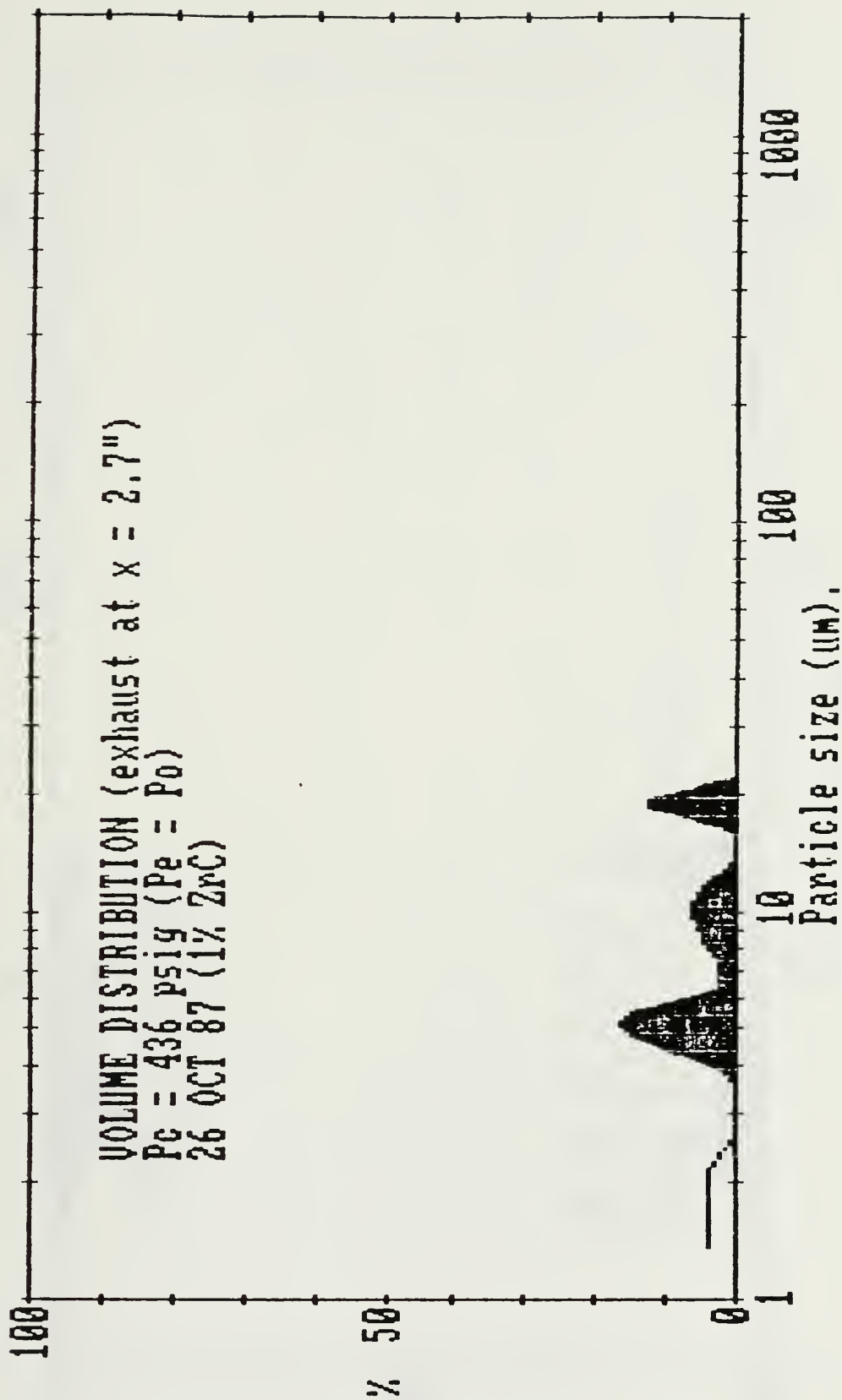


Figure 4.30 Volume Distribution, Exhaust ( $P_e = P_o$ ) Test No. 6 (436 psig)

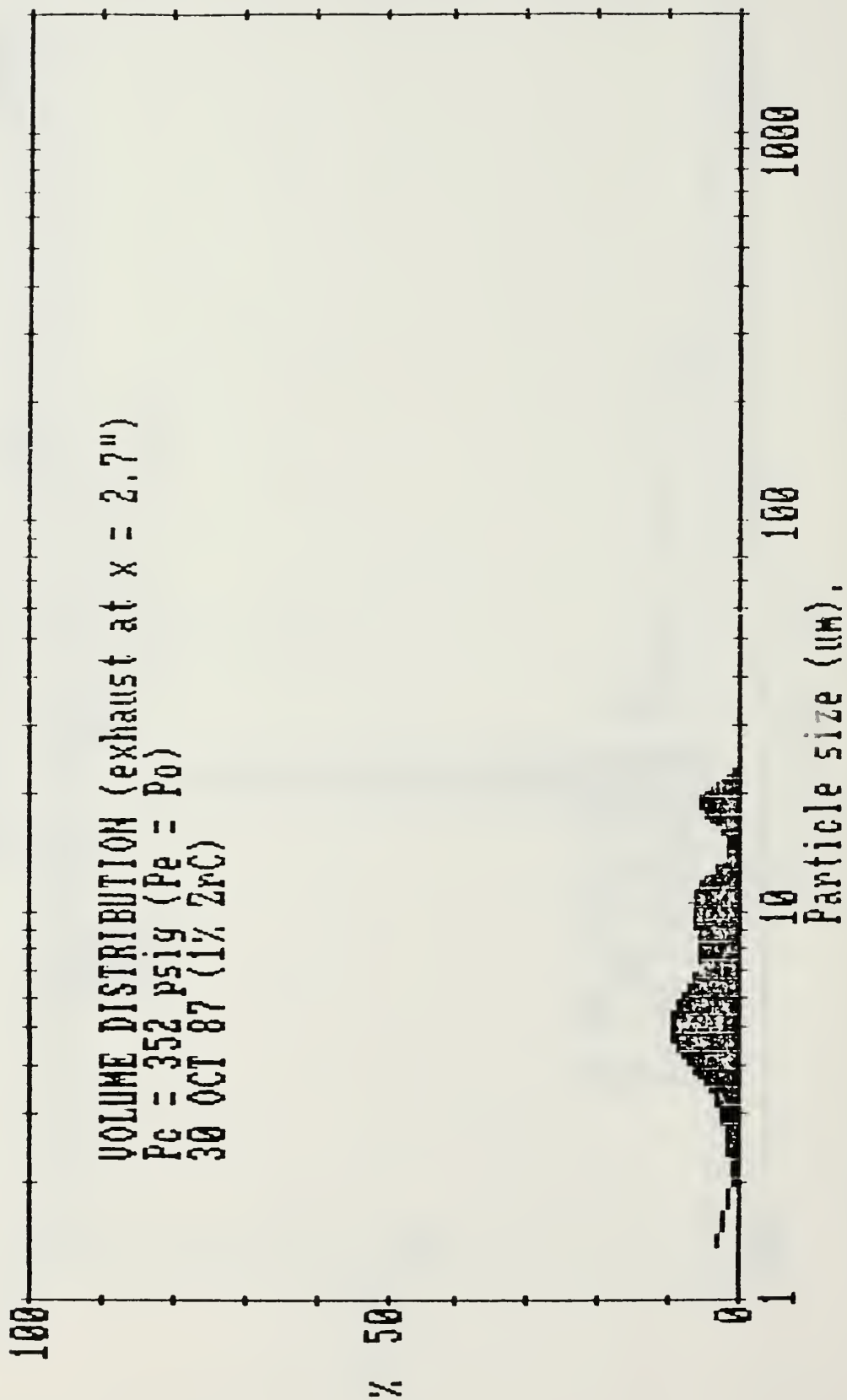


Figure 4.31 Volume Distribution, Exhaust ( $P_e = P_o$ ) Test No. 7 (352 psig)



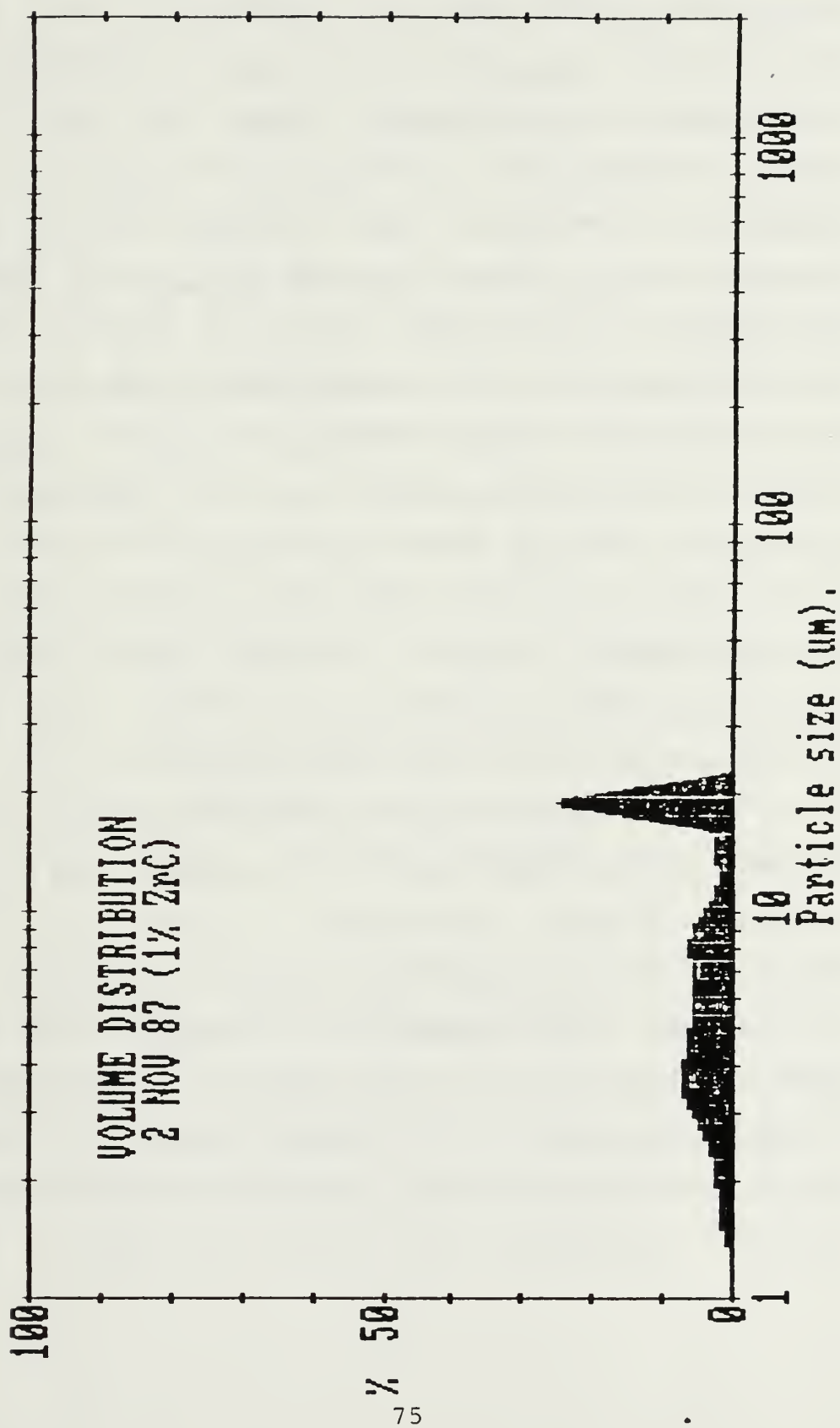


Figure 4.32 Volume Distribution, Exhaust ( $P_e = P_o$ ) Test No. 8 (300 psig)

The measurements were all made 2.7 inches downstream of the nozzle exhaust plane except for test five, where the distance was 0.6 inches. The tests run with the 2.7 inch distance were necessary because laser diffraction data were being obtained simultaneously through the motor, and the physical dimensions of the apparatus limited the minimum distance to 2.7 inches. Test 5 results indicated that the majority of the particles remained monomodal and essentially unchanged in mean diameter (19 microns) from the throat to the exit plane. The measurements made further aft had one mode centered at the same 19 micron diameter. However, the number of these particles were less, and significant numbers of smaller particles were observed in a bi- or tri-modal distribution. The reduced particle size could be due to particle breakup. However, it may have resulted from the reduced number of particles in the scattering volume, which was located through the center of the spreading exhaust jet.

The presence of strong thermal gradients along the boundary of the exhaust jet initially caused some problem in obtaining exhaust measurements. During initial runs, scattering data indicated the presence of abnormally large particulates in the exhaust, on the order of 127 microns. Knowing that particle size entering the nozzle was substantially less than 127 microns, typically around 70 microns for 150 psig runs, a search for causal factors was pursued. Conversation with Hughes and Taylor at MALVERN

Instruments confirmed the idea that thermal gradients or density gradients were indeed biasing the scattered light data, i.e., the presence of strong thermal gradients along the boundary of the hot gas jet, or density gradients associated with a shock. The solution to this difficulty was a rather simple procedure. When unstable refractive index of the suspending medium is present as a result of strong thermal gradients, a steering effect occurs that steers light to low angles, hence biasing particle size to the large end of the scale. The procedure employed when using the Master Sizer program was to inhibit data from the affected inner rings, using the "KILLDATA" command. Once the user had examined the raw data and observed which rings had been affected, then those rings were inhibited by the software command "KILLDATA." Care must be exercised in this procedure to ensure that no scattering data will be lost as a result of inhibiting data from the affected inner rings. In the latter case there is no recourse, scattering data at that point becomes no longer separable from the steered light.

Figure 4.33 is a graphical depiction of particle size (SMD) versus motor chamber pressure. There was a slight reduction in particle size with increasing pressure. Figure 4.34 plots both exhaust conditions. The reduced size in the downstream, spreading plume is apparent.

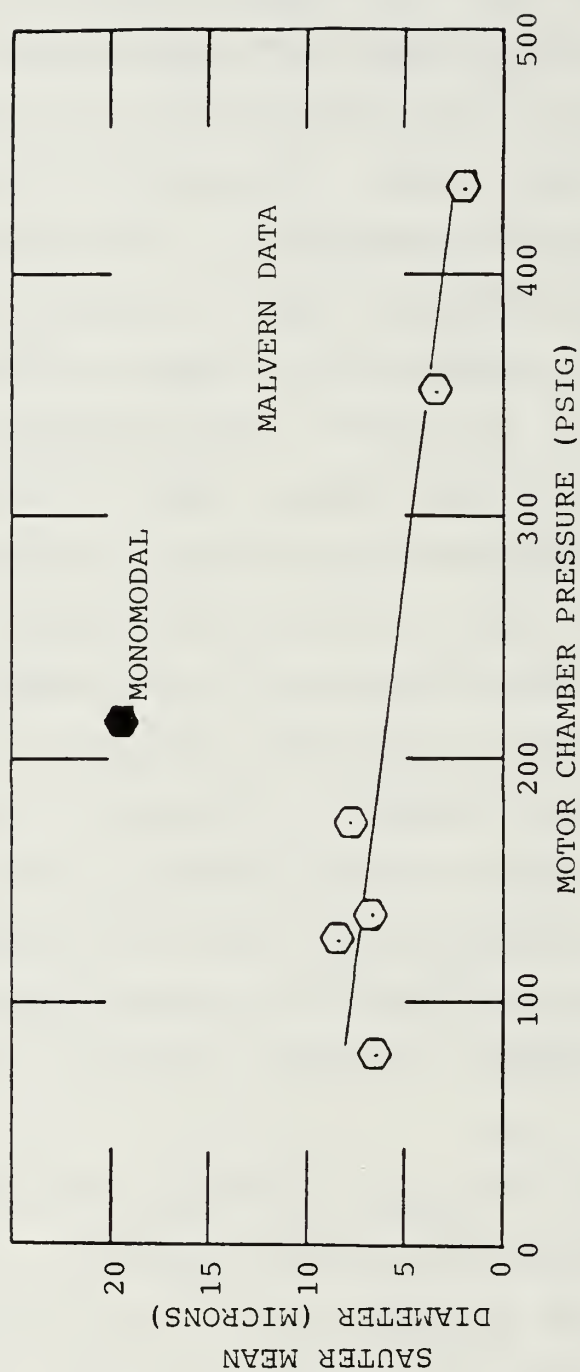


Figure 4.33 Exhaust Scattering Measurement Results ( $P_e = P_o$ )

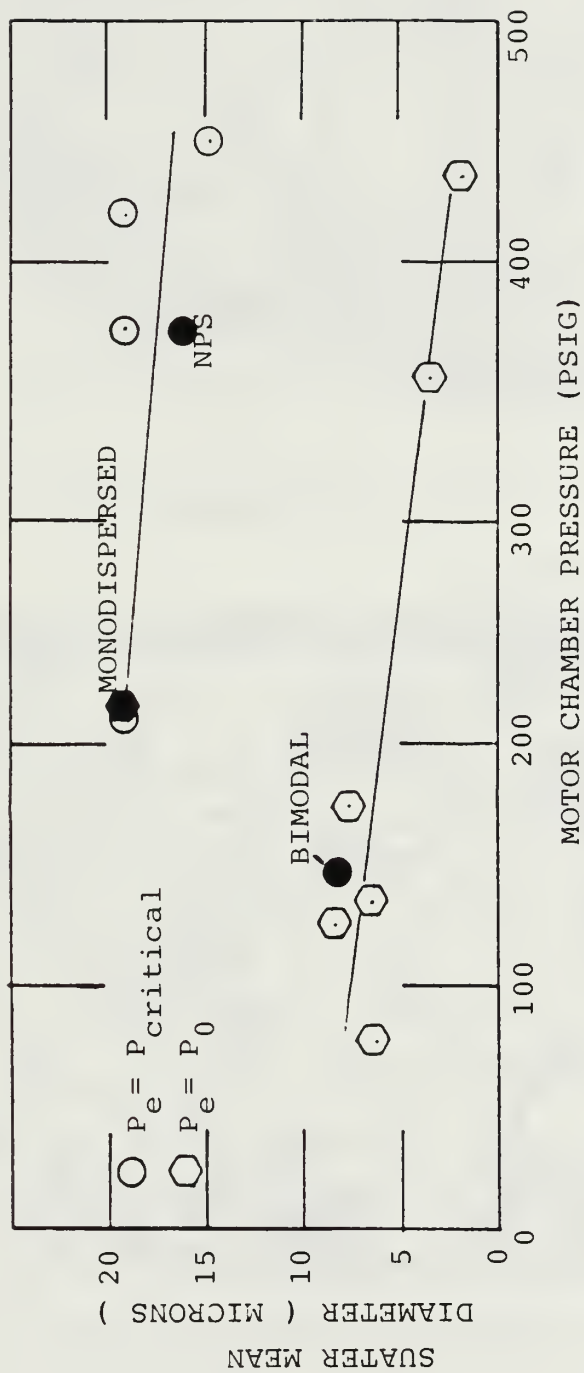


Figure 4.34 Comparative Results, Exhaust ( $P_e = P_{critical}$ ) and Exhaust ( $P_e = P_0$ ) Data

Exhaust measurements were made for both  $P_e = P_o$  and  $P_e = P_{critical}$  to determine if any change in particle size was incurred as a result of the supersonic expansion of the jet. Particle breakup downstream of the nozzle exhaust was observed. The limited data at approximately 200 psi indicated that little breakup occurred within the nozzle, downstream of the throat. In aluminized propellants, one might reasonably expect that vapor condensation occurring during the expansion process might well affect the size distribution of exhaust particles. However, in the case of zirconium carbide, the temperature in the chamber is not sufficiently high for appreciable amounts of either Zr, ZrC or  $ZrO_2$  to be present in a vapor phase.

#### 6. SEM Analysis

As a means of independently verifying the scattering results, residue was collected from the face of the nozzle converging section. This residue was then placed in a solution of lab grade acetone and put into an ultrasonic cleaner, mixed, and allowed to settle. After repeated cleanings, the acetone was evaporated off in an oven under reduced pressure. Using this powder, seven samples were prepared for examination with the scanning electron microscope. Three of the samples were prepared using a non-conducting epoxy base which had to have a gold flashing applied in order to provide for a conducting surface. The remaining samples were mounted using a conducting colloidal carbon. Figures 4.35 and 4.36 are SEM photographs taken of the samples. Particles were counted from each sample in an attempt to get a representative size distribution. Some 218



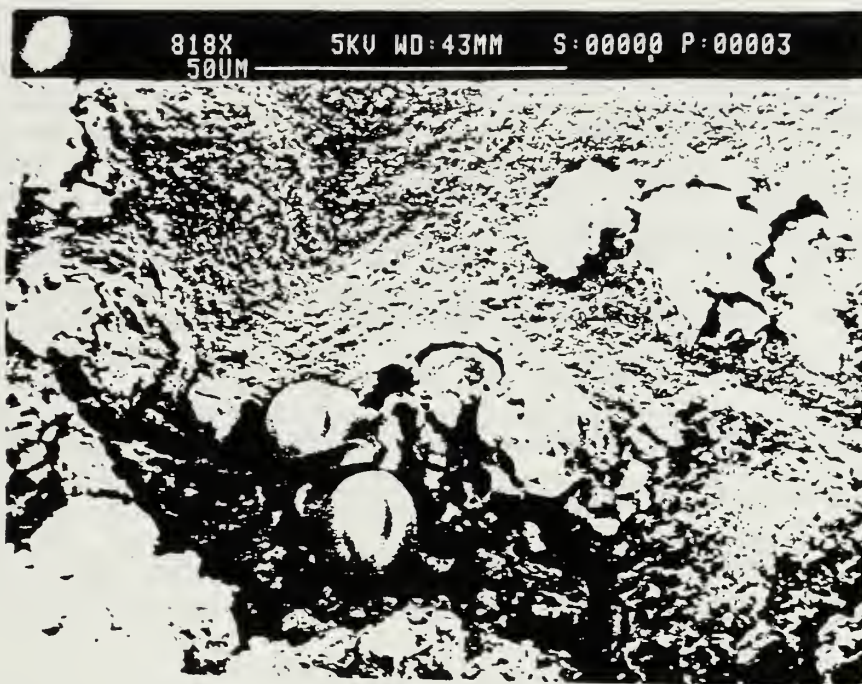


Figure 4.35 SEM Photograph of Residue Collected from Exhaust Nozzle

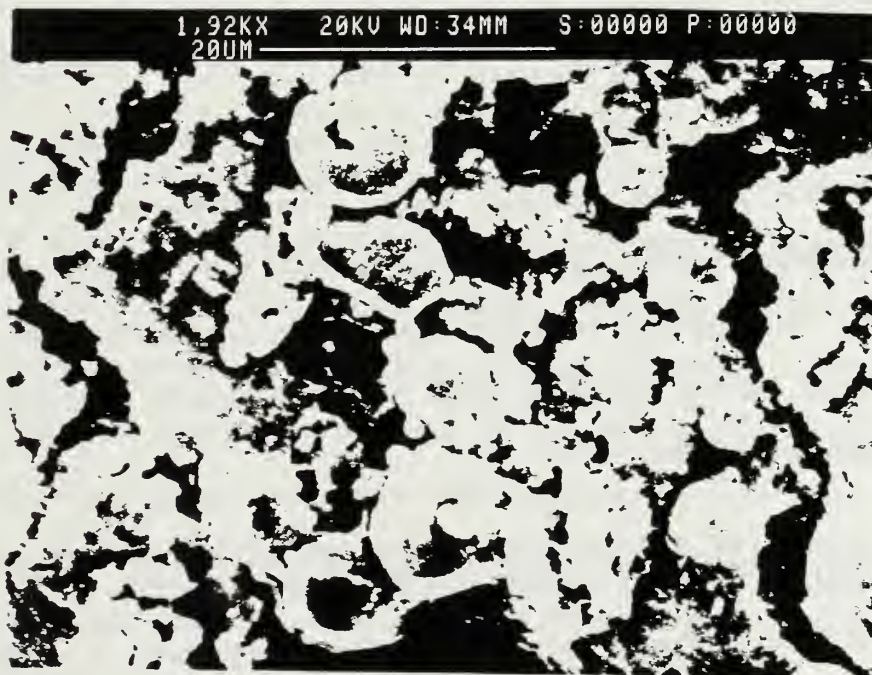


Figure 4.36 SEM Photograph of Residue Collected from Exhaust Nozzle

particles were counted with sizes ranging from 1-20 microns. The smaller particles (3 microns and less) were difficult to see, but did exist in the sample. No particle larger than 20 microns was observed, but this by no means implies that no larger particles were present. Collection of residues and/or exhaust products is a crude method. When collected in small quantities from wall surfaces it cannot yield a valid statistical sample. However, it does provide some reassuring insight as to what was physically present in the sample.

The particles were grouped strongly in 2 bands, one band from 5-12 microns and the other from 14-17 microns. The sample was taken from the 427 psig run where the mean particle size (SMD) prior to the nozzle entrance was 27.6 microns and in the nozzle throat region it was 19 microns. Thus, the SEM data were in reasonably good agreement with the optical data. In Figures 4.35 and 4.36 the larger irregular-shaped particles have reasonable sources, one being residue from the binder/inhibitor, and the second being residue from the lab grade acetone used to clean the samples.

#### D. COMPARATIVE EVALUATION OF THE MALVERN 2600 AND THE LOCALLY DESIGNED LASER DIFFRACTION SYSTEM

From the outset of this investigation, a comparative analysis of the two diffraction instruments was a primary goal. Some of the limitations of the NPS system were

obvious, based on a review of the system hardware and software.

The differences in software and in data reduction algorithms were significant. The NPS algorithm is based on a ratioing technique developed by Buchele [Ref. 10]. This method yields the size parameter  $D_{32}$  by the process of fitting a theoretical curve for monomodal distributions to a measured intensity profile. The technique is discussed in detail in Chapters II and III. The MALVERN Master-Sizer operating system, by comparison, inverts the scattered data to obtain a size distribution. The NPS system could be upgraded in this area by adopting one of the quadrature methods described by Koo [Ref. 16].

The differences in hardware are highlighted by the design of the detector system photodiode arrays. The MALVERN systems annular array design allows for the detection of much weaker intensities. The field of view of the NPS system was also limited by the array dimensions.

A comparison was made using the NPS laser system to measure particle size at the nozzle entrance. Figure 4.37 is a plot of comparable through-motor measurements made by the MALVERN system and the NPS system in the motor section just prior to the nozzle entrance. As can be seen from the plot, the NPS system underestimated the mean particle sizes at low pressures where the distributions were multimodal. As discussed above, the NPS data reduction algorithm assumes

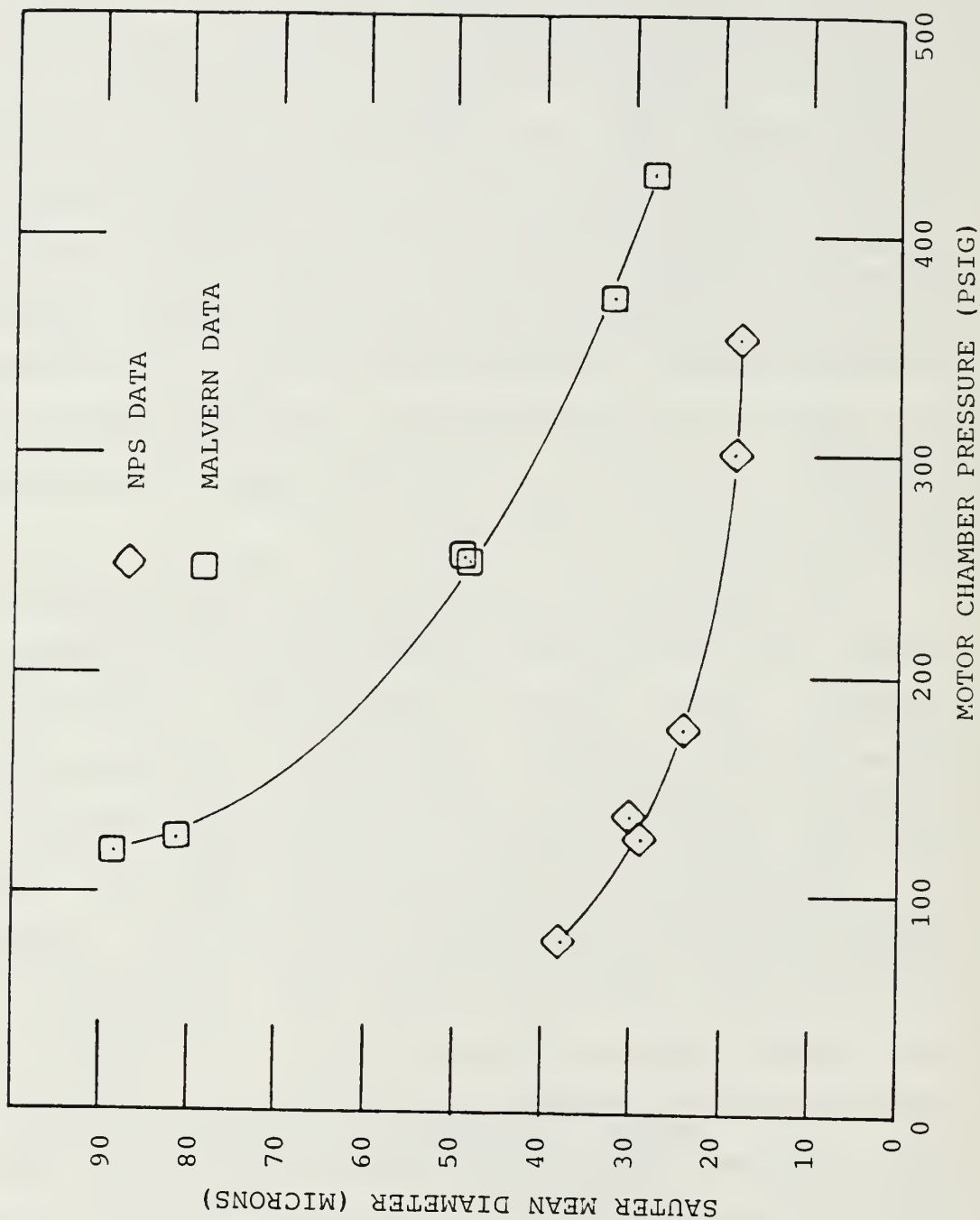


Figure 4.37 Comparative Result, NPS and MALVERN Data for the Nozzle Entrance



a monomodal distribution. The larger particles in the bimodal distribution (60-70 microns), scattered light at angles below the range of the NPS detector. To further verify this effect, the MALVERN data for the run at 161 psig was reduced, after inhibiting data that were outside the field of view of the NPS system. Figure 4.38 depicts the resulting distribution. What occurred was that an artificial mode appeared at 24.7 microns. Figure 4.39 is a measurement made at a similar pressure (175 psig) with the NPS system. A SMD of 24 microns was obtained. Thus, when distributions are multimodal, accurate values of  $D_{32}$  are not obtained with present data reduction algorithm used with the NPS apparatus. Figures 4.40, 4.41 and 4.42 are included for completeness. These figures represent the data used to construct Figure 4.37. At higher chamber pressures (400 psig class), where the distributions became more monomodal and the dominant scattered light was within the field of view of the NPS system, better agreement of data existed (Figure 4.37).

The conclusion is that the NPS system functions well when the distribution of particulates is monomodal and the linear diode array is placed such that the majority of the scattered light is within the field of view of the detector.

#### E. SOURCES OF MEASUREMENT ERROR (UNCERTAINTY)

In the course of this investigation a number of measurement errors were encountered from a variety of

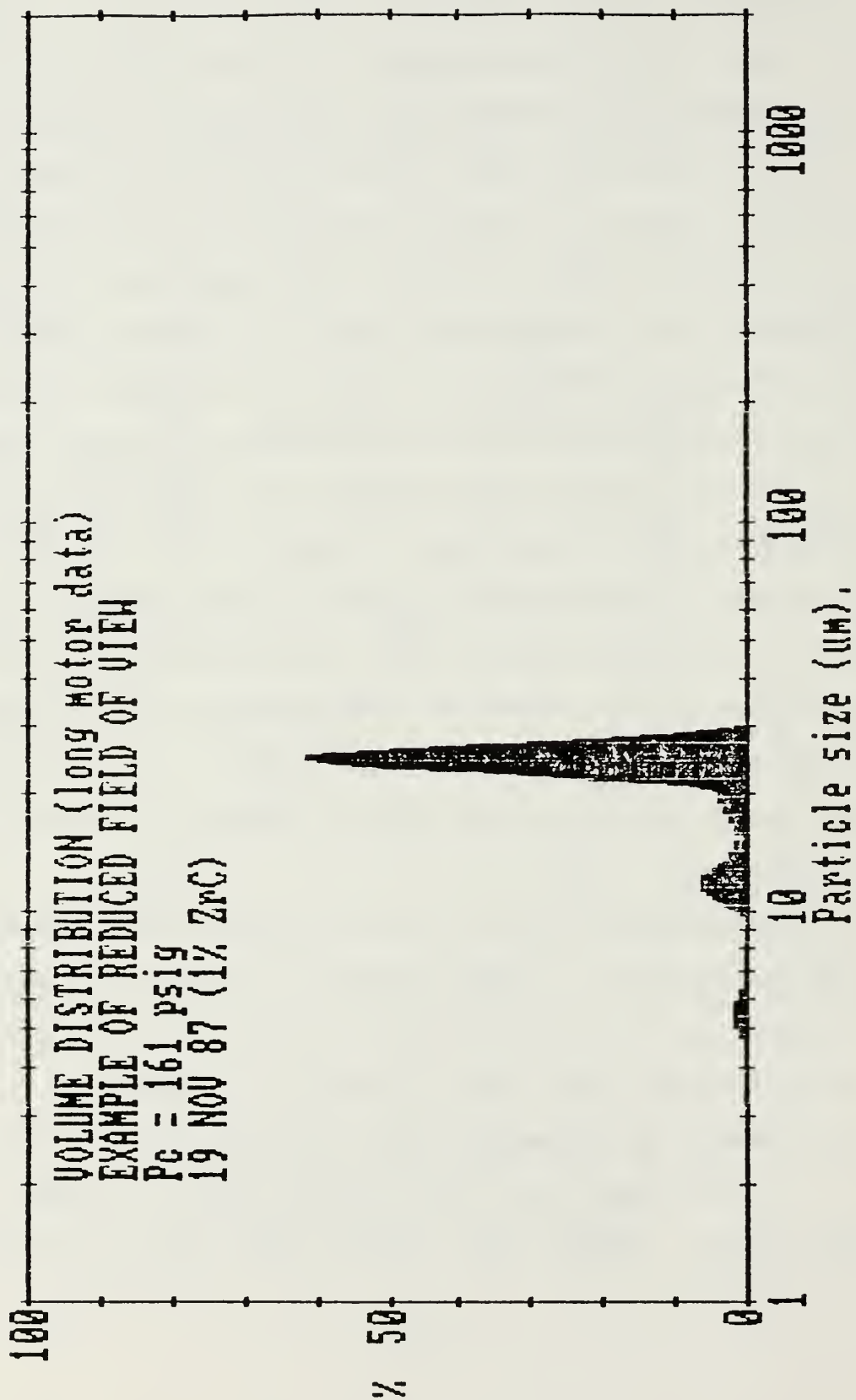


Figure 4.38 Example of the Effects of a Reduced Field of View



# CURVE FIT RESULTS INTENSITY VS. THETA

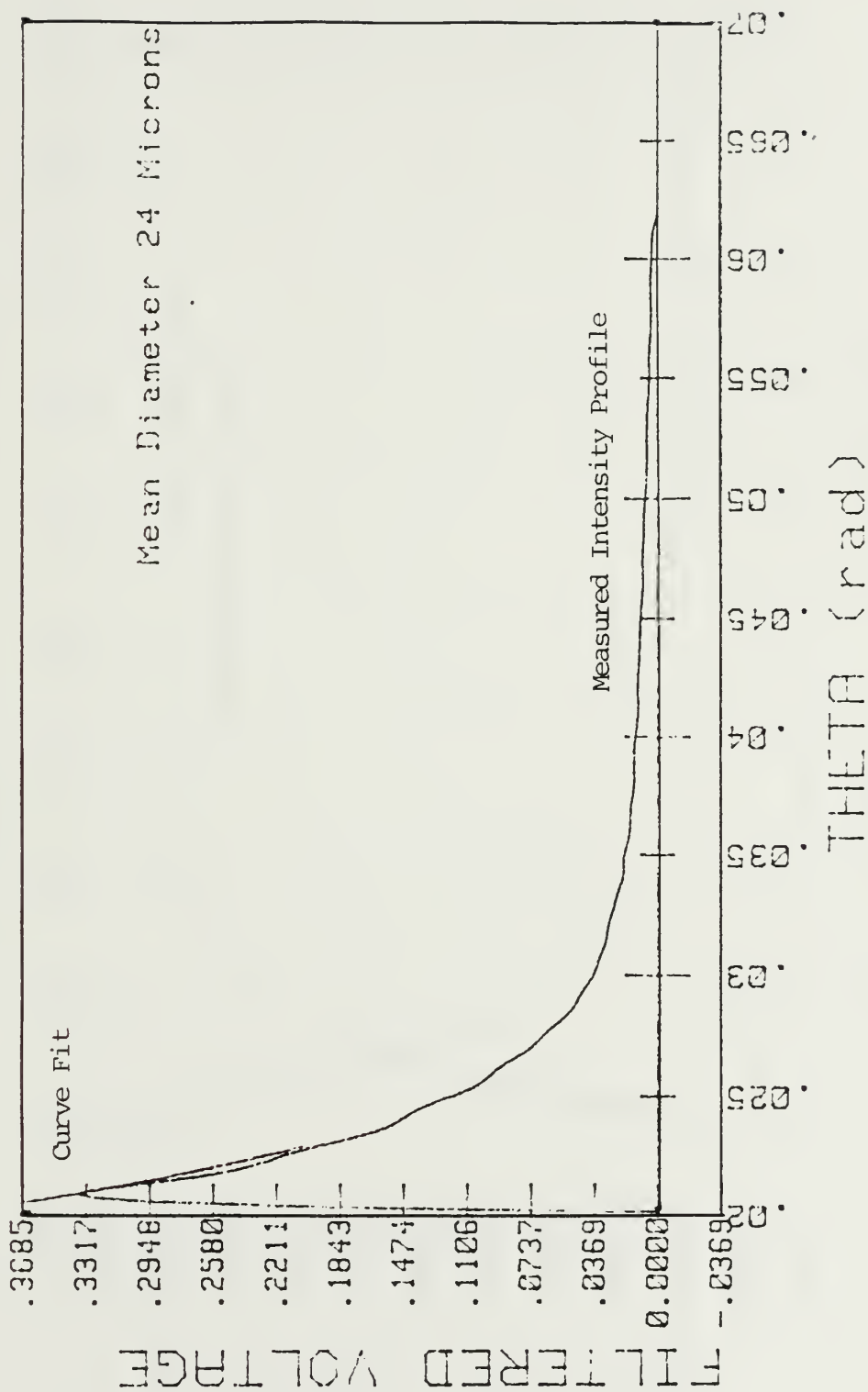


Figure 4.39 Motor Profile, Nozzle Entrance Test No. 4 (175 psig)

# CURVE FIT RESULTS INTENSITY VS. THETA

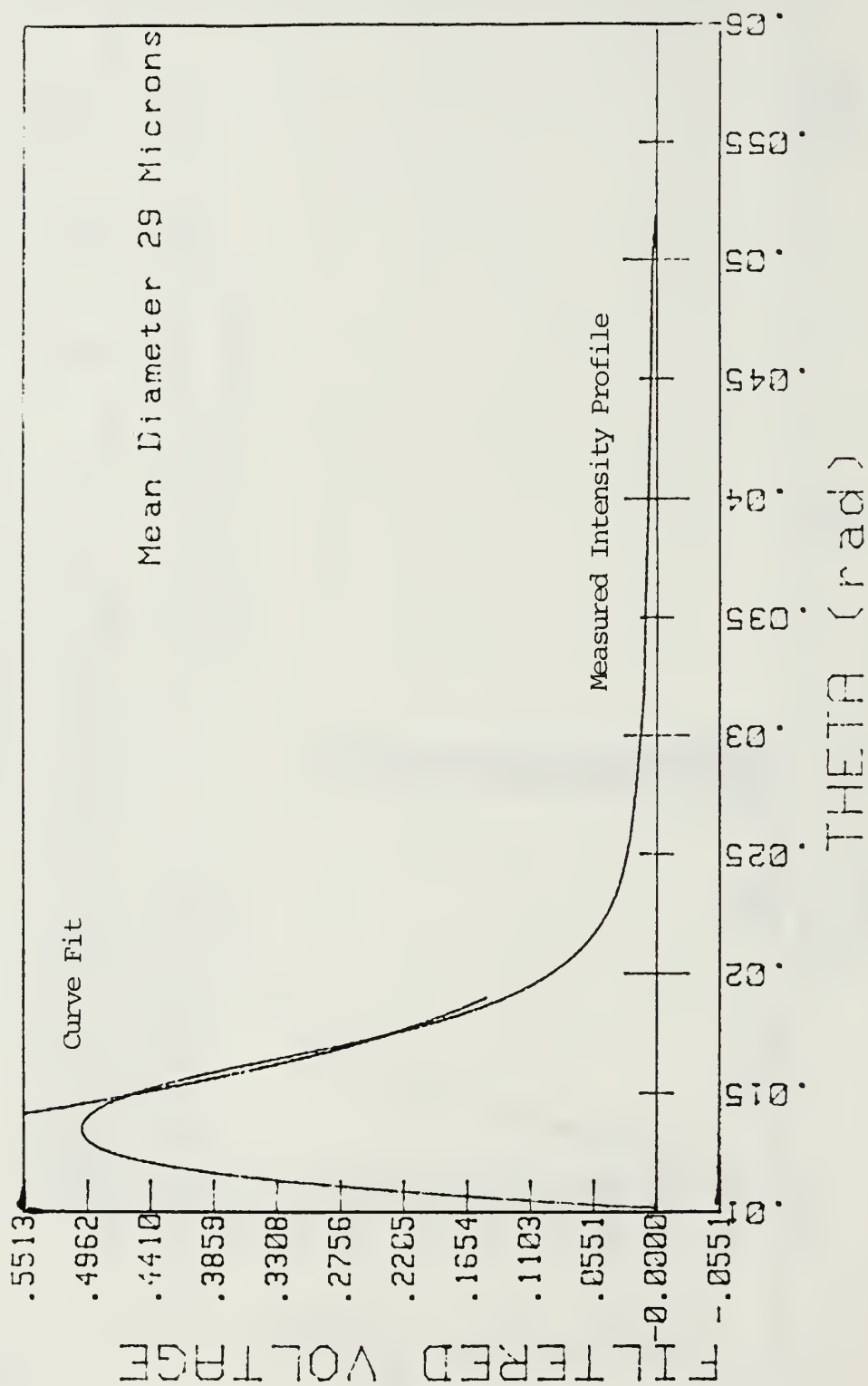


Figure 4.40 Motor Profile, Nozzle Entrance Test No. 5 (125 psig)

# CURVE FIT RESULTS INTENSITY VS. THETA

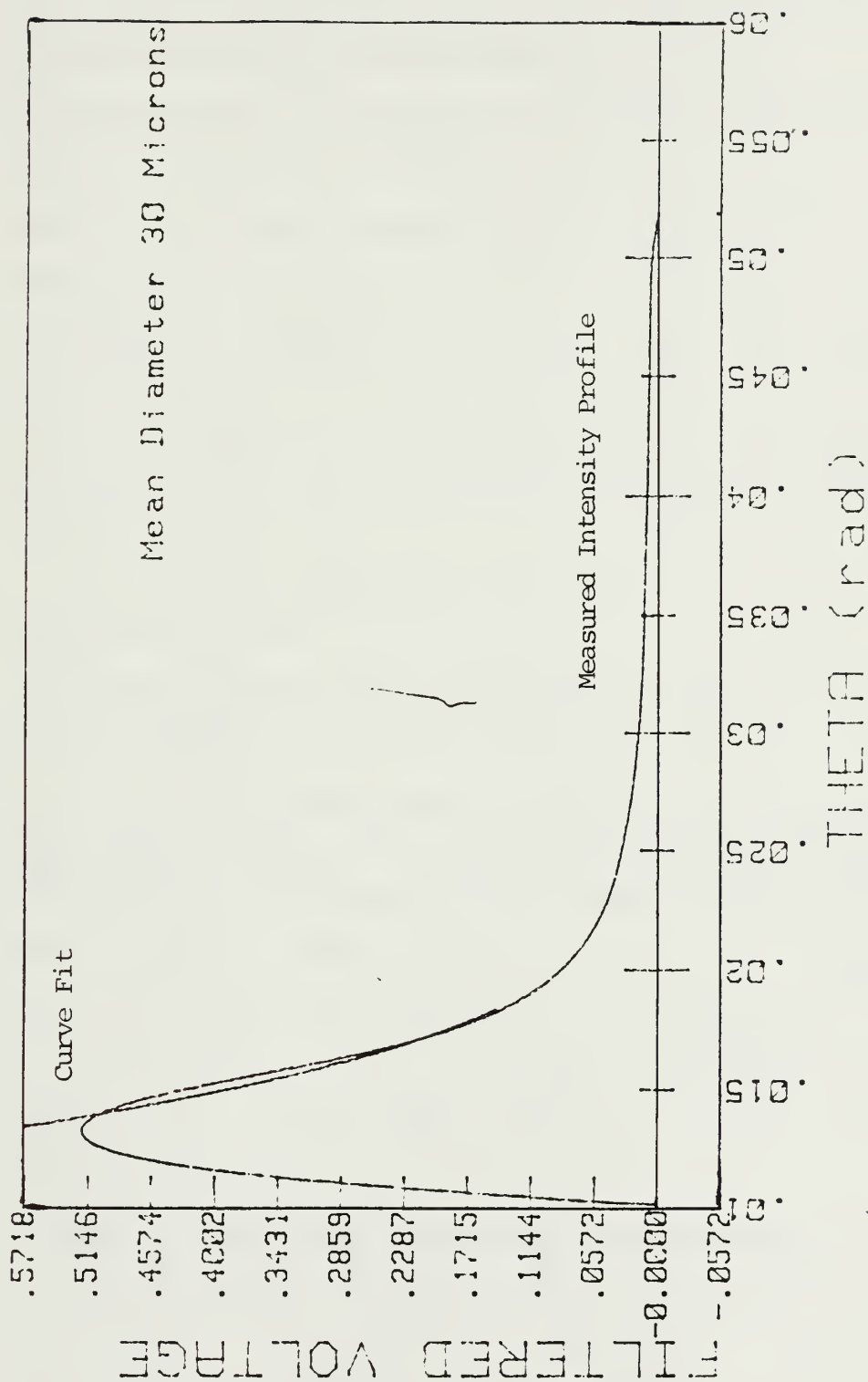


Figure 4.41 Motor Profile, Nozzle Entrance Test No. 6 (135 psig)

# CURVE FIT RESULTS INTENSITY VS. THETA

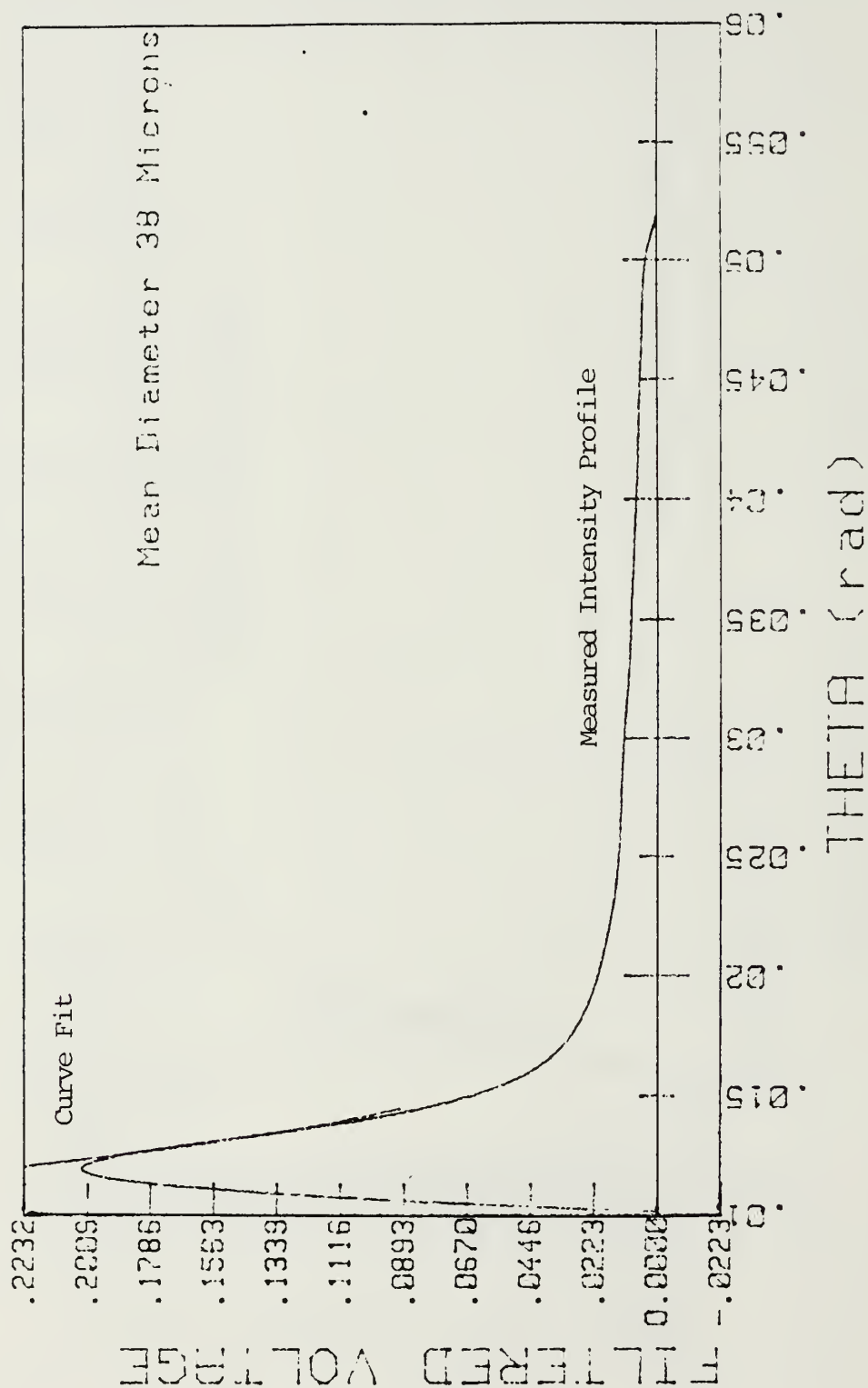


Figure 4.42 Motor Profile, Nozzle Entrance Test No. 7 (79 psig)

sources. Measurements were made in both the motor chamber and exhaust environments, and each environment presented a slightly different set of difficulties.

Measurements made in the motor environment were subject to the following sources of uncertainty:

- (a) scattering by the aperture (window frame)
- (b) limited field of view
- (c) multiple scattering effects due to dense concentrations
- (d) surface reflections from the windows in the motor
- (e) diameter of aperture limited scattering angle to a maximum of  $6^{\circ}$
- (f) cleanliness of window surfaces
- (g) extraneous light
- (h) quenching effects due to chamber walls, and the introduction of nitrogen used as a purge for the window surfaces
- (i) vignetting of scattered light, i.e., sample not completely within the range of the focal length of the receiving lens. In the event vignetting occurs, particle size is biased to the larger sizes.

Scattering by the aperture is discussed in some detail by Buchele [Ref. 10]. Although some scattering from this source does occur, if the particle concentration is sufficiently high (as in the present case), particle scattering will dominate.

The limited field of view of the NPS system did significantly impact the scattering data obtained. In the case of the present investigation, the physical dimensions of the photodiode array did not allow for scattered light to

be detected at angles less than .01 radians. Also in the current configuration of the NPS scattering device, the largest particle size which could reasonably be detected was 40 microns. The problem may be overcome in large part by increasing the dimension of the array. A 4096 diode RETICON array has been purchased, and should be installed in the near future. This will provide a much enhanced field of view for the NPS instrument.

Multiple scattering effects tend to occur when the separation distance between particles becomes small. Correction methods have appeared in the literature [Refs. 27,28]. These effects were present in the motor measurements and empirical corrections of the data were required. A reduced combustion chamber width is required to reduce this problem.

The problems associated with windowed surfaces are three-fold in nature. The first is that some reflections are present. The MALVERN system in the align mode allows sufficient adjustment of the detector in order to eliminate the effects due to reflections. The second problem was a result of the physical diameter of the window which could pass light. This restricted the maximum scattering angle to  $6^\circ$ . If very small particles had been present, this would have had a biasing effect on the received scattering data. The apparent size would have been larger than the actual size. The third problem associated with the windowed surface was to provide sufficient purge to keep these



surfaces clean. A trial and error method of adjusting purge flow rates was employed. If the windows had become contaminated in a previous run, the flow rate was increased until the surfaces remained clean and usable data were obtained.

The introduction of the purge nitrogen, along with the walls of the motor chamber, had some undetermined quenching effect on the gas and particle temperatures. Although the percent of gas flow comprised by the nitrogen purge was estimated to be between 3 and 9 percent for the given range of pressures, it was not possible to determine what influence the quenching effect had on particle size, or the extent to which it actually occurred.

Extraneous light can also be a factor. Buchele [Ref. 10] details these effects. The ratioing method adopted in the data reduction algorithm for the NPS system has the desirable feature of eliminating this effect. Reference 10 points out the fact that extraneous light is most likely to be a problem at small angles.

Vignetting effects occur when scattered light is not captured by the receiving lens. This tends to bias particle size toward the larger size bands. The way to overcome this difficulty is to ensure that the field of particulates is well within the focal length of the receiving lens, so that all of the light scattered by the sample will be captured by

the (Fourier transform) lens and focused onto the detector array.

The measurement errors that were found to be associated with obtaining scattering data in the exhaust are listed below:

- (a) unstable refractive index of the suspending medium which result from thermal or density gradients
- (b) turbulence along the jet boundary
- (c) shocks associated with a jet which is not ideally expanded
- (d) the location at which the measurements are taken aft of the nozzle can affect the measured distribution
- (e) vignetting, similar to that described previously
- (f) extraneous light (also discussed previously in conjunction with motor measurement errors).

Thermal gradients play a significant role in measuring particle size in hot gas jets. Close to the exit plane of the exhaust, the jet was slightly smaller than the MALVERN laser beam diameter. As discussed above, scattering data were influenced by the thermal gradients along the jet boundary. Also as discussed earlier, the "KILLDATA" command can be used to inhibit data from the inner rings where the steering effect is most prominent. Buchele [Ref. 10] points out that turbulence compounds these effects. It was impossible to separate the effects of turbulence and thermal gradients on the beam steering. In either case, so long as the user is reasonably assured that no scattering data are present as a result of large particles in the exhaust flow,

the "KILLDATA" command may be used to inhibit data from the light steered to low angles.

The presence of shocks in the exhaust jet which is not ideally expanded, is to be expected. The density gradients in the region of a shock can also adversely affect scattered data. If shocks are identified as a problem, a schlieren may be used to establish shock location so that on subsequent runs the apparatus can be positioned upstream of the shock.

The location at which diffraction measurements are made in a supersonic exhaust can influence the resulting distribution of particulates which are observed. The further back in the jet, the less concentrated the particle field becomes. This may have biased the measurements to the smaller particles which were present.

The effects of extraneous light and vignetting have been previously discussed and will not be discussed further, except to say that the measurement and subtracting of background light plays a role in reducing the effect of extraneous light.

## V. CONCLUSIONS AND RECOMMENDATIONS

The results of this investigation have demonstrated that laser diffraction methods can be an effective means for determining particle sizes in solid-propellant rocket motors. Measurements were successfully made in both the motor chamber and exhaust environments. Each environment presented a different set of difficulties.

The MALVERN and the locally designed diffraction system produced data which correlated quite well when the particle distributions were monomodal, and the dominant scattered light was within the field of view of the NPS linear diode array. When the distributions were multimodal, the NPS system did not accurately measure the Sauter mean diameter.

This problem was the result of both a limited field of view and the data reduction algorithm. The latter was based upon monomodal distributions. The system could be significantly improved by using larger arrays and by using data reduction techniques which are based on quadrature methods [Ref. 16].

The NPS system will always be limited to higher number density flows since the linear array only intercepts a very small fraction of the light scattered at a given angle.

The MALVERN 2600 has proven to be well suited for use in solid propellant combustion experiments. The beam diameter,

however, is larger than optimum for the current application. The acquisition of a new beam expander to reduce the diameter of the collimated beam would enhance both in-situ motor measurements and exhaust measurements.

A transition from the axisymmetric motor to a two-dimensional motor would improve through-motor measurements in the following ways:

- (a) advantage of reduced optical depth
- (b) reduction or elimination of multiple scattering effects that may be present in the motor chamber environment due to dense particle concentrations
- (c) increased range of scattering angles
- (d) allows operation to higher pressures.

The motor data suggested that ZrC reacts to form  $\text{ZrO}_2$  on or near the propellant surface. Surface agglomerations occurred and were observed to decrease in size as chamber pressure increased.

At the low Mach numbers in the present motor the  $\text{ZrO}_2$  particles appeared to remain practically unchanged as they passed down the length of the motor port at very low pressures. At higher pressures (above 250 psig), particle growth/agglomeration occurred.

At low pressures the  $\text{ZrO}_2$  particles were multimodal. At higher pressures (greater than 350 psi) the distributions approached monomodal.

ZrO<sub>2</sub> particles broke up in the nozzle converging section to a monomodal distribution with a D<sub>32</sub> between 15 and 19 microns, independent of the particle size entering the nozzle. Limited data indicated that no appreciable change in particle size occurred in the supersonic nozzle flow. Aft of the nozzle, in the expanding plume, the particle size was significantly smaller (2-8 microns). This could be due to particle breakup, or to measurement location biasing.

SEM analysis of particles collected from the converging nozzle wall showed particles with sizes in good agreement with the optically obtained data.



## LIST OF REFERENCES

1. Netzer, D.W. and Powers, J.P., "Smokeless Propellants," AGARD Conference Proceedings No. 391, September 1985.
2. Shorr, M. and Zachringer, A.J. (Editors), Solid Rocket Technology, John Wiley and Sons, Inc., New York, 1976.
3. Coats, D.E., Nickerson, G.R. and Hermesen, R.W. et al., "A Computer Program for the Prediction of Solid Propellant Rocket Motor Performance," Volume I, Interim Report AFRPL-TR-80-34, April 1981.
4. Hermesen, R.W., "Aluminum Oxide Particle Size for Solid Rocket Motor Performance Prediction," AIAA 19th Aerospace Sciences Meeting, January 12-15, 1981.
5. Kerker, M., The Scattering of Light and Other Electromagnetic Radiation, Academic Press, 1969, Chapter 3.
6. Van de Hulst, H.C., Light Scattering by Small Particles, John Wiley and Sons, Inc., New York, 1957.
7. Powell, E.A., Cassanova, R.A., Bankston, C.P., and Zinn, B., "Combustion Generated Smoke Diagnostics by Means of Optical Measurement Techniques," AIAA Paper No. 76-67 AIAA 14th Aerospace Sciences Meeting, January 1976.
8. Jones, A.R., "Error Contour Charts Relevant to Particle Sizing by Forward Scattered Lobe Measurements," Letter to the Editor, Journal of Physics, Applied Physics, Vol. 10, 1977.
9. Hodkinson, J.R., "Particle Sizing by Means of the Forward Scattering Lobe," Applied Optics, Vol. 5, No. 5, 1966, pp. 839-844.
10. Buchele, D.R., "Particle Sizing by Measurement of Forward Scattered Light at Two Angles," NASA Technical Paper 2156, May 1983.
11. Dobbins, R.A., Crocco, L. and Glassman, I., "Measurement of Mean Particle Sizes of Sprays from Diffractively Scattered Light," AIAA Journal, Vol. 1, No. 8, August 1963, pp. 1882-1886.

12. Mugele, R.A. and Evans, H.D., "Droplet Size Distribution in Sprays," Industrial Engineering Chemistry, Vol. 43, 1951, pp. 1317-1324.
13. Harris, R.K., An Apparatus for Sizing Particulate Matter in Solid Rocket Motors, M.S. Thesis, Naval Postgraduate School, Monterey, California, June, 1984.
14. 2600 Particle Sizer User's Manual, Spring Lane, MALVERN, Worcestershire, WR141AQ, England, Manual Version 2.1, 30 September 1985.
15. Dodge, L.G., Rhodes, D.J. and Reitz, R.D., "Drop-Size Measurement Techniques for Sprays: Comparison of MALVERN Laser-Diffraction and Aerometrics Phase/Doppler," Applied Optics, Vol. 26, No. 11, 1 June 1987.
16. Koo, J.H., Particle Size Analysis Using Integral Transform Techniques on Fraunhofer Diffraction Patterns, Ph.D. Dissertation, The George Washington School of Engineering and Applied Science Department of Civil, Mechanical and Environment Engineering, Washington, D.C., April 1987.
17. Pruitt, T.E., Measurement of Particle Size Distribution in a Solid Propellant Rocket Motor Using Light Scattering, M.S. Thesis, Naval Postgraduate School, Monterey, California, June 1987.
18. Walker, J.D., Holographic Investigation of Metallized Solid Propellant Combustion in Two Dimensional and Three Dimensional Rocket Motors, M.S. Thesis, Naval Postgraduate School, Monterey, California, September 1987.
19. MALVERN Instruments Particle Sizer Reference Manual, Spring Lane, MALVERN, Worcestershire, WR141AQ1, England, Manual Version 3.0, 22 July 1986.
20. Rosa, J.S., Particle Sizing in a Solid Propellant Rocket Motor Using Scattered Light Measurements, M.S. Thesis, Naval Postgraduate School, Monterey, California, December 1985.
21. Pokhil, P.F., Belyayev, A.G., Frolov, Yu.V., Logachev, V.A., and Korotkov, A.I., Combustion of Powdered Metals in Active Media, Nauka, Moscow, USSR, 1972.

22. Gany, A. and Caveny, L.H., "Agglomerates and Ignition Mechanism of Aluminum Particles in Solid Propellants," proceedings of 17th International Symposium on Combustion, August 1978.
23. Personal Communication with Mr. T. Rudy, Chemical Systems Division, United Technologies.
24. Summerfield, M. and Kuo, K.K., Fundamentals of Solid-Propellant Combustion, American Institute of Aeronautics and Astronautics, 1984.
25. Lynch, C.T., CRC Handbook of Material Science, CRC Press, Cleveland, Ohio, 1975.
26. Schwartkopf, P. and Kiefer, R., Refractory Hard Metals Borides, Carbides, Nitrides, and Silicides, The MacMillan Company, New York, 1953.
27. Gomi, H., "Multiple Scattering Correction in the Measurement of Particle Size and Number Density by the Diffraction Method," Applied Optics, Vol. 25, No. 19, 1 October 1986.
28. Gulder, O.L., "Multiple Scattering Effects in Drop Sizing of Dense Fuel Sprays by Laser Diffraction," AGARD 70th Symposium of the Propulsion and Energetics Panel on Combustion and Fuels in Gas Turbines, October, 1987.

INITIAL DISTRIBUTION LIST

	No. Copies
1. Defense Technical Information Center Cameron Station Alexandria, Virginia 22304-6145	2
2. Library, Code 0142 Naval Postgraduate School Monterey, California 93943-5100	2
3. Department Chairman, Code 67 Department of Aeronautics Naval Postgraduate School Monterey, California 93943-5100	1
4. Professor D. W. Netzer, Code 67Nt Department of Aeronautics Naval Postgraduate School Monterey, California 93943-5100	2
5. LCDR E. D. Youngborg 992 Cobblestone Drive Orange Park, Florida 32073	2
6. LT Marlow Moser, USAF Stop 24 Air Force Astronautics Laboratory Edwards AFB, California 93423-5000	2
7. Deputy Chief of Naval Operations (Air Warfare) OP-05 Pentagon Washington, D.C. 20361	1









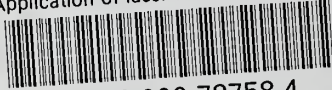


T Thesis  
Y Y745  
c.1 Youngborg  
Application of laser  
diffraction techniques  
to partical sizing in  
solid propellant rocket  
motors.

Thesis  
Y745 Youngborg  
c.1 Application of laser  
diffraction techniques  
to partical sizing in  
solid propellant rocket  
motors.



thesY745  
Application of laser diffraction techniq



3 2768 000 78758 4  
DUDLEY KNOX LIBRARY